CONTROL OF VAPOR DISPERSION AND POOL FIRE OF LIQUEFIED NATURAL GAS (LNG) WITH EXPANSION FOAM

A Dissertation

by

GEUN WOONG YUN

Submitted to the Office of Graduate Studies of
Texas A&M University
in partial fulfillment of the requirements for the degree of

DOCTOR OF PHILOSOPHY

August 2010

Major Subject: Chemical Engineering

Control of Vapor Dispersion and Pool Fire of Liquefied Natural Gas (LNG) with Expansion Foam

CONTROL OF VAPOR DISPERSION AND POOL FIRE OF LIQUEFIED NATURAL GAS (LNG) WITH EXPANSION FOAM

A Dissertation

by

GEUN WOONG YUN

Submitted to the Office of Graduate Studies of
Texas A&M University
in partial fulfillment of the requirements for the degree of

DOCTOR OF PHILOSOPHY

Approved by:

Chair of Committee,	M. Sam Mannan
Committee Members,	Mahmoud El-Halwagi
	Carl Laird
	N.K. Anand
Head of Department,	Michael Pishko

August 2010

Major Subject: Chemical Engineering

ABSTRACT

Control of Vapor Dispersion and Pool Fire of Liquefied Natural Gas (LNG) with Expansion Foam. (August 2010)

Geun Woong Yun, B.S., Sungkyunkwan University; M.S., Yonsei University, Republic of Korea; M.S., Texas A&M University

Chair of Advisory Committee: Dr. M. Sam Mannan

Liquefied Natural Gas (LNG) is flammable when it forms a 5 – 15% volumetric concentration mixture with air at atmospheric conditions. When the LNG vapor comes in contact with an ignition source, it may result in fire and/or explosion. Because of flammable characteristics and dense gas behaviors, expansion foam has been recommended as one of the safety provisions for mitigating accidental LNG releases. However, the effectiveness of foam in achieving this objective has not been sufficiently reported in outdoor field tests. Thus, this research focused on experimental determination of the effect of expansion foam application on LNG vapor dispersion and pool fire.

Specifically, for evaluating the use of foam to control the vapor hazard from spilled LNG, this study aimed to obtain key parameters, such as the temperature changes of methane and foam and the extent reduction of vapor concentration. This study also focused on identifying the effectiveness of foam and thermal exclusion zone by

investigating temperature changes of foam and fire, profiles of radiant heat flux, and fire height changes by foam. Additionally, a schematic model of LNG-foam system for theoretical modeling and better understanding of underlying mechanism of foam was developed.

Results showed that expansion foam was effective in increasing the buoyancy of LNG vapor by raising the temperature of the vapor permeated through the foam layer and ultimately decreasing the methane concentrations in the downwind direction. It was also found that expansion foam has positive effects on reducing fire height and radiant heat fluxes by decreasing fire heat feedback to the LNG pool, thus resulting in reduction in the safe separation distance. Through the extensive data analysis, several key parameters, such as minimum effective foam depth and mass evaporation rate of LNG with foam, were identified. However, caution must be taken to ensure that foam application can result in initial adverse effects on vapor and fire control. Finally, based on these findings, several recommendations were made for improving foam delivery methods which can be used for controlling the hazard of spilled LNG.

DEDICATION

- To God, Jesus, and the Holy Spirit: You did not forsake me when I was living in darkness with sins. You brought me to U.S. to become a Christian and give me a new life. Thanks for your endless love and blessing. You saved me.
- To my wife, Soonyung: Without your support and patience, I may not be able to make it. You also have been my soul mate and mediator with our God. You are the most precious thing in my life. I love you.
- To my son, Jeongwook: My sweetheart, son. You have been my source of joy in my life. Thanks for your patience about the deficiency of playing together. I will always love you.
- To mother and father: Thanks for raising me and giving full support for my previous educations. You have been teaching me how I should be diligent and responsible for my work through your life. You are my role model. Thus, I am able to achieve this degree. I do really appreciate your love and support. I love you.
- To my brother and sisters: I really appreciate your help and support when I grew up. Without your help, I may not be myself as it is. I love you.

ACKNOWLEDGEMENTS

I would like to thank my committee chair, Dr. M. Sam Mannan, and my committee members, Dr. Mahmoud El-Halwagi, Dr. Carl Laird, and Dr. N.K. Anand for their guidance and support throughout the course of this research. I also appreciate Dr. Jerald Caton for his help at my final exam. I specially thank Dr. Mannan for his wonderful and thoughtful guidance for this research as well as for my career life. I have been really happy with Dr. Mannan throughout my entire time at TAMU. There is no doubt that Dr. Mannan is one of best advisors (or professors) in the world.

I also appreciate the LNG team members (Dedy Ng, Morshed Rana, Ruifeng Qi, Benjamin Cormier, Jaffee Suardin, ByungKyu Kim) for their help and friendship. Thanks should go to all members of Mary Kay O'Connor Process Safety Center (MKOPSC) for their support. I also thank my friends (including church friends) and colleagues and the department faculty and staff for making my time at Texas A&M University a great experience.

Finally, I would like to thank BP Global Gas SPU (especially Mr. Robin Passmore and Dr. Ben Ho) for the financial support of this research. I thank the Texas Engineering Extension Service (TEEX) for providing supports and guidance on the field tests at Brayton Fire Training Field. I thank Randy Marek for helping to build my experimental setup.

NOMENCLATURE

BFTF	Brayton Fire Training Field
CFD	Computational Fluid Dynamics
LFL	Lower Flammable Limit
LNG	Liquefied Natural Gas
MKOPSC	Mary Kay O'Connor Process Safety Center
SEP	Surface Emissive Power

TABLE OF CONTENTS

Page

CHAPTER Page

CHAPTER Page

LIST OF FIGURES

Page

Page

Page

Page

LIST OF TABLES

Page

CHAPTER I

INTRODUCTION AND LITERATURE REVIEW

1.1 Introduction

1.1.1 Liquefied natural gas

Liquefied Natural Gas (LNG) refers to natural gas converted into liquid state by super cooling to -260 ^{o}F (-162.2 ^{o}C) at atmospheric pressure [1, 2]. LNG commonly consists of 85 % - 98 % methane with the remainder as a combination of nitrogen, carbon dioxide, ethane, propane, and other heavier hydrocarbon gases.

Because of the fact that the volume compresses 600 times from gas phase into its liquid phase by super cooling, it provides cost-effective LNG containment, and the liquid phase also permits cost effective LNG transportation across great distances onshore and offshore, at atmospheric pressure. Moreover, LNG is environmental friendly because of clean burning. Therefore, LNG demand has been growing to diversify the energy portfolios and fulfill the energy demand for LNG as a fuel of heating, cooling, cooking and power generation, etc. LNG may play an important role in filling the gap between supply and demand of energy in North America.

This dissertation follows the style of Journal of Hazardous Material.

1.1.2 LNG concerns

LNG is flammable when it forms a 5 – 15 % volumetric concentration mixture with air at atmospheric conditions. When the LNG vapor comes in contact with an ignition source, it may result in fire and/or explosion. Even though methane is lighter than air at ambient conditions, the released LNG forms a denser-than-air vapor cloud up to -173 ^{o}F (-114 ^{o}C, at which point gas density becomes equal to that of air at 15 ^{o}C) [3, 4]. Because of this dense gas behaviors and flammable characteristics, caution must be taken in considering safety measures for control of vapor dispersion and fire.

1.1.3 Expansion foam

According to the definition of NFPA 11 [5], expansion foam can be one sort of the air foam. Air foam is made by mixing air into a water solution, containing a foam concentrate, by means of suitable equipment, e.g., foam generators. The foam concentrate is mainly based on surface active agents. Foams may be subdivided into three ranges of expansion as follows: (1) Low-expansion foam – expansion up to 20; (2) Medium-expansion foam – expansion from 20 to 200; (3) High-expansion foam – expansion from 200 to approximately 1000 [5].

1.1.4 Motivation

With increasing demand for LNG, there are at least 113 currently active LNG facilities across the U.S., including importation terminals, operating and storage facilities for use during periods of peak natural gas demand or as a baseload source of natural gas. In addition, there are also a number of proposed projects for LNG terminals in North

America. Fig. 1 shows a typical process flow of LNG importation terminal. Usually, LNG is stored or treated in massive volume in LNG facilities, thus the fact may pose large consequences in unexpected cases [6].

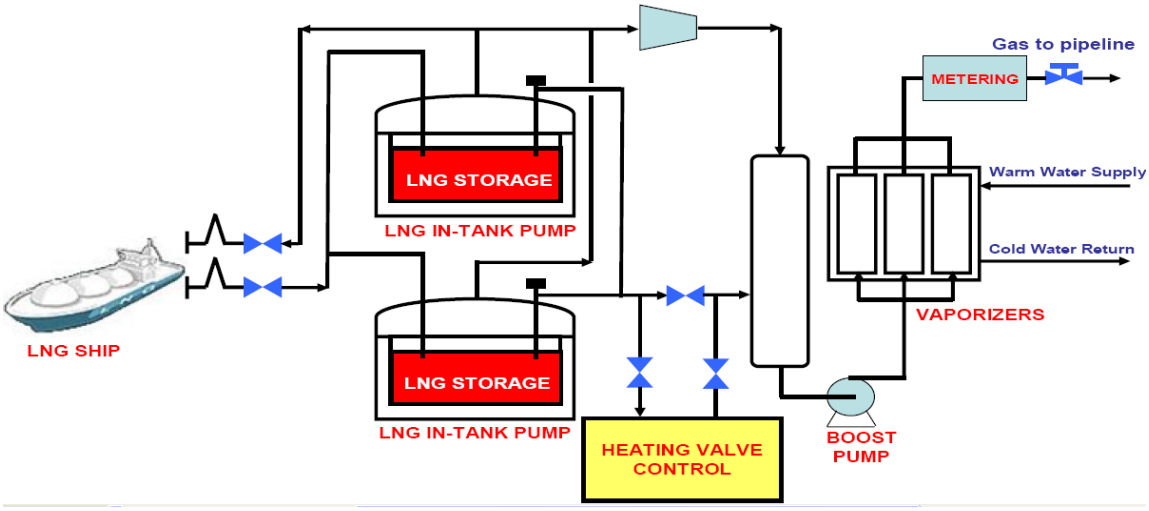

(Adapted from [7])

Fig. 1. Process flow diagram of typical LNG importation terminal

Therefore, NFPA 59 A [8, 9] requires a thorough evaluation of potential release consequence when developing LNG terminals. Especially, LNG storage tanks should have dike or impoundment, which is built around the storage tanks for holding accidental spill as shown in Fig. 2. This standard also requires LNG facilities to design "vapor exclusion zone" so that LNG vapor cloud will not affect beyond the property line based on vapor dispersion computations under 50 percent of the lower flammability limit (LFL), i.e., 2.5 % volume in air. In addition, this standard specifies that provisions shall be made to prevent thermal radiation heat flux of a fire from exceeding some limits, such as 5 kW/m^2 at a property line [10].

Consequently, application of expansion foam can be one of those safety provisions for vapor dispersion control and pool fire suppression. In order to use the expansion foam for LNG facilities, the effectiveness of expansion foam on control of LNG vapor dispersion and pool fire should be validated by experiments. Thus, this research focuses on determining the foam effectiveness on LNG control and identifying several key parameters regarding foam application.

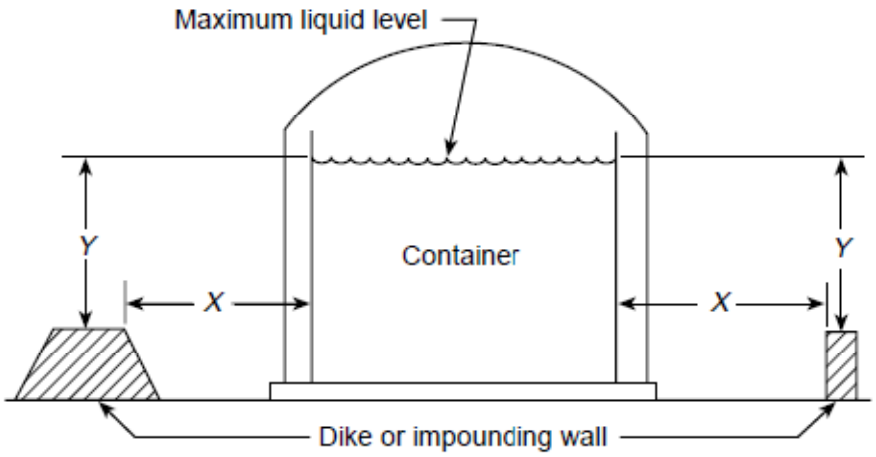

Notes:

- Dimension *X* shall equal or exceed the sum of dimension *Y* plus the equivalent head in LNG of the pressure in the vapor space above the liquid.
  Exception: When the height of the dike or impounding wall is equal to, or greater than, the maximum liquid level, X may have any value.
- Dimension *X* is the distance from the inner wall of the container to the closest face of the dike or impounding wall.
- Dimension *Y* is the distance from the maximum liquid level in the container to the top of the dike or impounding wall.

(Adapted from [8])

Fig. 2. Dike or impoundment wall proximity to storage tanks

1.2 Present status of question

1.2.1 Important parameters of LNG control

When LNG escapes from its containment, it will start to behave as a dense gas since its temperature is still very low. After having enough heat transfer with surrounding environments (including air, sun light, and ground), it becomes lighter than air and then dissipated. Due to the dense cloud behavior of LNG, vapor dispersion calculation of LNG is conducted with dense gas models, such as Britter and McQuaid model [11], DEGADIS model, or Slab model [12]. Currently, however, no models for LNG vapor dispersion controlled by expansion foam have been developed. The extent of LNG vapor dispersion can be affected by LNG release rate, vaporization rate, geometry of spill area, and the atmospheric conditions. In addition, it is important to know the LNG spreading behavior for estimating the size of liquid pool and/or fire. Fay [13] suggests the relationships between maximum pool area and vaporization rate as shown in equation (1). In this equation, it is known that the maximum pool area is a function of vaporization rate.

$$\mathbf{A_p} \sim \frac{\sqrt{\mathbf{g h_0}}\mathbf{A_h}}{\boldsymbol{\omega}} \qquad (1)$$

where, A_p: Maximum pool area

A_h: Rupture flow area

ω: Regression velocity, where volume rate of pool liquid vaporized per unit surface area

h_0: Initial value of hydrostatic head

g: Acceleration due to gravity

LNG pool fire models have been developed to evaluate the thermal hazard exclusion zones around LNG fires required by U.S. Regulations and NFPA 59 A [8, 14]. Two general approaches have been used to determine the threshold distance of heat flux from fire as follows; solid flame and point source models [14]. Nowadays, researchers have been attempting to use computational fluid dynamics (CFD) modeling for LNG pool fire modeling, but significant efforts for validating simulation results are still required. As such vapor dispersion models, however; any models for fire control with expansion foam have not been developed. In this literature review, point source model has been introduced in order to identify key parameters of pool fire modeling.

Heat flux to an object from the center of fire can be calculated using the point source model as shown by equation (2) [14]. The heat flux from fires is a function of mass burning rate (or mass evaporation rate), fire diameter, and fraction of combustion energy released that is radiated, which is also a function of fire diameter.

$$\dot{q}'' = X_R \frac{\frac{\pi}{4} D^2 \dot{m}'' \Delta H_c}{4\pi S^2} \qquad (2)$$

where, $\dot{q}''$: Radiative heat flux received by an object at distance S

X_R: Fraction of combustion energy released that is radiated

$X_R = 0.35e^{-(D/20)}$, D: fire diameter (m)

D: Fire diameter

$\dot{m}''$: Mass burning rate per unit area

ΔH_c: heat of combustion of the fuel burning

S: Distance from the center of the fire

In addition, equation (3) shows the relationship between the flame height and diameter of fire base by Thomas's correlation [14]. If LNG spills in an unconfined area and then catches fires, the fire height can be measured using visual devices, such as cameras. When mass burning rate of LNG is known, then the fire diameter for unconfined pool fires on land can be estimated using equation (3). Similarly, if fire diameter and mass regression rate are known, the flame height can be calculated. This estimated flame height may be used for calculation of surface emissive power (SEP) and geometric view factor for solid flame modeling of LNG pool fire.

$$\frac{L}{D} = 55\left(\frac{\dot{m}''}{\rho_a\sqrt{gD}}\right)^{2/3} \quad (3)$$

where, L: Height of fire

D: Fire diameter

$\dot{m}''$: mass burning rate

ρ_a: Density of air

g: Acceleration due to gravity

1.2.2 Previous study on expansion foam

Regarding expansion foam application on LNG pool, limited research and experiments have been done so far, but they were still capable of presenting useful knowledge to LNG industries for foam application on LNG.

In 1974, University Engineers, Inc. [15] investigated the effectiveness of expansion foam of LNG spills on land in vapor dispersion control by measuring methane concentration and in fire control by measuring the reduction of radiant heat fluxes emitted from LNG fires. This research presented several methane concentration graphs which had both data before and after foam application to recognize differences, and also radiant heat flux curves which showed the extent of heat reduction by foam. In this research, it was concluded that expansion foam can reduce the gas concentrations, foam can affect the LNG evaporation rate, and foam blankets with depth ranging from 0.46 m (1.5 ft) to 1.22 m (4 ft) have no effect on vapor dispersion control. In addition, University Engineers, Inc. also concluded that expansion foam provides effectiveness on fire control by reducing levels of flame emissive power. However, the report does not provide the mechanisms of foam change when contacting with LNG, temperature profile of expansion foam and fire, and temperature changes of LNG vapors after foam application. Moreover, it does not include what is the minimum effective foam depth and how LNG and foam spreading affect the temperature profile of foam.

Specifically, for LNG liquid level measurement, University Engineers, Inc. [15] and Suardin [16] used differential pressure meters using nitrogen gas as a bubbling material. In this technique, a pressure transducer is connected to the nitrogen line so that it can sense the sum of pressure drop required to discharge nitrogen gas through the supply tube and also the pressure required to overcome the static pressure of the liquid head. In case of foam application, foam itself on top of LNG may be influence on the liquid head, thus resulting in gaps or uncertainty in level measurement. Therefore, it may

be better if thermocouples, which can measure the temperature of cryogenic liquid (including LNG), are used together with differential pressure meters to compare both measurement results.

Radiant heat fluxes were measured only in a crosswind of the fire at several locations by Suardin [1, 14, 16]. In the test of University Engineers, Inc. [15], the radiometers were positioned in two wind directions (downwind and crosswind) of the fire to determine hazardous distance. However, in this research, it is attempted to obtain heat flux contours for estimating 360 degree angle of thermal radiation distances in plane by positioning radiometers in four directions. NFPA 59 A [8] specifies that provisions shall be made to prevent thermal radiation flux by a fire based on a design spill from exceeding 5 kW/m^2 at a property line. Therefore, measuring distances of this radiation threshold can be applied to determine LNG plant design and layout [15, 17].

Takeno [3] studied effects of high expansion foam dispersed onto leaked LNG on the atmospheric diffusion of vaporized gas. He performed two types of experiments. One experiment was to identify the effects of expansion foam application on the temperature increase of vaporized gas, using a small-scale liquid pool to simulate an actual scale as shown in Fig. 3. However, he used liquid nitrogen (LN_2) instead of LNG to secure safety in experiments. In the experimental apparatus, fourteen stationary thermocouples were arranged along a pole installed vertically to verify the liquid level and measure the temperature profile within and above the expansion foam. The other experiment was to measure the change of evaporation rate after applied expansion foam contacts with the LN_2 as shown in Fig. 4. The evaporation rate which can be one of the input parameters

for overall heat balance modeling was measured by a laboratory scale apparatus that included a load cell, which converts weight into voltage. However, it was a laboratory scale experiment by using LN_2, not outdoor field test using LNG. Thus, the resulting evaporation rate may not reflect the atmospheric outdoor conditions (e.g. wind effects, solar radiation, humidity) and actual LNG release scenarios in the LNG facilities. Currently, to measure the evaporation rate of LNG, two direct measurement methods can be used. One is the use of thermocouples, which can also be called as “thermocouple trees”. The thermocouples can detect the liquid level of LNG by measuring the LNG boiling temperature, -162.2 ^{o}C. Thus, with the given surface area of LNG pool and its level, the volumetric evaporation rate can be obtained and then it can be converted into mass evaporation rate using specific gravity of LNG. The other one is the use of differential pressure transmitters, which can be called as “bubble meters”. It measures the pressure difference between the atmospheric pressure and the hydrostatic pressure of LNG at the bottom of pit. The hydrostatic pressure of LNG differs as LNG liquid level decreases. The pressure difference can be converted into the level of LNG decrease to obtain evaporation rate. In addition, the differential pressure transmitter includes nitrogen line at the bottom end of the pipe to avoid any back flow. However, Takeno [3] did not use those direct measurements for evaporation rate.

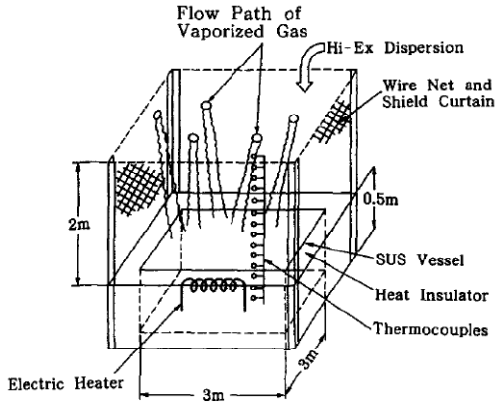

(Adapted from [3])

Fig. 3. Experimental apparatus of expansion foam using LN_2

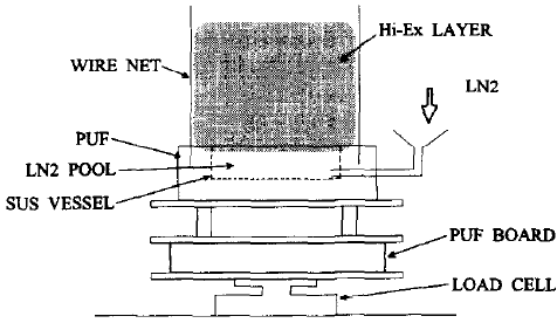

(Adapted from [3])

Fig. 4. Experimental apparatus for evaporation rate

Takeno's paper also discussed the heat balance of expansion foam layer, LN_2, and surroundings. The paper indicated three layers of expansion foam as shown in Fig. 5 and Fig. 6; frozen layer [18], no-frozen layer, and dissipated layer. It considered two modes of heat transfer: (1) convection of water traveling downwards caused by dissipation of expansion foam; (2) thermal conduction through the expansion foam layer.

In this paper, the total heat balance was expressed in the following equation; $Q_B + Q_D + Q_E = Q_A + Q_C$ (see each description in Fig. 6). However, it didn't include thermal conduction from concrete dike or wall which is one of the requirements for LNG storage tank systems and facilities. The paper also assumed that the radiation from the sun, Q_E, was zero since the experimental apparatus had the shield curtain. However, the assumption may not be realistic in the LNG or other facilities because industrial safety practices recommended that released flammable liquid from the containments should not be enclosed. It implies that spilled LNG may have energy inputs from solar radiation, only if sunlight exists. Moreover, in case of foam application to fire, the heat transfer balance is different with the case without fire, but the paper did not address this issue. For LNG pool fire cases, convective and radiant heat from fire to expansion foam and LNG, and the change of latent heat due to vaporization of water should be considered additionally.

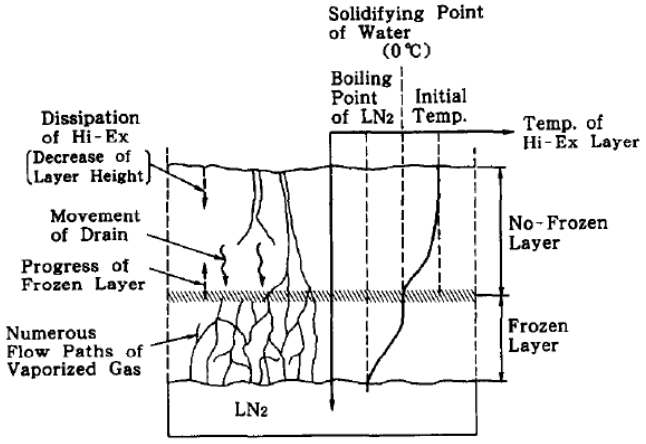

(Adapted from [3])

Fig. 5. Model of heat transfer of expansion foam using LN_2

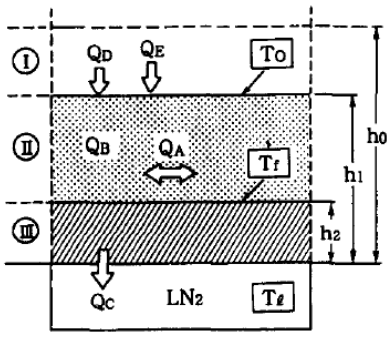

h_0 : Initial Height of Dispersed Hi-Ex (m)
h_1 : Height of Dispersed Hi-Ex (m)
h_2 : Thickness of Frozen Hi-Ex Layer (m)

Q_A : Heat Transfer from Hi-Ex to Vaporized Gas (J/m^2)
Q_B : Change in Latent Heat of Hi-Ex Layer (J/m^2)
Q_C : Heat Transfer from Bottom Side of Hi-Ex Layer to LN_2 (J/m^2)
Q_D : Heat Transfer from Ambient Air by Conduction and Convection (J/m^2)
Q_E : Heat Transfer from Ambient Air by Radiation (J/m^2)

T_o : Initial Temperature of Hi-Ex 15 (℃)
T_f : Solidifying Point of Water 0 (℃)
T_ℓ : Boiling Point of LN_2 −195.6 (℃)
H_f : Heat of Solidification of Water 3.34×10^5 (J/kg)

(Adapted from [3])

Fig. 6. Heat balance in the whole expansion foam system using LN_2

Recently, a few field tests concerning expansion foam application on LNG pool were conducted in College Station, Texas [16]. These tests attempted to identify several key parameters, such as mass evaporation rate, optimum foam application rate, and radiant heat reduction by foam. However, there are still several research gaps which need to be filled or improved to obtain the strategy for foam application on LNG.

1.2.3 Summary of research gaps

Previous works have confirmed that the expansion foam represents one of the promising techniques to control both LNG vapor dispersion and pool fire. However, those experimental works do not present clear ideas how to design effective expansion foam system and how much foam can reduce potential hazards of spilled LNG. There are still important key issues which should be discovered, such as: (1) the minimum effective foam depth for both vapor dispersion and pool fire scenarios; (2) underlying mechanism of expansion foam on LNG; (3) effects of LNG and/or foam spreading on

foam temperature profile; (4) the extent of reduction of LNG vapor concentration and radiant heat flux by expansion foam; (5) the change of mass evaporation rate and temperature of LNG vapors by foam; and (6) the foam collapse rate on LNG. In addition, previous researchers provided only one dimensional experimental results (e.g. heat flux measurements in only a cross wind direction or temperature measurements of foam in only a vertical axis), thus it might not be sufficient to convince or make conclusions about the foam effects.

Therefore, more studies are required to fill the research gaps and also determine the key parameters in designing expansion foam system for the purpose of controlling accidentally released LNG vapors and pool fire.

1.3 Proposed research

1.3.1 Objectives

It was recognized by previous literature review that the expansion foam is one of the promising techniques for mitigating accidental LNG spills. The main purpose of this research is to experimentally determine the effect of expansion foam application on LNG vapor dispersion and pool fire. Specifically, this research is proposed to obtain: (1) minimum effective foam depth for vapor dispersion and fire control; (2) the extent of reduction of vapor concentration and radiant heat flux; (3) temperature profiles of expansion foam, LNG vapors, and fire; (4) heat flux profiles of fire; and (5) mass evaporation rate during vapor dispersion and pool fire. In addition, this research focuses on understanding the underlying mechanism of expansion foam when it contacts with

LNG and obtaining foam breaking rate on the basis of theoretical modeling and experiments.

Finally, this work will determine effectiveness of expansion foam on controlling LNG vapor and fire. Furthermore, this work will provide LNG industries or regulators with experimentally determined specific guidelines for foam system design.

1.3.2 Methodology

To study the expansion foam on LNG, the research outline is developed as shown in Figure 7. In this research, two methods were employed: (1) field experiments and (2) theoretical study. Foam effectiveness and several key parameters were identified by field experiments and some of them are used for validation of theoretical calculation results. In this study, two types of experiments are performed: (1) a small-scale field test for indentifying expansion foam changes on LNG; and (2) medium-scale field tests for verifying foam effectiveness on vapor dispersion and pool fire suppression. From the small-scale test, foam breaking rate and foam changes on a LNG pool are identified, and medium-scale tests are used to identify mass evaporation rate of LNG, temperature profiles, vapor concentration profiles, and radiant heat flux profiles as summarized in Fig. 7.

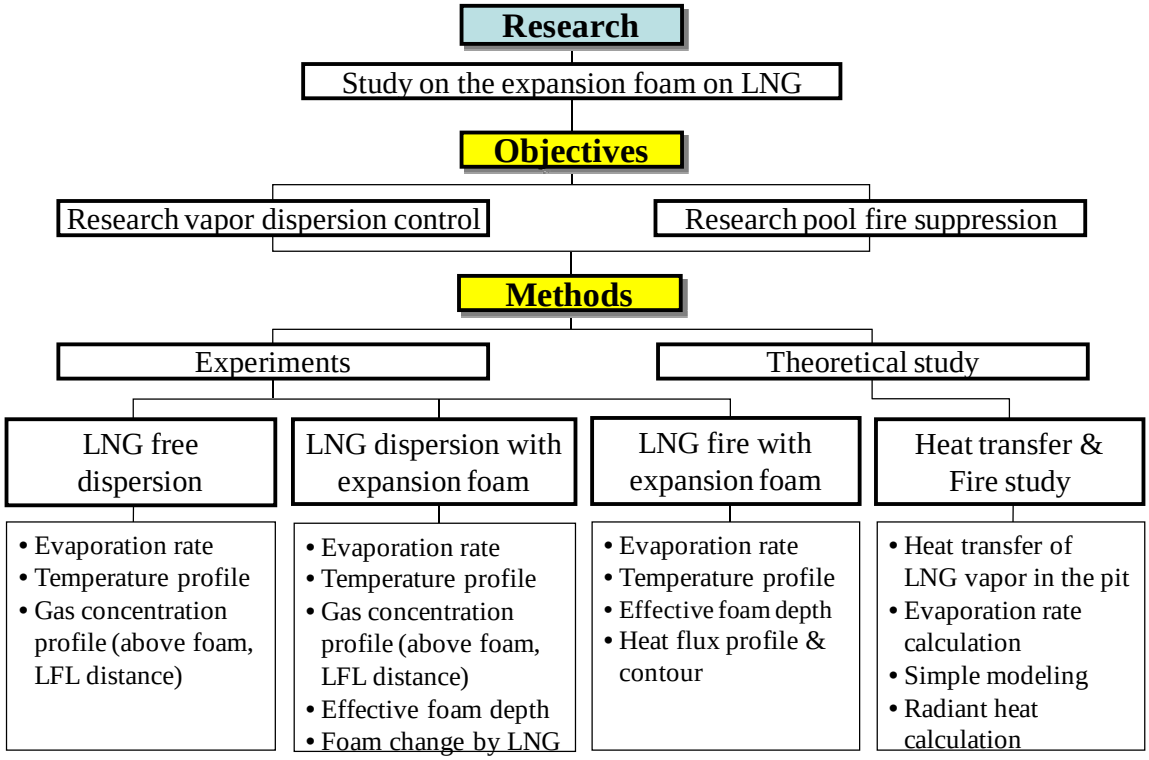

Fig. 7. Research outline

1.3.3 Experimental design

Outdoor small and medium scale experiments were designed to release LNG onto a confined concrete pit (or wooden box lined with concrete boards in a small-scale test) to simulate LNG release scenarios in LNG facilities on land. Prior to investigation of the foam effectiveness on LNG, it should be observed the changes and mechanisms of expansion foam when it is applied on LNG and how much foam can be broken by contacting with LNG and other factors such as wind streams. To achieve this objective, a small-scale field test was designed and conducted on March 2009. Medium-scale field tests were conducted to observe foam effectiveness on LNG control and also identify

other key parameters on March and December 2009. Experiments were designed to be carried out on the LNG test facility at the Brayton Fire Training Field (BFTF), which is affiliated with the Texas A&M University System, as shown in Fig. 8. The facility is composed of three concrete pits and its flat ground is also made of concrete. Detailed information on the test setup is presented in Chapter II and III.

1. Small pit : 3.05 m x 3.05 m x 1.22 m
2. Large pit (65 m2 pit) : 10.06 m x 6.71 m x 1.22 m
3. L-Trench
4. Small pit : 6.71 m x 6.71 m x 2.44 m

Fig. 8. LNG props at TEEX's Brayton Fire Training Field

1.3.4 Overall procedure of medium-scale tests

Both March and December tests had the same test procedure as shown in Fig. 9. LNG was initially released into a large pit through a 10.16 cm diameter stainless steel pipeline up to 20.32 cm depth. After that, high expansion foam (expansion ratio 500:1) was applied by two foam generators and filled up to wooden wall level with 2.44 m

depth. When vapor dispersion control test as shown in Fig. 9(b) was over after some period of time, the wooden walls around the pit were removed. Finally, LNG was ignited by a torch for fire test as shown by Fig. 9(d). All tests for the control of vapor dispersion and pool fire by foam application were conducted in a series manner. Real landscapes of vapor dispersion test and pool fire test with expansion foam are presented in Fig. 10 and Fig. 11.

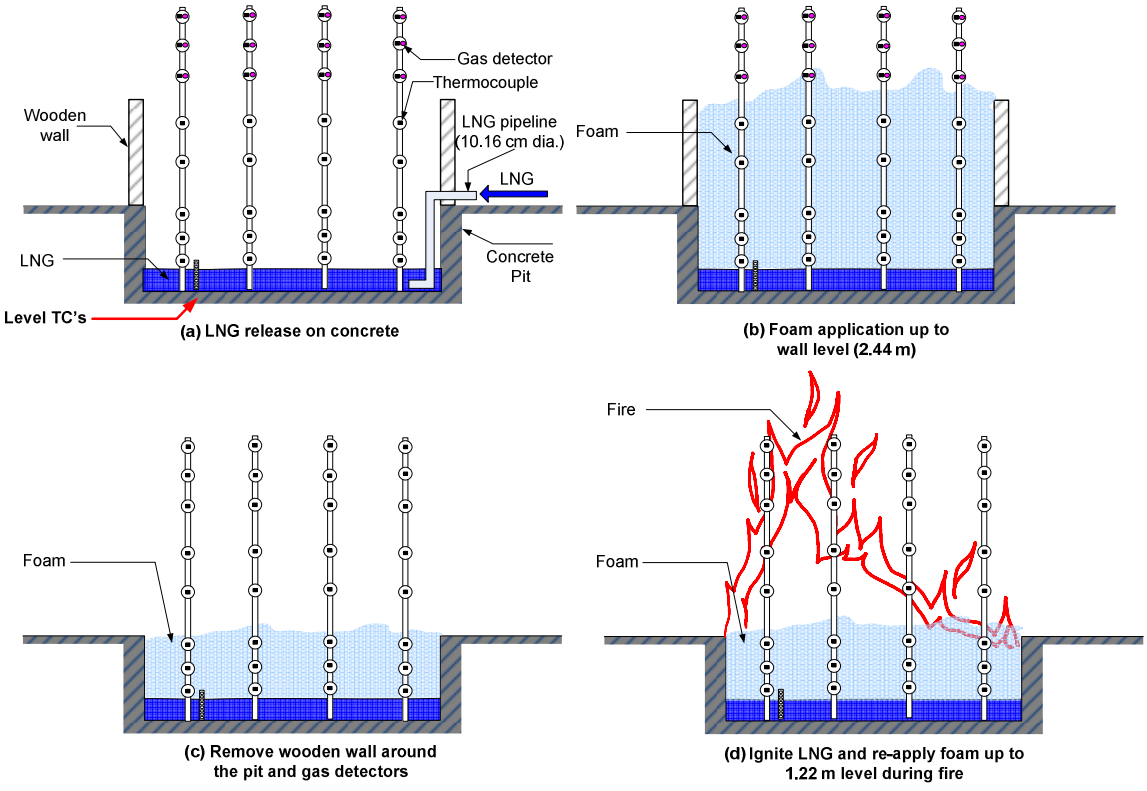

Fig. 9. Experimental procedure

Fig. 10. Real landscape of vapor dispersion test with expansion foam

Fig. 11. Real landscape of pool fire test with expansion foam

CHAPTER II

CONTROL OF VAPOR DISPERSION

2.1 Introduction

Liquefied Natural Gas (LNG) is natural gas that has been converted into liquid form by super cooling to -162.2 ^{o}C (-260 ^{o}F) at atmospheric pressure [1, 4, 6]. LNG primarily consists of 85% - 95% methane with the remaining compounds consisting of nitrogen, carbon dioxide, ethane, propane, and other heavier hydrocarbons [1, 19]. Even though methane is lighter than air at ambient conditions, the release of LNG on any substrate results in its rapid boiling and the formation of a cold, denser than air vapor cloud, which is visible (white) due to the condensation of water vapor from the atmosphere [3, 4]. The vapor is flammable in air at concentrations between 5 – 15% [1, 4]. When the LNG vapor comes in contact with an ignition source, it may result in fire and/or explosion. Because of the dense gas behavior and flammable characteristics, caution must be taken when considering safety measures for preventing and/or mitigating an accidental LNG release.

With increasing demand for LNG, there are currently at least 100 active LNG facilities spread across the U.S. LNG is typically stored or treated in massive volume at LNG facilities, thus may pose large consequences in the event of an accidental release [6]. Potentially catastrophic pool fires or vapor cloud fires could arise from a serious accident or deliberate attack against LNG facilities. Faced with growing concerns about

LNG safety, standard NFPA 59A requires a thorough evaluation of potential release consequences concerning LNG facility siting [8, 9]. This standard also requires LNG facilities to design “vapor exclusion zones” so that LNG vapor clouds will not affect the population beyond the property line based on vapor dispersion computations under 50 percent of the lower flammability limit (LFL), i.e., 2.5% volume in air [10, 20].

Expansion foam has been recommended as a safety provision for LNG vapor dispersion control and fire mitigation [5]. The foam is made by mixing a foam concentrate with water and then aerating and agitating the solution to form a bubble structure. The foam concentrate is typically made of surface active agents. Foams can be categorized into three expansion ranges: (1) Low-expansion foam – expansion up to 20; (2) Medium-expansion foam – expansion from 20 to 200; (3) High-expansion foam – expansion from 200 to approximately 1000 [5]. Although expansion foam has been used for fire mitigation, the application of this foam to an LNG fire and vapor control has not been thoroughly investigated.

In 1974, University Engineers Inc. investigated the effectiveness of expansion foam for vapor dispersion control in the event of LNG spills on land by measuring the downwind methane concentration [15]. Results were depicted through the changes in methane concentration before and after foam application. Summary of their test findings is as follows: expansion foam reduced the gas concentrations in the downwind direction; foam influenced the LNG evaporation rate; and foam blanket depths from 0.5 to 1.2 meter (1.5 - 4 feet) did not show any effect on vapor dispersion control. On the other hand, Takeno et al. [3] studied the effects of high expansion foam dispersion on the

temperature and evaporation rate of liquid nitrogen (LN_2). Because the tests were conducted using LN_2 in a laboratory setting, the resulting evaporation rate may not reflect the atmospheric conditions (e.g., wind effects, solar radiation, and humidity) and may not likely depict the release at LNG facilities. Since 2005, a series of medium-scale field tests of expansion foam application on LNG pools were performed by the Mary Kay O'Connor Process Safety Center at the Brayton Fire Training Field (BFTF), which is affiliated with the Texas A&M University System [16, 21]. These tests attempted to identify several key parameters, such as mass evaporation rate and optimum foam application rate.

Although previous work has confirmed that the expansion foam represents one promising technique to control LNG vapor dispersion [3, 15, 21, 22], it is still unclear from such experimental work how to design effective expansion foam systems. Therefore, more studies are needed to fill the knowledge gaps and distinguish the key parameters in designing expansion foam system for controlling LNG vapor.

The objective of the present investigation is to experimentally determine the effects of expansion foam application on LNG vapor dispersion. Specifically, this study aimed to determine: (1) minimum effective foam depth for vapor dispersion control; (2) the extent reduction of vapor concentration; (3) temperature profiles of expansion foam and LNG vapor; and (4) change in mass evaporation rate with foam application. In addition, this study focused on understanding the underlying mechanisms of expansion foam when it contacts with LNG as well as obtaining foam breaking rates. Results from

this investigation can be used to provide guidelines on expansion foam system designs for LNG industries and regulators.

2.2 Field test

Two types of LNG spill test were performed at the BFTF in March and December 2009: (1) small-scale field test for indentifying expansion foam mechanisms when it contacts with LNG; and (2) medium-scale field test for verifying foam effectiveness on vapor dispersion control. Through the small-scale test, foam breaking rates and foam variations on an LNG pool were identified, whereas the medium-scale tests determined mass evaporation rates of LNG, temperature profiles of foam and LNG vapor, and vapor concentration profiles.

2.2.1 Apparatus

To apply expansion foam, two types of air foam generators (Angus Fire) were used as seen in Fig. 12. For the medium-scale tests, two large foam generators as seen in Fig. 12(a) were employed and a smaller foam generator as seen in Fig. 12(b) was used for the small-scale test. The foam generators were designed to mitigate LNG hazards and were mounted around the pit area. Through these foam generators, expansion foam was produced by blowing air across a metal mesh screen with foam solution, which is the solution of water and foam concentrates. The foam concentrate is composed of several components, such as surface active agents, ethyl alcohol, lauryl alcohol, glycol, and inorganic salts. The foam solution was sprayed on the metal mesh net to produce a uniform size of bubbles.

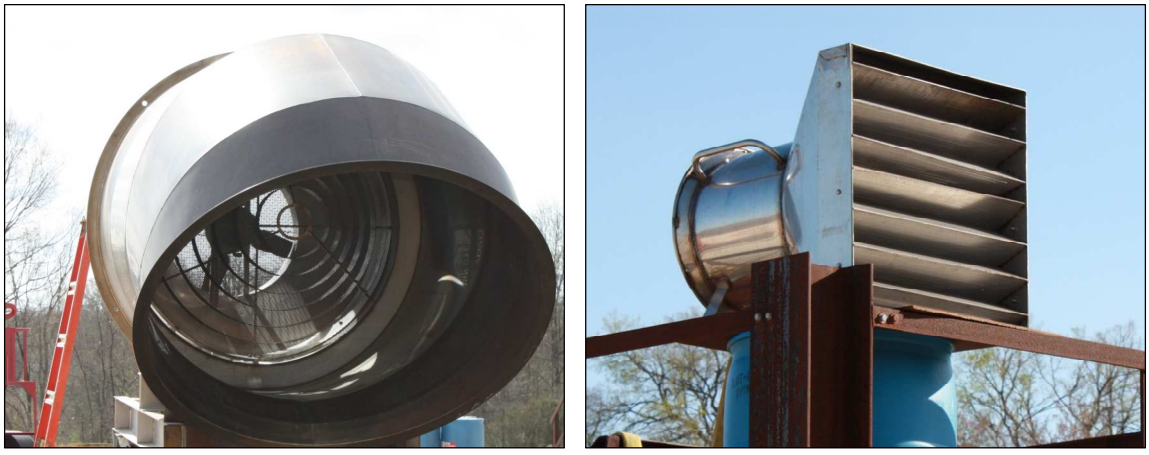

(a) For medium-scale test **(b) For small-scale test**

Fig. 12. Foam generators

Chromega/Alomega thermocouples (type K, Omega Engineering Inc.) with a wire diameter of 6.4 mm and a length of 10.67 m and 6.10 m were used to measure liquid LNG and vapor temperatures. Each thermocouple was linked to data acquisition system and computer. The software program was configured to simultaneously record the input data every second from the thermocouples at a continuous sampling rate for each thermocouple, with an accuracy of ± 2.2 ^{o}C. To ensure all thermocouples are working properly in the cryogenic temperature of LNG, they were custom-designed with some protection features. The thermocouple bead was made of Inconel collar, filled with ceramic and the junction of lead wires was insulated with ceramic fiber to prevent moisture accumulation.

To measure methane concentration, two types of infrared gas detectors (Honeywell Analytics, Inc.) were used: point gas detector and handheld gas detector. “Searchpoint Optima Plus” point gas detector uses the dual wavelength infrared

absorption technique to detect methane gas concentration in full range. It is designed to protect against dust and water ingress and is supplied with weather protection assemblies to operate in severe conditions. For ease of use and convenience, infrared type portable gas detectors were also employed. During the tests, these handheld gas detectors were mounted at designated locations to monitor and record methane concentration continuously into an XD memory card. It also provides audible and visual alarms to alert the user when high concentrations of methane are detected.

2.2.2 Small-scale field test setup

The small-scale field test was designed to spill an LNG onto a confined concrete-lined wooden box. In this test, a 0.91 m × 0.91 m × 0.61 m wooden box (lined with concrete boards) was constructed for LNG containment and a 0.91 m × 0.91 m × 1.83 m transparent box made of Pirex glass was built for containing foam as seen in Fig. 13. Six thermocouples in 8.89 cm interval up to 53.34 cm (0.53 m) were mounted on the wooden box at different elevations to observe the changes in LNG level. A measuring tape was applied on each side of the transparent box to record the changes of foam level during the experiments.

Before mounting the transparent box on the wooden box, LNG was released into the wooden box through a 10.16 cm diameter pipeline wherein the thermocouples started to record the temperature changes. As soon as the LNG level reached 0.53 meter level, the transparent box was mounted on the wooden box, and then followed by the application of expansion foam by a foam generator to the top of the transparent box. The changes of foam level were measured and still photos were taken.

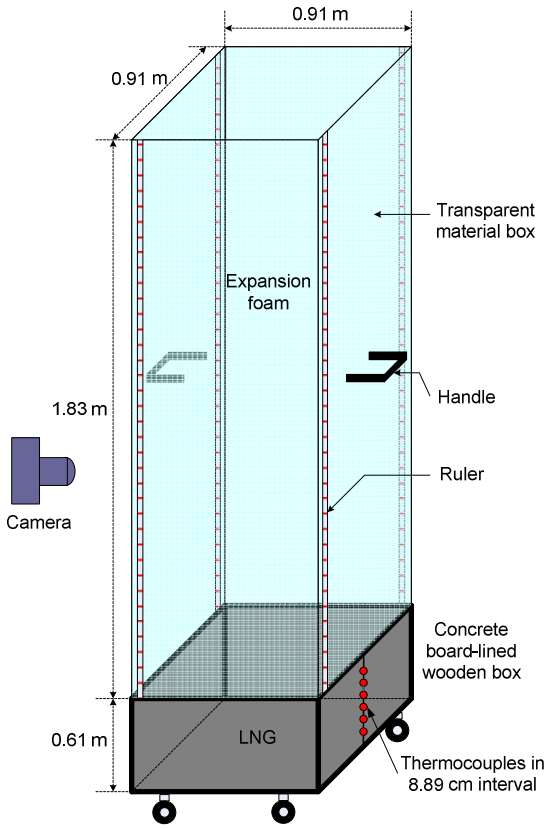

Fig. 13. Setup for small-scale field test

2.2.3 Medium-scale field test setup

A medium-scale test was performed in the large LNG training pit (6.40 m × 10.06 m × 1.22 m) at BFTF. As shown in Fig. 14, more than one hundred thermocouples were mounted vertically on steel frames inside the pit to measure the temperatures of LNG vapor and expansion foam. Several thermocouples were also installed at a 1.27 cm elevation up to 20.32 cm to determine the changes of LNG level. Additionally, three thermocouples were installed on one side of the concrete wall to measure the foam temperature near the concrete wall.

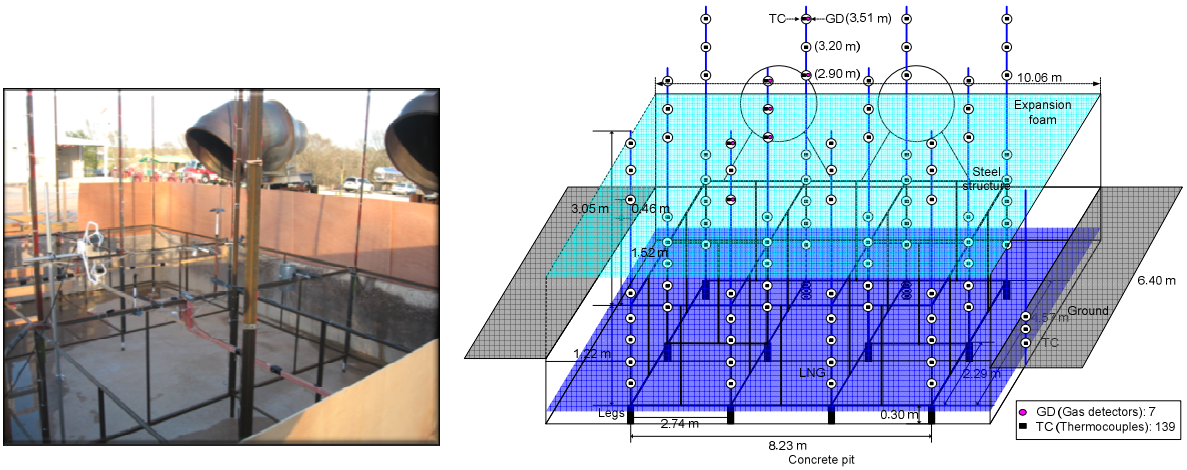

(a) Real landscape (b) Schematic diagram

Fig. 14. Setup for medium-scale field test in March 2009

In the March test, in order to measure the LNG vapor concentration, seven infrared point gas detectors were placed above the pit to measure concentration profiles. As seen in Fig. 15, two or three gas detectors were mounted on steel frames, with upper positions depicted on the drawing being the higher elevation (e.g., GD 22 is higher than GD 21. The height is seen in Fig. 14 (b)). Fig. 16 presents gas detector setup for the December test. Five infrared point gas detectors were placed above the foam level in the pit. In the downwind direction, twelve handheld gas detectors (i.e., six full range and six LFL range gas detectors using infrared sensors) and two infrared gas detectors were installed downwind.

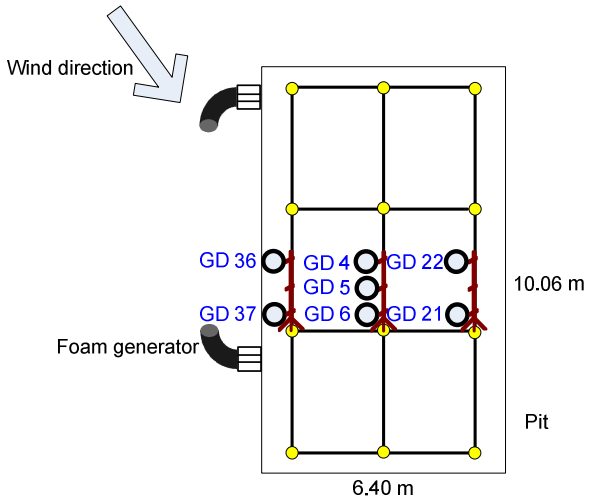

Fig. 15. Setup for gas detectors in March 2009

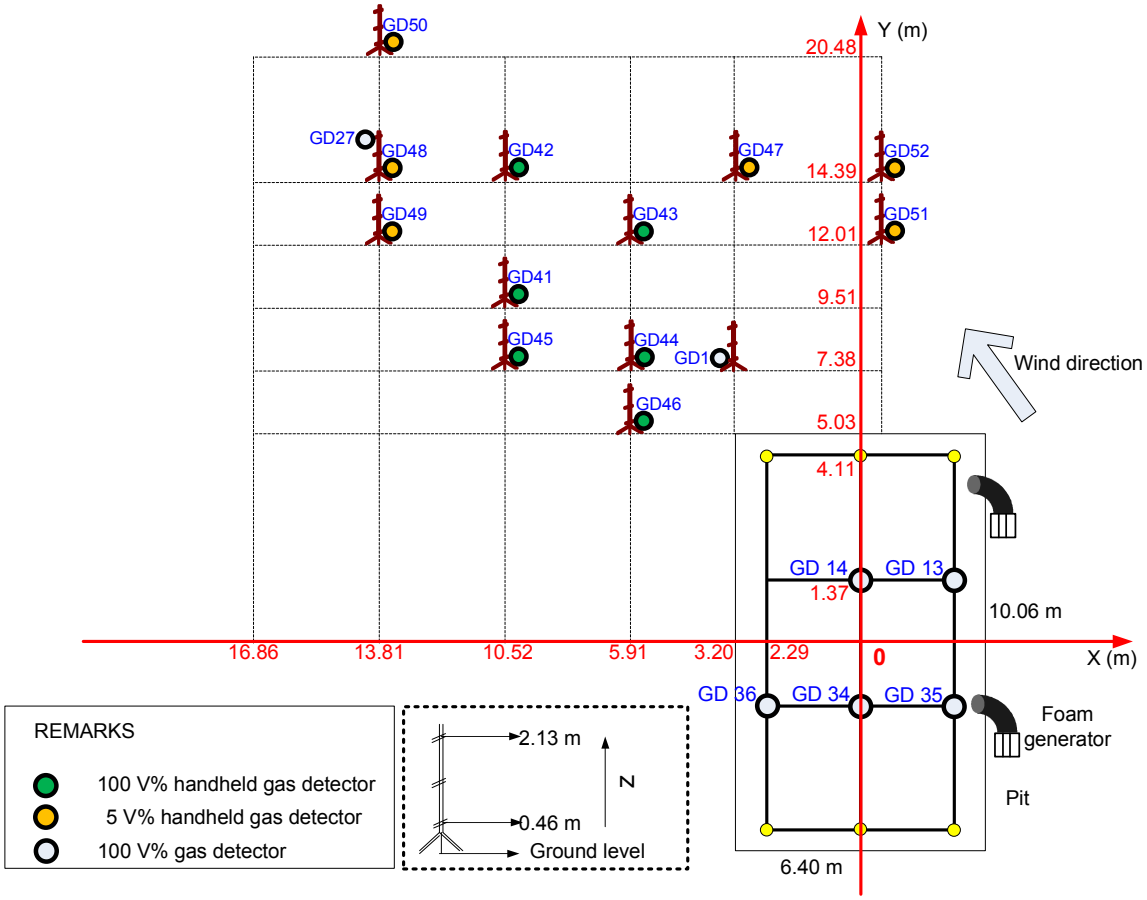

Fig. 16. Setup for gas detectors in December 2009

Fig. 17 shows the schematic drawings of the experimental procedure for a medium-scale test. LNG was released initially into a large pit with a 1.22 m vapor fence of wooden wall through a 0.10 meter stainless steel pipeline up to 0.20 meter depth. Subsequently, high expansion foam (expansion ratio of 500:1) was applied by two foam generators that were installed at a 1.22 m elevation near the pit and filled the pit up to 2.44 m depth. Temperature and concentration data were collected from the beginning of the LNG being released into a pit.

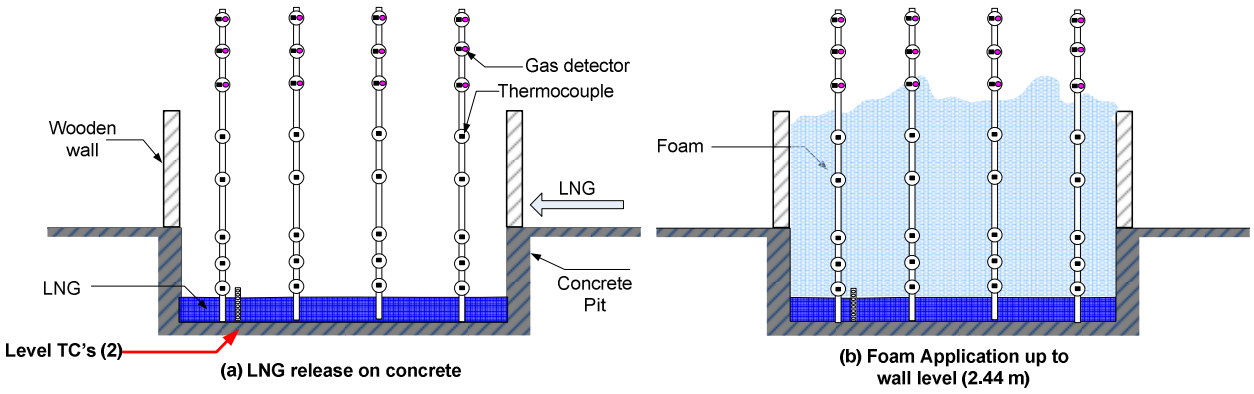

Fig. 17. Schematic of experimental procedure for medium-scale test

2.2.4 Summary of experimental facts

The field experiment test was conducted on March and December 2009. The atmospheric and foam conditions during the field tests for vapor dispersion control are summarized in Table 1.

Table 1 Summary of experimental facts for 2009 vapor dispersion tests

Conditions	Variables	March 2009	December 2009	Note
Atmospheric conditions	Temperature	24.37 ± 0.98 °C	13.24 ± 0.51 °C	
	Wind speed	3.70 ± 0.99 m/s	1.51 ± 0.58 m/s	Maximum wind speed (March test: 11.20 m/s, December test: 3.10 m/s)
	Wind direction	S and SSE&W	N and ENE	
	Relative humidity	45.02 ± 4.50 %	46.89 ± 3.12 %	
	Solar radiation	8.21 ± 13.75 W/m^2	223.71 ± 52.06 W/m^2	
LNG conditions	Methane composition (%)	99.85	99.87	Other components: nitrogen and ethane
Foam conditions	Expansion ratio	500:1	500:1	Classfied as "high expansion foam"
	Foam application rate	6.5 l/m^2·min	6.5 l/m^2·min	
	Foam concentrate	Jet-X	Jet-X	Components: HMIS surface active agents, ethyl alcohol, lauryl alcohol, glycol, inorganic salts

2.3 Results and discussion

2.3.1 Foam behavior during LNG spills

Fig. 18 shows the on-site test photos of the collapsed foam blanket on top of the LNG pool surface and formation of ice passages during the foam application. When the foam was initially applied to the LNG pool surface, foam started to collapse due to contact with LNG and other factors, such as wind and normal shrinkage. Consequently, some water content in the collapsed foam is released and reaches the LNG pool surface and warms the LNG vapor escaping from the pool surface. During this process, the water is cooled down forming ice tube passages along the LNG vapor pathways. This formation of ice passages is shown in Fig. 18. During the initial period of vaporization, it

was observed that the upper surface of foam layer was lifting, followed by the vaporized methane gushing out of the layer which is similar to the observation made by Takeno et al [3]. Additional observation showed that expansion foam was not broken uniformly across the LNG pool surface as shown in Fig. 18. The phenomena of uneven foam collapse and irregular formation of ice tube passages may imply that the mass evaporation rates across the LNG pool surface were not uniform due to the different heat transfer characteristics amongst LNG, foam, concrete walls and the atmosphere as well as foam spreading behavior. Because of the different rates of heat transfer over the LNG pool surface, it was not possible to identify the shape and reasoning for temperature contours of foam and its vertical temperature profiles. Thus, these unknown phenomena are addressed in medium-scale test results.

In order to provide guidelines on expansion foam system design, it is important to know how much foam will break down when it contacts with the LNG pool surface. Standard NFPA 11 §5.2.4.2 states “in determining actual solution flow requirements, consideration shall be given to potential foam losses from wind and other factors [5].” However, the standard does not give any details when considering the foam collapse on the pool surface. Therefore, this study attempts to obtain foam breaking rates by observing changes in foam and LNG levels. The foam level changes were measured visually by using a measuring tape attached on the four sides of the Pirex glass box, whereas the LNG level changes were identified automatically by measuring temperature changes from thermocouples in the wooden box.

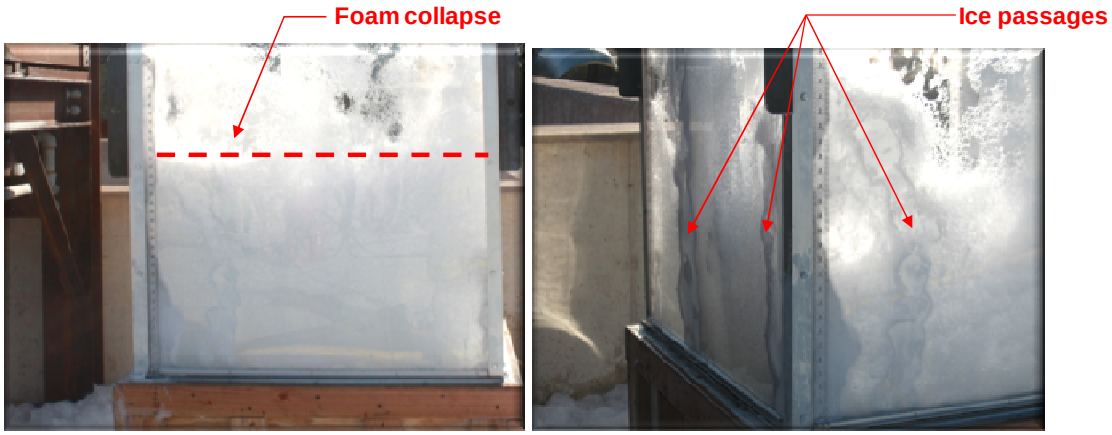

Fig. 18. Foam collapse on LNG pool surface and formation of ice passages in the foam layer

Fig. 19 shows the profiles of foam and LNG levels versus time. The foam level decreases rapidly in the first one minute interval followed by a continuous decrease over time, which is attributed to the collapse of foam blanket due to contact with the LNG pool surface and other factors. On the contrary, the LNG level decreases much slower. The graph of net foam level change is obtained by subtracting LNG levels from the foam levels. In order to subtract the LNG levels from the foam levels at the exact same time and provide an accurate estimation, a trendline from three LNG level data with 0.9825 R^2 value was used. This net foam level change has been converted into volume using dimensions of Pirex box for practical applications. Fig. 20 shows the foam breaking rate profile at around the 23 minute interval in which the foam filled the Pirex box. The foam collapsed relatively fast in the first five minutes followed by a slow decline. We believe that faster collapse rate was due to large conductive heat losses when contacting with

cold pool surface at the beginning of foam application. The collapse rate was stabilized as it reached the foam steady-state in the LNG and the atmosphere.

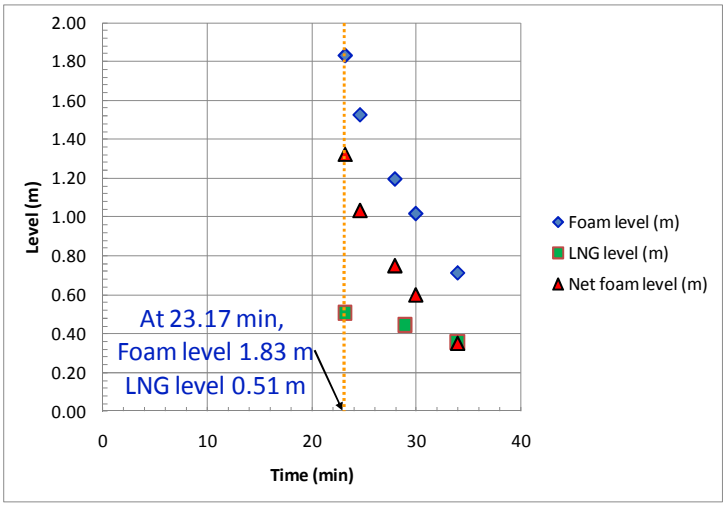

Fig. 19. Profiles of foam and LNG level versus time

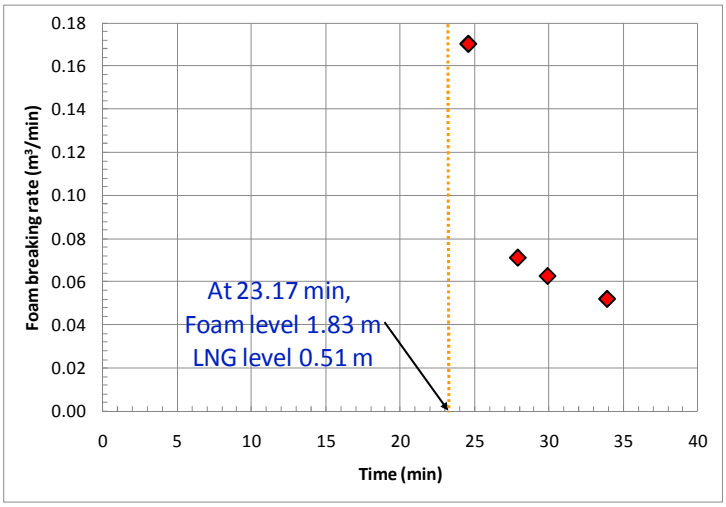

Fig. 20. Profile of foam breaking rate versus time

2.3.2 Mass evaporation rate

Mass evaporation rate of liquid is one of the important parameters to predict the size of LNG pool and the resulting vapor cloud. In this medium-scale experiment, the mass evaporation rate of LNG was determined from the temperature measurements using the thermocouples. The thermocouples were installed within LNG levels before and after the foam application and are capable of measuring the temperature ranging from -270 ^{o}C to 1372 ^{o}C. Fig. 21 shows the profile of mass evaporation rate of LNG before the foam application. The vaporization rate was estimated by using the mass balance with the following assumptions: (1) input is the LNG flow rate with a mean value of 2.566 kg/s (90 gpm), (2) accumulation is the formation of an LNG pool on the concrete floor over time, and (3) output is equal to the evaporation rate. Numbers on Fig. 21 (1.27 cm, 3.81 cm, etc.) depict the heights of thermocouple measured from the bottom of the pit. Fig. 21 implies that LNG vaporized quickly upon release due to a large conductive heat input from the concrete floor and the convective heat input from the atmosphere. After 1,720 sec, the vaporization rate gradually became slower and finally reached equilibrium. It is important to note that Fig. 21 does not include the mass evaporation rate after the foam application; the time needed for thermocouples at higher elevation to sense any temperature difference was not sufficient during the March experiment. This may be an indication that the expansion foam insulated LNG pool surface and subdued vaporization after the foam application, thus requiring a much longer time to sense any temperature difference. It was therefore addressed in the vaporization analysis of December test.

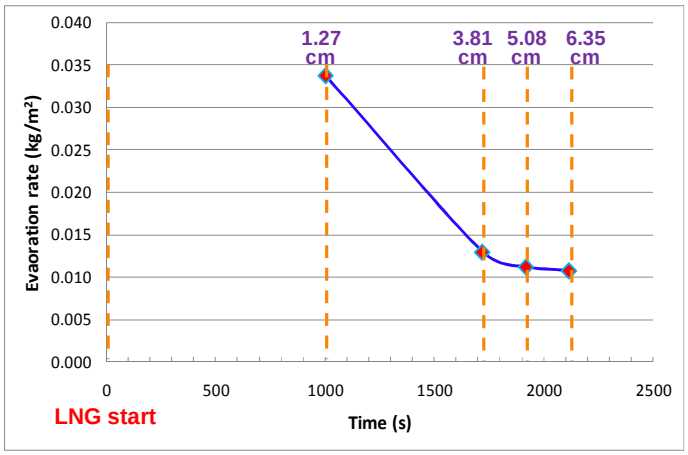

Fig. 21. Mass evaporation rate of LNG before foam application

For boiling liquids, mass evaporation rate can be estimated by using the following equations given by TNO and Briscoe et al. [23, 24]. This equation is one of the simple models, which have several assumptions as follows; (1) instantaneous release, and (2) neglecting the effects of spreading. The LNG evaporation rate was computed with this equation and compared with experimental data to identify and fill the gaps.

$$q_v(t) = \frac{H_c(t)}{L_v(T_b)} \times A \tag{4}$$

$$H_c(t) = \frac{k \times (T_{g,0} - T_b)}{\sqrt{a_s \times \pi \times t}} \tag{5}$$

$q_v(t)$: Mass evaporation rate (kg/s)

$H_c(t)$: Heat flux by conduction (J/m^2s)

$L_v(T_b)$: Heat of vaporization at T_b (J/kg)

A: Liquid pool area (m^2)

k: Thermal conductivity of concrete (J/(m·s·K))

$T_{g,0}$: Initial concrete temperature (K)

T_b: Boiling point of liquid (K)

a_s: Thermal diffusivity of concrete (m^2/s)

t: Time from the start of the release (s)

To calculate vaporization rate of LNG, Table 2 presents summarized properties of LNG and concrete. Several values were adopted from publications by TNO and Briscoe et al. [23, 24]. Here Fig. 22 depicts mass evaporation rates obtained by experimental measurement (blue curve which is identical to the graph shown in Fig. 21) and theoretical calculation (red curve). It is clearly shown that calculated vaporization rate is smaller than measured evaporation rate. This may be explained with following several reasons regarding calculation results using equation (4) and (5): (1) the equations do not take into account the heat transfers from concrete walls to LNG, but only include one-dimensional heat conduction from concrete ground of the pit to LNG and (2) atmospheric convective heat input and solar radiation are neglected, even though these factors are able to impact the LNG vaporization. Another uncertainty may arise from experimental measurement due to the fluctuation of temperature readings of thermocouples. It is therefore recommended that alternative experimental measurements for LNG level changes (for example, use of differential pressure meters) be used together with thermocouples.

Table 2 Properties of concrete and LNG

Materials	Properties	Values	Units
Concrete	Density	2300	kg/m^3
	Specific heat	961.4	J/kgK
	Thermal conductivity (k)	0.92	W/mK
	Thermal diffusivity (a_s)	4.16E-07	m^2/s
	$T_{g,0}$ (initial concrete temperature)	296.55	K
LNG	Latent heat of LNG (L)	5.02E+05	J/kg
	T_b (boiling temperature of LNG)	110.95	K

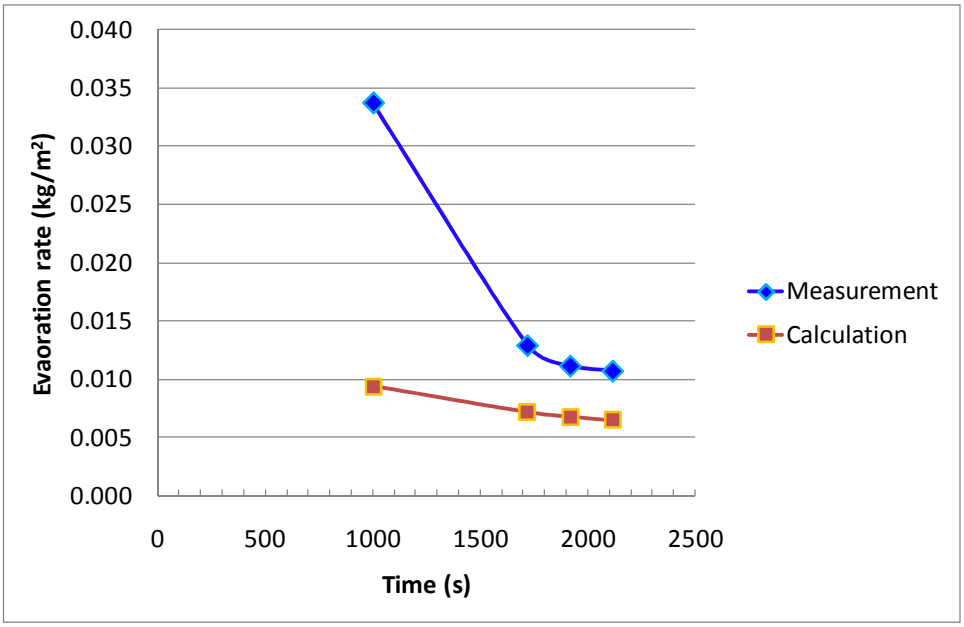

Fig. 22. The comparison of vaporization rate between experimental measurement and theoretical calculation

It can be inferred from Fig. 21 that the mass evaporation rate of LNG depends greatly on heat flow to the concrete pit. Herein we illustrate the different modes of heat transfer in a concrete pit as depicted in a schematic diagram in Fig. 23. The dominant heat source for vaporization comes from the ground. Initially, the heat flux into the pool is controlled by the rate of heat conduction from the ground. In the later stage, the heat convection from atmosphere and solar radiation are also significant contributors to the total heat input [24, 25]. In the case of LNG spills into impounding dike (or inside a pit), the convective heat input may decrease over time. This is attributed to the reduced ambient temperature inside the pit due to insufficient mixing with fresh air.

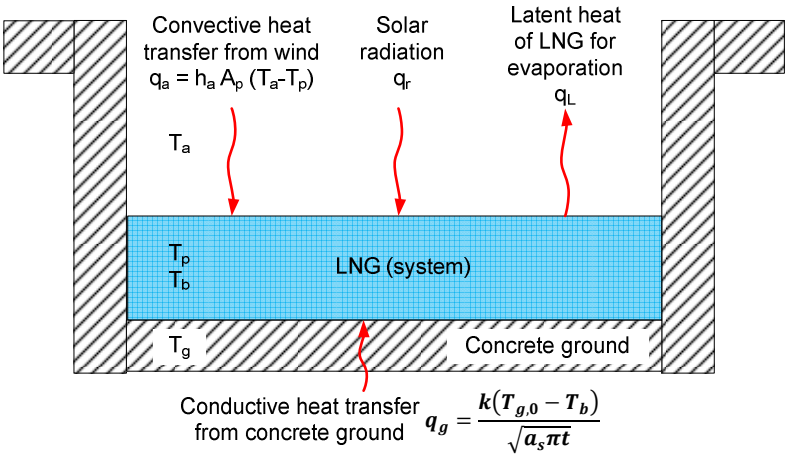

Fig. 23. Heat transfer of LNG in a concrete pit

There is no doubt that expansion foam can impact mass evaporation rate of LNG to some extent. It is therefore necessary to identify that how much foam can increase or decrease LNG vaporization. Herein, we attempt to measure LNG level changes with

thermocouples in 0.64 cm (1/4 inch) interval up to 20.32 cm (8 inches) after foam application during the December tests as shown in Fig. 24. Fig. 25 shows that thermocouples installed for LNG level measurement generated sharp temperature increases when foam was applied on LNG. The foam application made significant temperature increases up to 5.08 cm (2 inch) depth from the surface of LNG since the foam affected temperature readings of eight thermocouples. This phenomenon resulted in initial significant increase of mass evaporation rate after foam discharge, thus causing subsequent increase of methane concentration on top of expansion foam in the pit (see section 2.3.6). The affected LNG depth, 5.08 cm, may be used when theoretical models of vaporization rate with foam application are developed. In Fig. 25, a green curve at the bottom represents water pressure of a foam generator and its four peaks up to 5 bar in gauge pressure (note secondary vertical axis) imply the action of foam discharge. In order to retain 1.22 m thickness of foam throughout the test period, the foam generator had to be turned on four times intermittently.

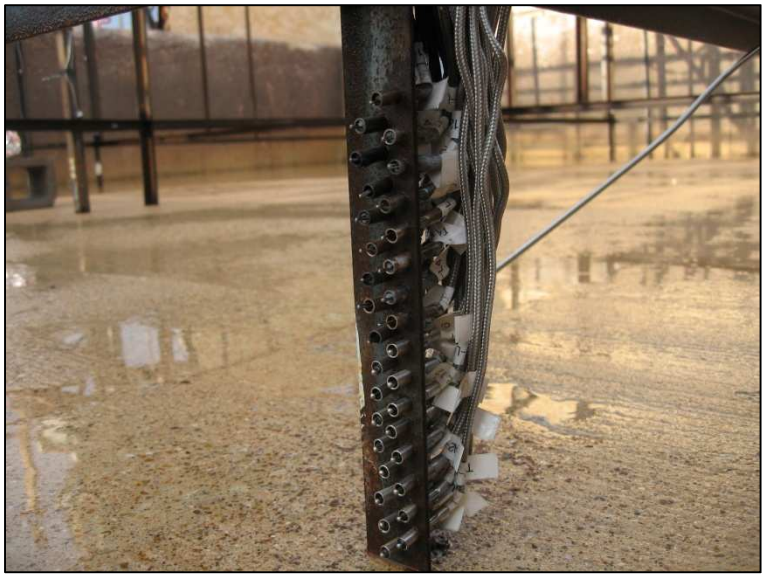

Fig. 24. Installation of thermocouples for LNG level measurement

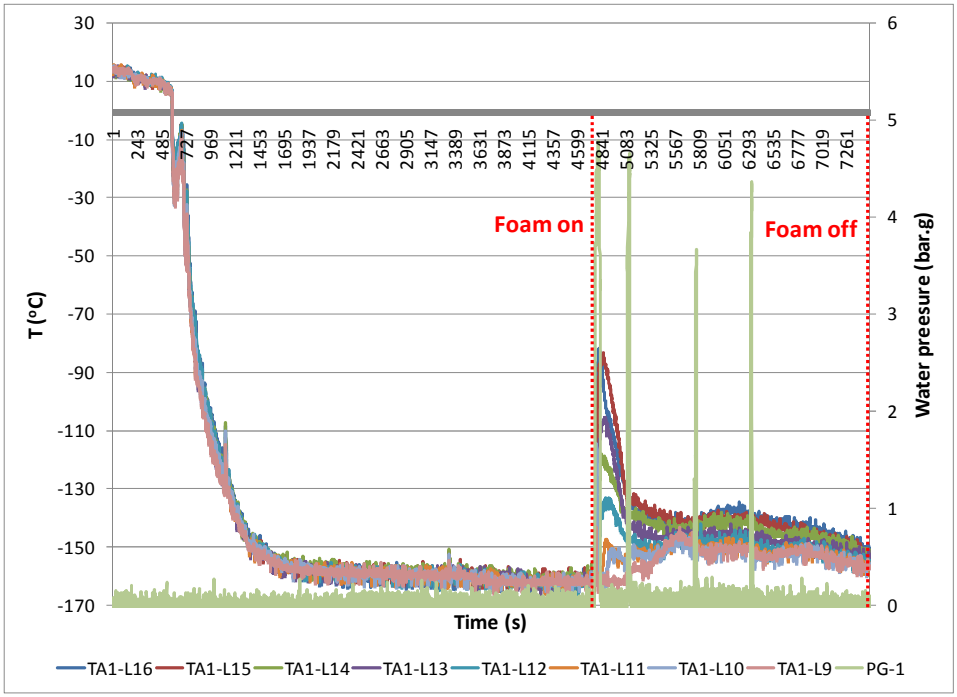

Fig. 25. Influence of foam on LNG temperature

Therefore, for the accurate level measurement of LNG after foam application, the thermocouples installed below this depth (e.g., from 10.16 cm (TA1-L1) to 15.24 cm (TA1-L8) height of thermocouples) were used. Fig. 26 presents some of the temperature profiles of LNG after foam discharge. Each curve shows an actual measurement in color curve and also a trendline of 10 seconds moving average in black curve. As seen in Fig. 26, each curve shows the time of temperature increase from the LNG boiling point (-162 ^{o}C) which implies vaporization of LNG. The time differences of thermocouples were examined such as Δt_1 and Δt_2. From the known density of LNG (450 kg/m^3 [19, 26]) and dimensions of the pit, mass evaporation rates were calculated by dividing these time intervals. These measurements, however; may have some degree of uncertainty due to the fluctuation of temperature readings. Despite this weakness, the vaporization measurements can still provide good experimental results. With this process, mass evaporation rates after foam were obtained as shown in Fig. 27. After foam application, vaporization was initially high due to larger heat transfer with fresh foam layers and then decreased to reach steady state. This trend can be related to the influence of foam on LNG temperature (see Fig. 25) and methane concentration profile inside the pit (see Fig. 33). Based on findings from concentration profile (see section 2.3.6), it was stated that the LNG pool can reach a steady state with surrounding environments at around 9 minutes. It is shown in Fig. 27 that the statement made a good agreement since the vaporization decreased to be stable after 9 minutes as 0.009±0.002 kg/m^{2}s. Caution must be taken, however; to the fact that the occurrences of intermittent reapplication of foam

to keep 1.22 m thick foam may affect the vaporization slightly even after reaching stable control status.

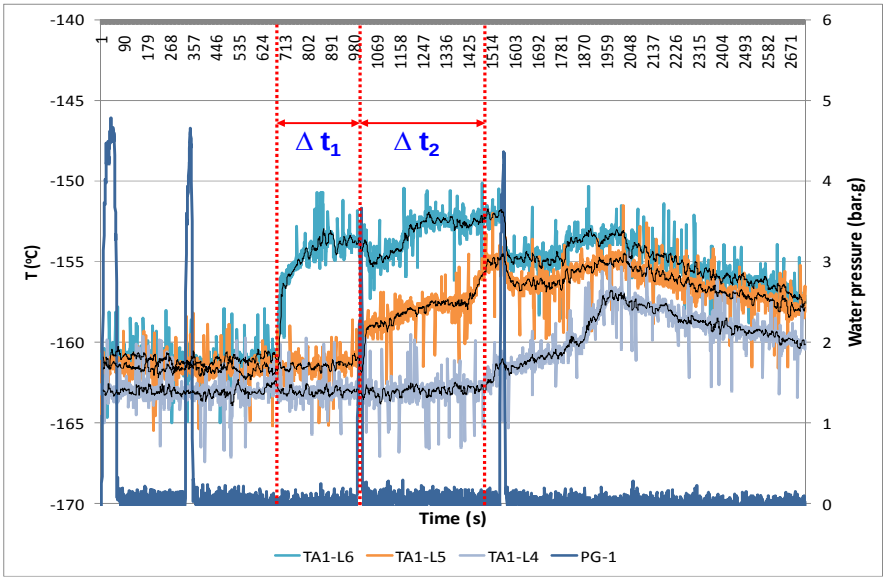

Fig. 26. Level measurement of LNG

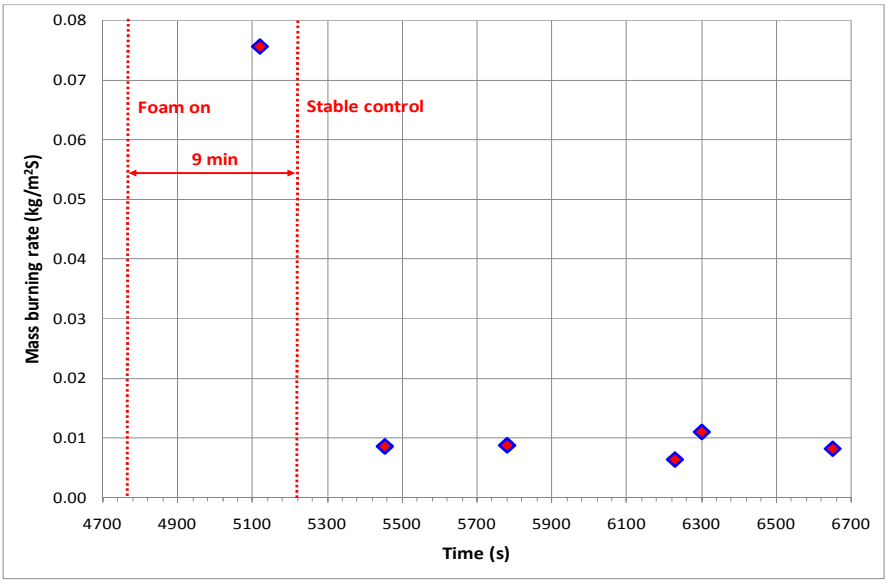

Fig. 27. Mass evaporation rate after foam application

2.3.3 Minimum effective foam depth

Currently there are no publications regarding the effective foam depth in the literature, here we attempt to achieve this objective from the medium-scale field test by pinpointing the changes in the foam level and the temperature readings from the thermocouples. Fig. 28 shows the temperature profiles of expansion foam and LNG vapor taken by thermocouples at different elevations above the liquid level. As shown in top and front views of the pit, six thermocouples (TA1-1 through TA1-6) were placed at the foam level.

Typically, when LNG is released onto ground, LNG is vaporized quickly and the LNG vapor is mixed with adjacent air and then diluted to lower methane concentration. Additionally, the temperature of LNG vapor gradually increases with convective or wind currents so that the specific gravity of methane-air mixtures becomes less than 1. As seen in Fig. 28, when LNG was released into a pit, there was an initial decrease in temperature of LNG vapor in the pit due to larger LNG vaporization, followed by a rise in temperature at approximately 1,716 seconds and become gradually stabilized. The fluctuations shown in Fig. 28 before the foam application were due to wind gustiness and turbulence close to the spill area. The temperature variations of LNG vapor before the foam application form a “v-shaped pattern”. When expansion foam was applied, the thermocouples started to measure the temperature of foam, not LNG vapor, because the thermocouples were covered by aggregated foam bubbles. The thermocouples initially read out the fresh foam temperatures, thus resulting in initial temperature increases. After that, the foam temperature gradually decreased because foam continuously lost its

heat to the newly vaporized LNG vapor. After some period of time, the decrease of foam temperature became steadier. This implies that initial foam application provides sufficient heat to warm up the LNG vapor, but the effectiveness becomes less over time. As shown in Fig. 28, all temperature profiles at different elevations are above -114 ^{o}C after the foam application, at which pure methane vapor is assumed to be positively buoyant as its specific gravity is less than 1.0 at -114 ^{o}C. This implies that even a 0.26 m (0.46 m foam level minus 0.20 m of liquid level) foam depth can provide heat to warm up the LNG vapor and become more buoyant.

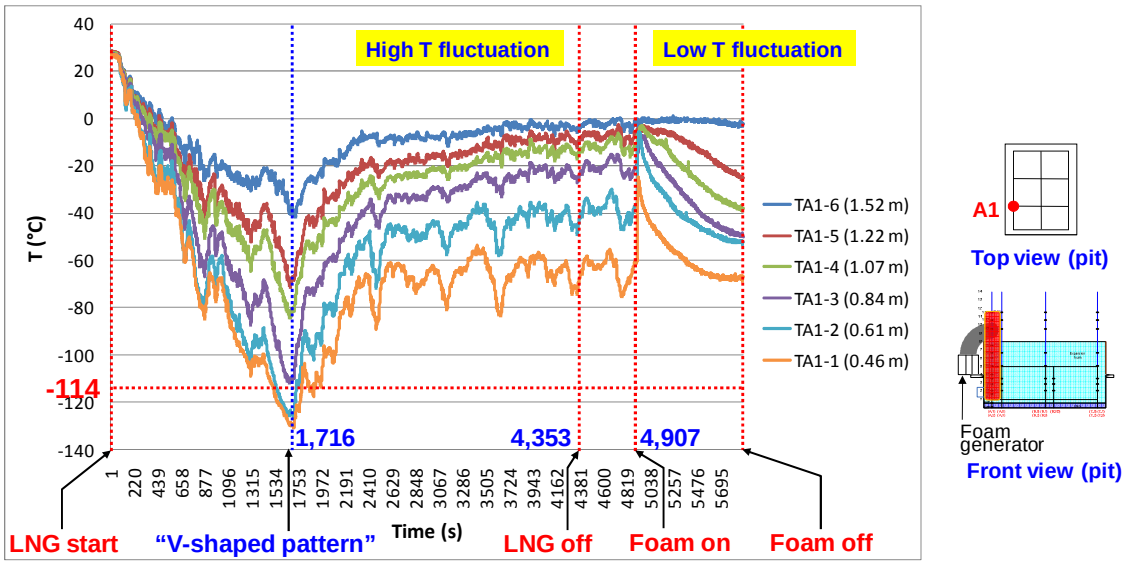

Fig. 28. Temperature profile of foam and LNG vapor

However, in determining the effective foam depth, it is important to note that this minimum foam depth (0.26 m) may not be sufficient to promote positive buoyancy of LNG vapor. Due to the variation of foam blanket on the pool surface, effective foam

depth should be given as a range. Moreover, the foam temperatures in other locations may be different than the one shown in Fig. 28. For instance, other thermocouples at different locations such as TW-2 (at 0.61 m elevation) gave temperature readings below -114 ^{o}C (Fig. 29), whereas most thermocouples installed at 0.84 m elevation showed temperature readings above -114 ^{o}C (Fig. 30). Using the 0.84 m elevation as a baseline for the minimum effective foam depth, it can be concluded that the thickness of expansion foam should be at least 0.64 m (0.84 m foam level minus 0.20 m of liquid level) for vapor dispersion control. Even though this conclusion can provide minimum guideline for effective foam depth, uncertainty may arise from using only the "pure methane vapor neutral buoyancy temperature (-114 ^{o}C)" as the metric in determining effective foam depth to infer the buoyancy of mixed LNG vapor and air. In some aspects, however; the adopted method in this research may have a rationale since the foam layer contains significantly smaller amount of air than open atmosphere. In addition, expansion foam plays a role as a medium to present heat to cold LNG vapor. Thus, if the foam has higher temperature than -114 ^{o}C, then it can be considered that foam contains some extent of potential of heat supply to LNG vapor. However, to obtain more accurate conclusion of effective foam depth, a heat transfer analysis of the interaction of vapor and foam should be associated with this conclusion.

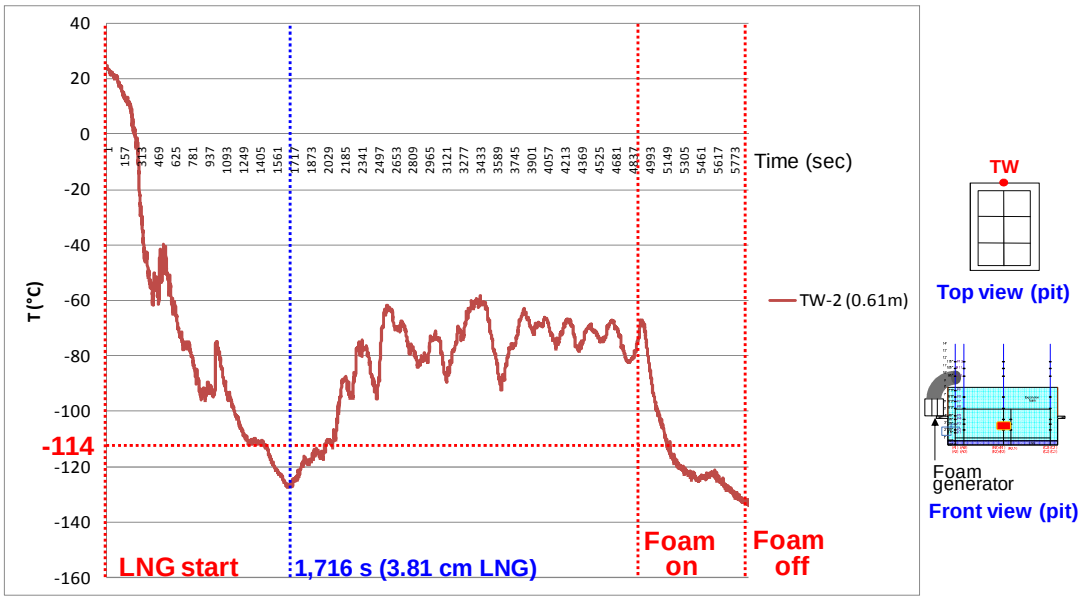

Fig. 29. Temperature profile of expansion foam at 0.61 m elevation near the concrete wall

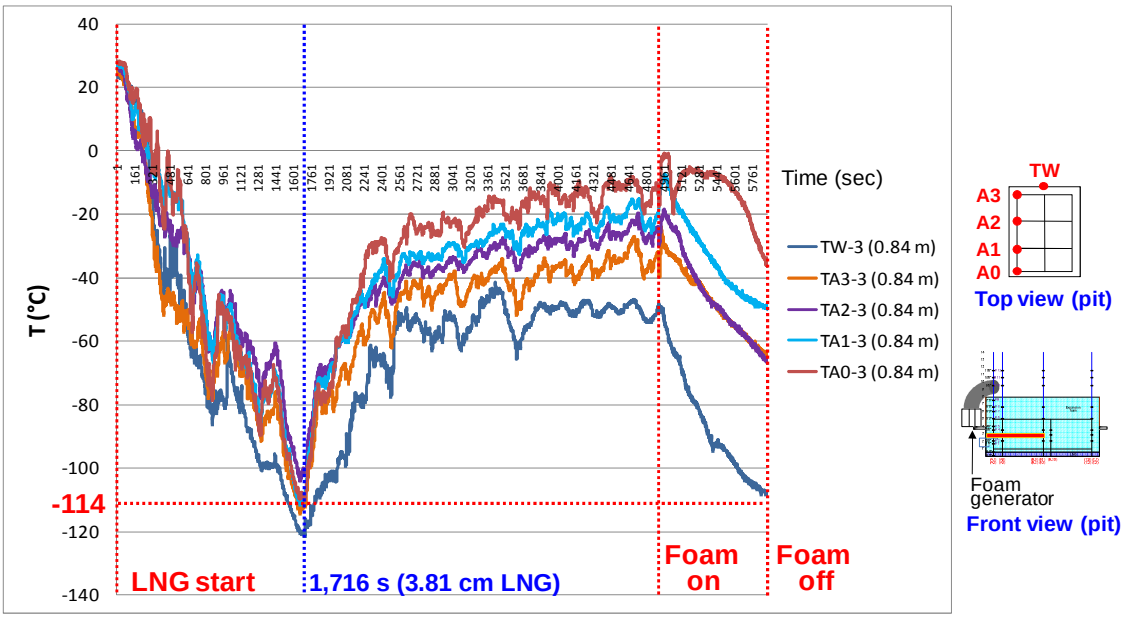

Fig. 30. Temperature profile of expansion foam at 0.84 m elevation

As stated above, the temperature profiles of LNG vapor form a v-shaped pattern prior to the foam application. Here, a discussion was made from a schematic diagram of the different modes of heat transfer in a pit provided in Fig. 23 to explain this phenomenon. LNG pool may have different types of heat transfer, for example conductive heat transfer from concrete ground, convective heat transfer from wind, and solar radiation. According to Briscoe et al. [24], the vaporization of cryogenic liquids on land is predominantly controlled by the rate of conductive heat through the ground. Initially, the heat flux into the pool is controlled by the rate of heat conduction from the ground. In the later stage, the heat convection from atmosphere and solar radiation begin to contribute to the total heat input [24, 25]. In the case of LNG spills into impounding dikes (or inside a pit), the convective heat input may decrease over time. This is attributed to the reduced ambient temperature inside the pit caused by insufficient mixing with fresh air.

If it is assumed that LNG vaporization is primarily dominated by the conductive heat input from the ground and contribution of the heat convection and solar radiation are assumed to be negligibly small, then mass evaporation rate can be derived with heat flux by conduction from concrete ground and heat of vaporization of LNG at T_b from equation of change for temperature as shown in equation (4) and (5) [23-25]. As seen in equation (5), the mass evaporation rate is a function of temperature difference between initial concrete ground temperature and boiling point of LNG. When LNG releases into a pit, initial temperature difference is relatively large, thus resulting in higher evaporation of LNG. The resulting nucleate boiling phenomenon creates a rapid temperature

decrease in the mixture of LNG and air in the pit as seen in Fig. 28. After some period of time, the temperature driving force decreases due to the heat loss of concrete to LNG and becomes stabilized because of reaching steady state between LNG and concrete ground. In this transition period, the temperature of air-LNG vapor mixture reaches the lowest value at 1,716 seconds and continues to increase gradually due to lower vaporization and air mixing in the concrete pit. Thus the resulting temperature profiles resemble a “v-shaped pattern”.

2.3.4 Effects of foam application on vapor temperature

The benefit of using expansion foam is actually influenced by the fact that the LNG vapor can be made buoyant, so in turn, they are dispersed more upward instead of downward. To observe the temperature rise of LNG vapor, some thermocouples were installed above the foam level at different elevations. Fig. 31 depicts temperature profiles of the mixture of LNG vapor-air above the foam layer in a 20 second moving average. Prior to the foam application, all thermocouples gave low temperature readings due to the rapid heat transfer from the concrete floor and ambient air. At some period of time, the vaporization began to decrease and the vapor temperature began to stabilize. However, small temperature fluctuation is seen due to the movement of cold vapor in the pit by wind and other effects (e.g., configuration of pit and wooden walls). When the foam was first generated, water would often go through holes in the foam-forming screen without being converted to foam and discharged to the pool surface. This resulted in a rapid decrease in vapor temperature, followed by excessive vaporization. The vapor temperature readings indicate that immediately after the application of foam, the vapor

temperature decreases due to the release of excess cold vapor from the water droplets that come in contact with LNG, thereby, increasing the vapor concentration (this topic is discussed in more detail in section 2.3.6). It is apparent from Fig. 31 that the vapor temperature after foam discharge attains the initial, stabilized vapor temperature before foam application within about 200 seconds (3.3 minutes). As the foam accumulated on the pool surface, further temperature rise was dominated by the warm LNG vapor passing through the foam layer. After the foam application, further heat transfer was subdued due to the insulation effect from the foam. Based on this observation, we can conclude that foam application promotes its buoyancy, however it can also raise a potential safety issue due to the aggregate vapor production during the initial stage of foam application.

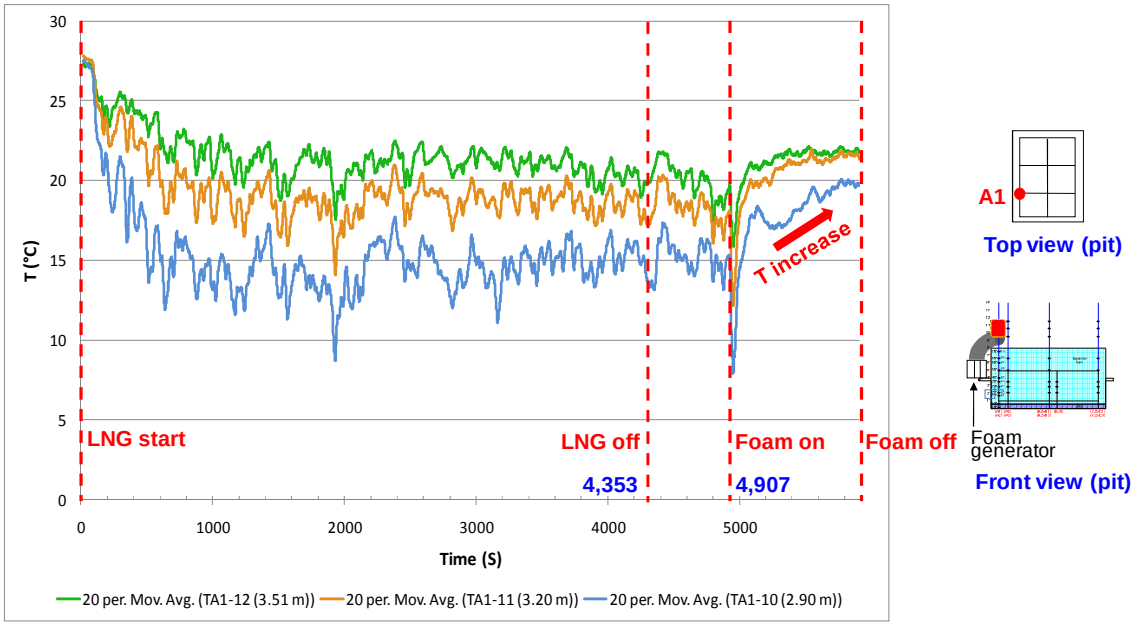

Fig. 31. Temperature increase of LNG vapor by expansion foam

2.3.5 Effects of LNG/foam spreading behavior on the temperature distribution in the pit

Results from experimental observation of temperature distribution in the pit before and after the foam application can provide a deeper understanding of LNG spreading, foam spreading, and effective foam depth. Here, we attempt to show the temperature contour of the pit area by plotting the mean temperature before and after the foam application. Fig. 32(a) and (c) are the temperature contours of LNG vapor at 0.84 m elevation (above the liquid level) before foam application and Fig. 32(d) and (f) are the temperature contours of expansion foam at the same elevation after the foam application. The darkest color denotes the lowest temperature while the brightest color represents the highest temperature. In order to consider temperature fluctuation of LNG vapors, the temperature values were averaged in 5 seconds.

The top right corner of Fig. 32(a) shows the location of LNG discharge into the concrete pit prior to foam application. The spreading of an LNG pool is influenced by several factors, such as the geometry and surface properties of the spill area and the release rate [2]. It was observed that the LNG pool initially spread down to the left side of the pit, where the pit was drained. While moving, the LNG exchanged heat up to its boiling point with the concrete floor and filled the pit up gradually to the right side with the boiling LNG. As the LNG spread on the concrete floor, a large amount of vaporization was generated. As seen in Fig. 32(a) and (b), this LNG spreading behavior results in temperature differences of the mixture of cold LNG vapor and air in different locations of the pit. It is interesting to note that, as seen in Fig. 32(c), although the LNG

covered the entire pit bottom about 20.32 cm thick, the LNG vapor-air mixture showed different temperatures (e.g. largest difference was 41.04 ^{o}C) in a different location. It may imply that vaporization of LNG differs over the LNG surface because of an uneven conductive heat transfer from concrete ground, which is caused by LNG spreading behavior in a different location (see Fig. 23). Additionally, these contours may also be affected by aerodynamic characteristics and turbulence resulting from the combination of LNG vaporization, wind effects, and surrounding geometry (i.e., pit, wooden walls, and foam generators). Fig. 32(d) and (f) show the resulting temperature contours after the foam application. Foam was applied by two foam generators located on the left side in a horizontal plane at 4,907 seconds as seen in Fig. 32(d). Fig. 32(e) depicts the foam temperature contours when foam was fully filled up to wooden walls (2.44 m height) in the pit. It can be observed in Fig. 32(f) that even after the foam reached a foam-control state (approximately 9 minutes after foam application, referring to section 2.3.6), the temperatures of expansion foam in different locations show large gaps (i.e., largest difference is 61.15 ^{o}C) even though the readings were taken at the same point. We believe that these temperature differences are normally affected by the characteristics of foam spreading, as well as LNG spreading. This discovery has important implications, as it provides understanding for siting foam generators and choosing the direction of foam spreading. Additionally, this finding should be used when determining minimum effective foam depth since foam layers in different locations may have different temperatures. Based on this finding, and the buoyancy perspective of LNG vapor in terms of its temperature, it is recommended that foam generators should be placed closer

to potential leak sources and directed in the same way as release motions. However, at this moment, it is not sufficient to explain the underlying mechanisms of these contours completely since it requires further investigations. Future work should focus on the effects of turbulence on vapor temperatures and its concentrations, and the influence of expansion foam on vaporization as seen by uneven foam collapse across LNG pool surface.

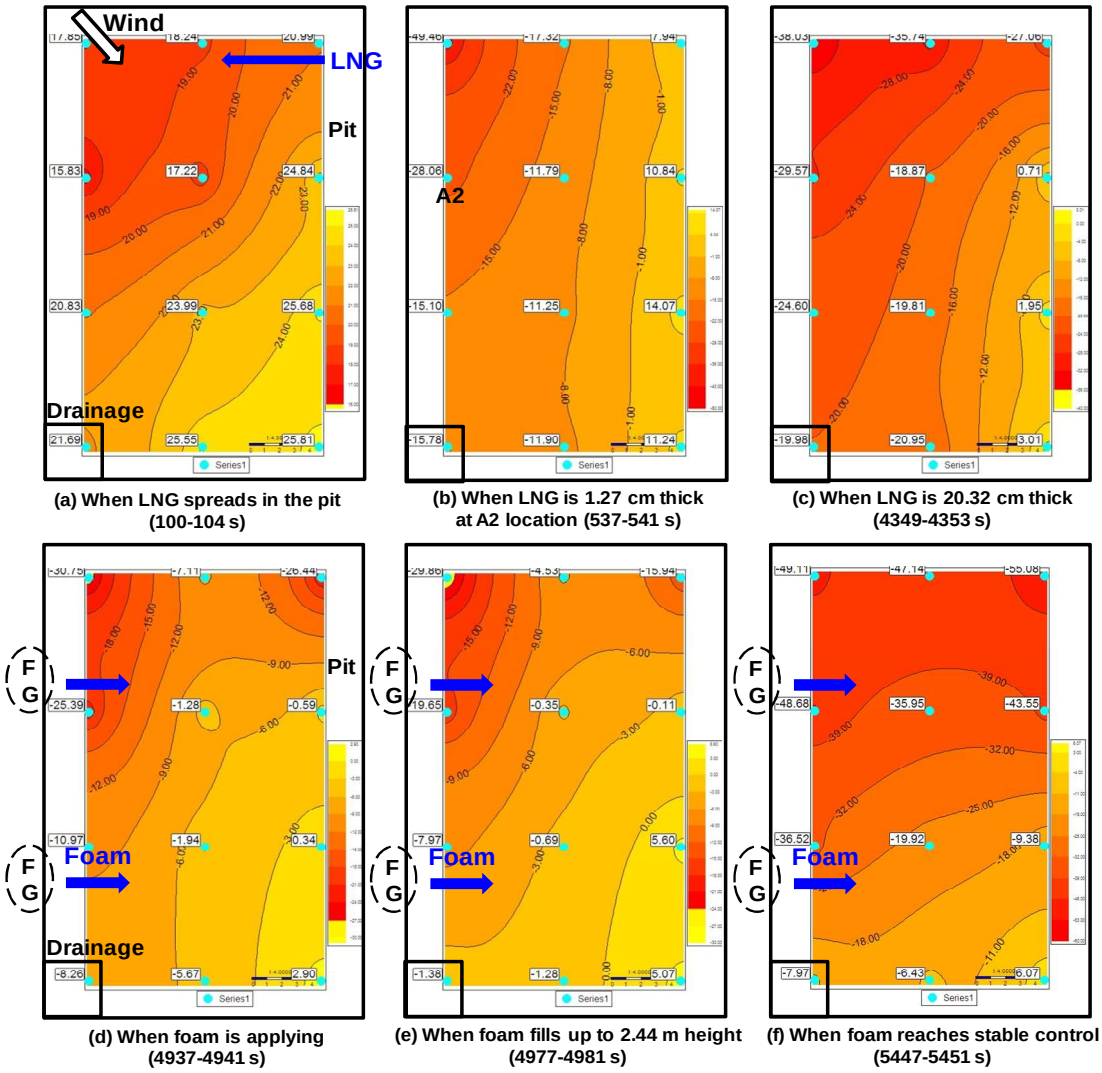

Fig. 32. Temperature contours of LNG vapor and foam inside a pit

2.3.6 Concentration profile

To be effective in controlling the vapor release from the spill area, expansion foam should demonstrate the reduction in gas concentration after the foam application. Fig. 33 shows the plots of methane concentration measured by two gas detectors above the foam layer in the pit. The concentration data were averaged in 100 seconds to present a clear trend of concentration. The locations of these detectors are seen in the top and front views of the pit. As shown in Fig. 33, GD 21 was installed at 0.46 m higher than the foam surface while GD 22 was installed at 1.07 m higher than foam. As seen in Fig. 33, the methane concentrations increased rapidly when expansion foam was first applied to the LNG pool. After the foam had filled up to 2.44 m depth in 70 seconds, it then reached a foam-control status with the LNG pool and surrounding environments at around 9 minutes. This phenomenon may be explained as follows: when foam was applied to the LNG pool, water in the foam accelerated the boil-off rate of LNG and after the initial phase, foam contained the vapor within the foam mass so a vapor-liquid equilibrium can be maintained, thus reducing the driving force towards vaporization. It becomes clear that expansion foam can reduce the methane concentration after the foam application by forming a barrier to prevent vaporization, but a caution should be taken to the initial negative effect on concentration.

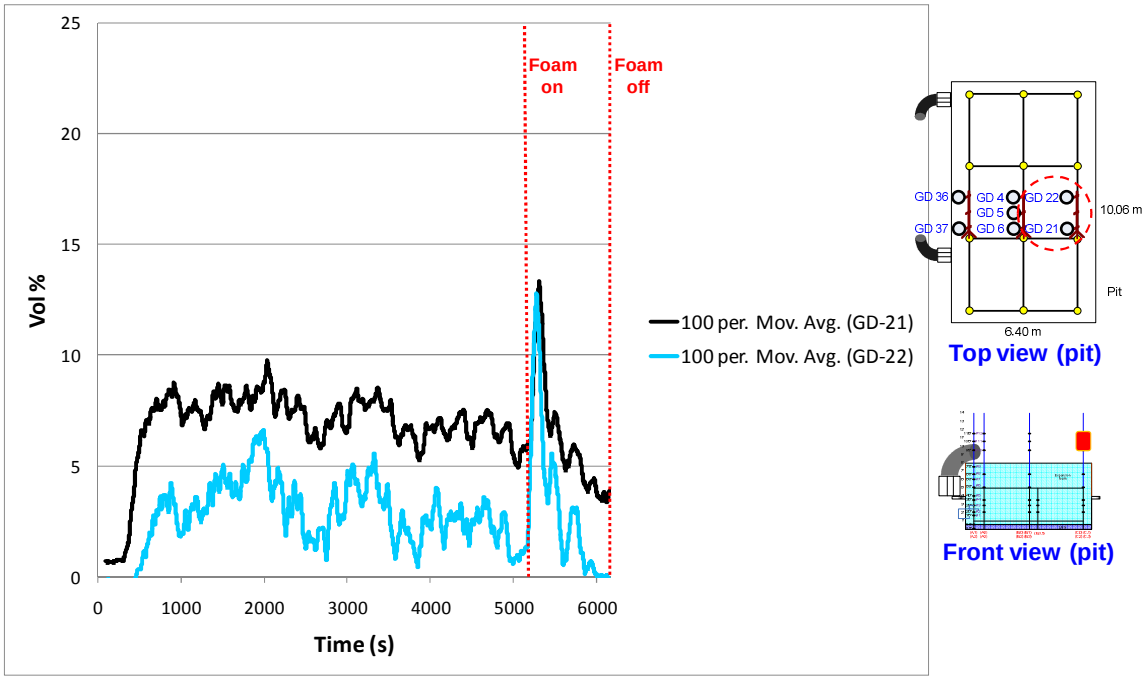

Fig. 33. Methane concentration profile inside the pit

Furthermore, the reduction of methane concentration was also observed in the downwind direction. Fig. 34 shows the graph of methane concentration measured at 3.59 m distance from the pit corner, using a 100 % v/v gas detector before and after the foam application. The measured methane concentration varied from 0.5% v/v to 7 % v/v. Other concentration measurements in different locations outside the pit are summarized in Appendix A. The fluctuation in concentration readings was due to the changes of prevailing wind direction and speed during the test period.

In addition to the buoyancy promotion effect and the blanketing effect by foam, the decrease in methane concentration downwind was also attributed to vapor fences surrounding the pit, which obstructed the flow path of the vapor in the downwind direction. From these results it can be summarized that expansion foam can reduce methane concentration, both above the pit (Fig. 33) and the downwind direction (Fig. 34).

It is reported in a literature that the methane concentration at higher elevation downwind becomes higher than the lower level concentration due to natural dilution and dispersion of LNG vapor [27]. Fig. 35 presents the methane concentration profiles in 0.46 m (a) and 2.13 m height (b) at 14.15 m downwind distance. In Fig. 35, both curves of (a) and (b) show almost identical profiles except the magnitude of concentration, thus providing the validity of measurements. It is clearly shown that regardless of expansion foam application, concentrations in 2.13 m height are larger than 0.46m height concentrations through-out the test period. This dispersion process implies that LNG vapor becomes more buoyant as the mixing process with air progresses. Ultimately, this process results in richer concentration in higher elevation.

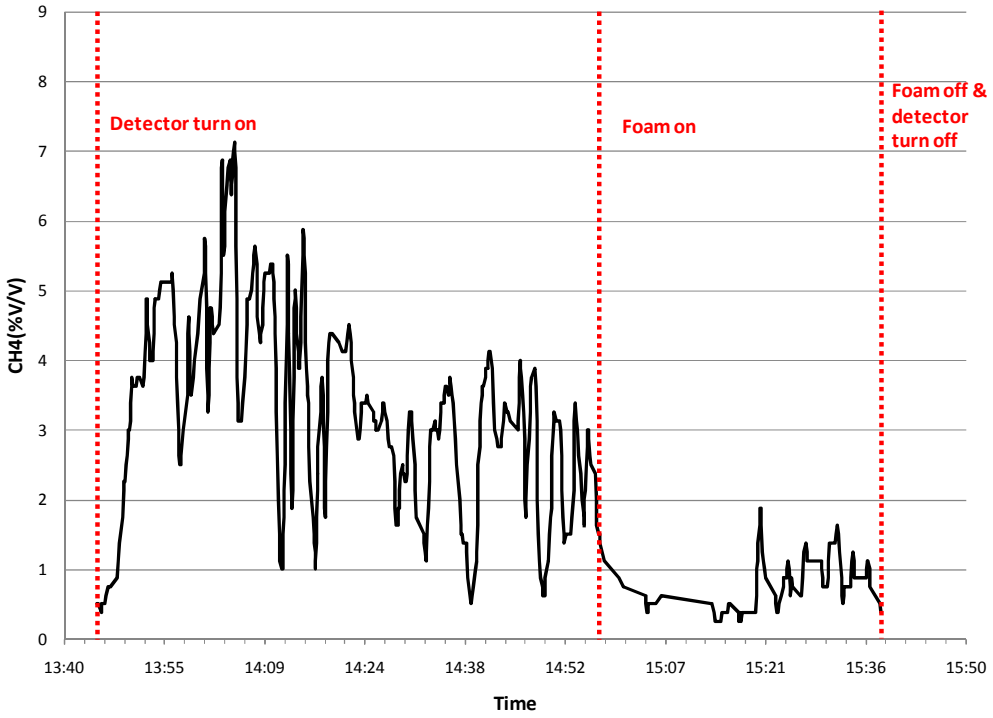

Fig. 34. Methane concentration profile at 3.59 m downwind distance (GD 44)

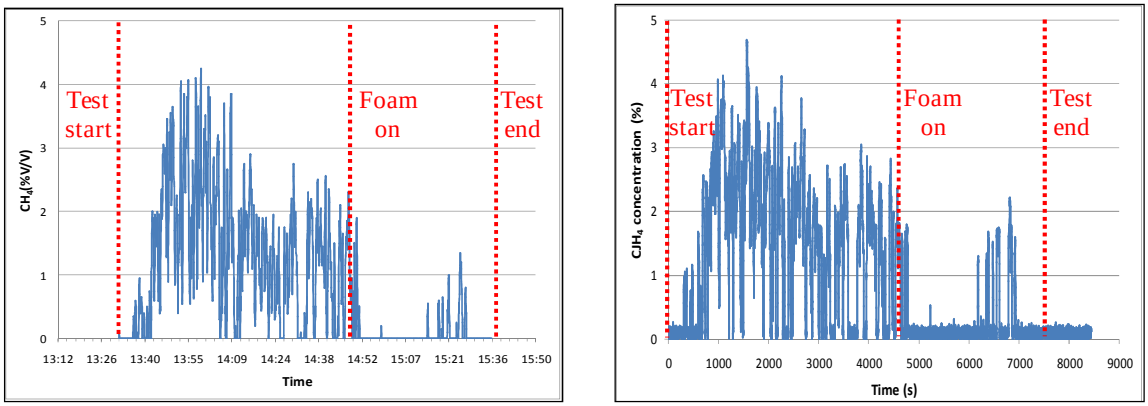

(a) GD 48 in 0.46 m height

(b) GD 27 in 2.13 m height

Fig. 35. Methane concentration at different elevations in downwind

In order to measure the vapor exclusion zone, methane concentration contours were developed on the basis of the aforementioned concentration observations. Fig. 36(a) represents the maximum methane concentration contours before the foam application at 2:03:54 pm (local time) and Fig. 36(b) presents maximum concentration at 1,208 seconds after foam discharge at 3:17:30 pm. The times at which maximum concentration were obtained after comparing all concentration profiles from gas detectors. As seen in Fig. 36(a) and (b), the red curve represents the contour of LFL (5 V% of methane) and yellow curve indicates ½ LFL distance (2.5 V% of methane). It is apparent that the LFL and ½ LFL distances were reduced significantly after the foam application. In summary, the expansion foam can reduce the LFL distance of methane in the downwind direction. In order to quantify the reduction of hazardous distances, we attempted to compare the distances before and after foam discharge as shown in Fig. 37. The LFL and ½ LFL distances were estimated using the coordinates of contours in diagonal direction, because the majority of gas detectors were placed in ENE (East North East) direction based on the weather forecast. However, the prevailing wind direction was shifted to the North during the test. Fig. 37 presents the reduction of LFL and ½ LFL distances, measured from the existing setup. Before foam application, LFL and ½ LFL distances were estimated 8.50 m and 16.41 m respectively while after foam discharge they were estimated 0.93 m and 3.32 m. It shows that the hazardous distances of LFL and ½ LFL were reduced to 89 % and 80 % respectively, thus confirming the effectiveness of foam in reducing vapor exclusion zone. It is important to note that these

values may vary dependent on the location of the pit. In addition, the generated contours may differ if gas detectors are placed closely in the downwind direction.

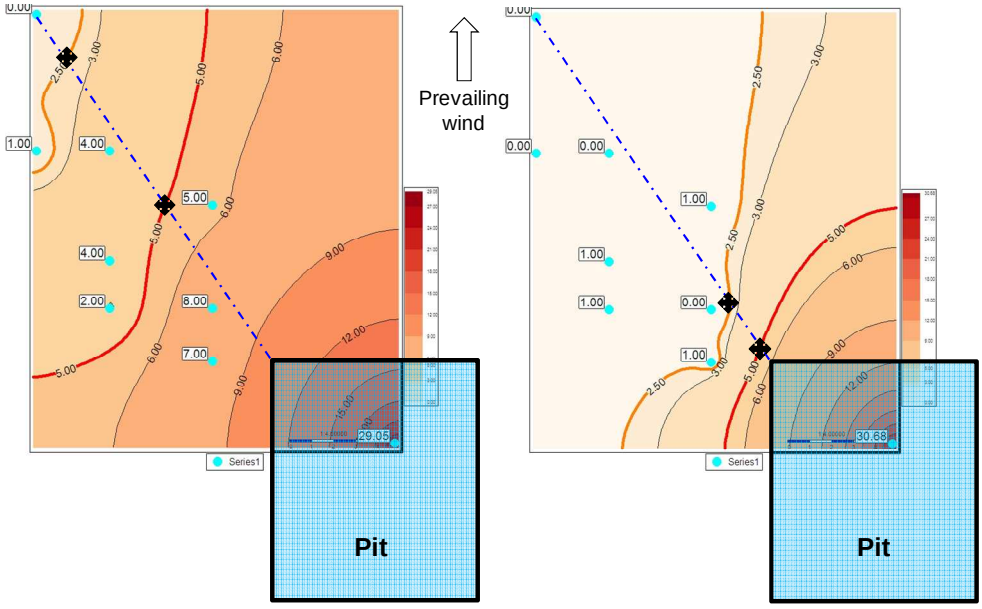

(a) Before foam discharge **(b) After foam discharge - at steady state**

Fig. 36. Maximum methane concentration contours in downwind

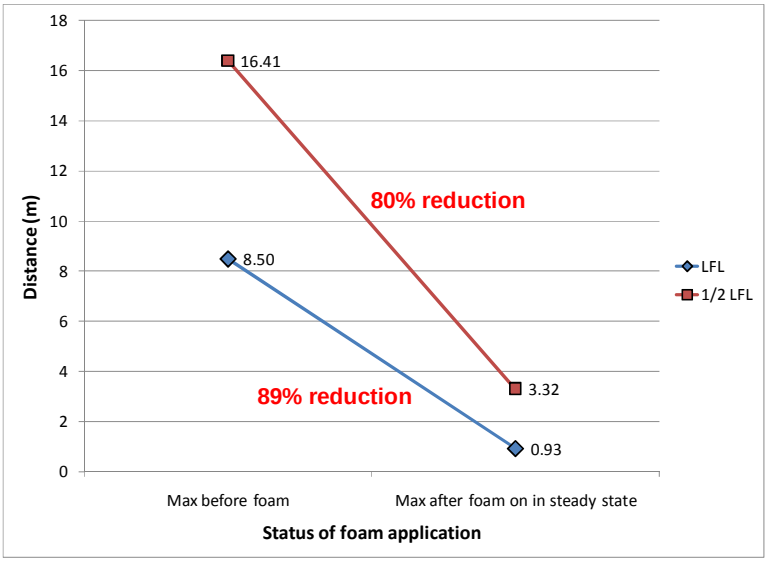

Fig. 37. Reduction of LFL and 1/2 LFL distance by foam application

2.3.7 Simplified model of LNG-foam system

In the medium-scale test during December 2009, it was observed that ice plates were formed after the vapor dispersion experiment as seen in Fig. 38. It can be further explained that when foam was applied on LNG, some of the water drained through the foam layers on LNG surface, and which then became ice plates due to heat loss to LNG. The ice plates could be methane hydrate, which contains a certain volume percent of methane and may be developed from the captured methane vapor while it penetrates the frozen foam layers. However, the ice plates were not observed during the March 2009 test. This can be explained due to the time duration of the test. In the December test, expansion foam was applied on LNG for 41 minutes while the foam in the March test was applied on LNG for 17 minutes. In other words, a longer period of contact time of foam with LNG results in greater heat losses of foam and more water drainage onto LNG surface. Therefore, it can be concluded that the formation of ice plate is dependent on the length of contact time with LNG. However, it should also be noted that the ice plate formation may be initiated by other factors, for example, the amount of water composition in foam bubbles and expansion ratio of foam.

Based on our findings from small and medium scale tests, a simplified model of expansion foam and an LNG system is proposed in Fig. 39. This model assumes that foam may form two layers when applied to an LNG pool: a non-frozen layer and a frozen layer. Other assumptions are that if the fresh foam is not applied continuously or intermittently on top of old foam, then the existing foam will be shrunk due to foam collapse and gradually lose its effectiveness to warm up the LNG vapor. Thus, in order

to maintain the foam effectiveness during the vapor dispersion process, a continuous or intermittent supply of foam should be applied. Furthermore, the temperature value -114 ^{o}C is presumed in the frozen layer and may serve as a threshold level for evaluating minimum foam depth required to warm up the LNG vapor and promote its buoyancy. However, caution should be taken to ensure the discussions about the use of temperature value -114 ^{o}C as a metric of determination of effective foam depth made in section 2.3.3. The lower frozen layer can also include ice plates which may affect the vaporization in the interface between foam and LNG [18, 22]. We believe that when expansion foam is applied on LNG the water droplets in the foam drain through foam layers up to the LNG surface, and then they freeze to become ice plates due to the contact with LNG. On the other hand, the non-frozen foam layer is assumed to have a temperature higher than 0 ^{o}C and may be used to evaluate the maximum effective foam depth. Based on this simplified model of LNG-foam system and the understanding of heat flow inside a concrete pit (Fig. 23), a new heat transfer model can be generated to better understand the dynamic characteristics of an LNG spill in confinement.

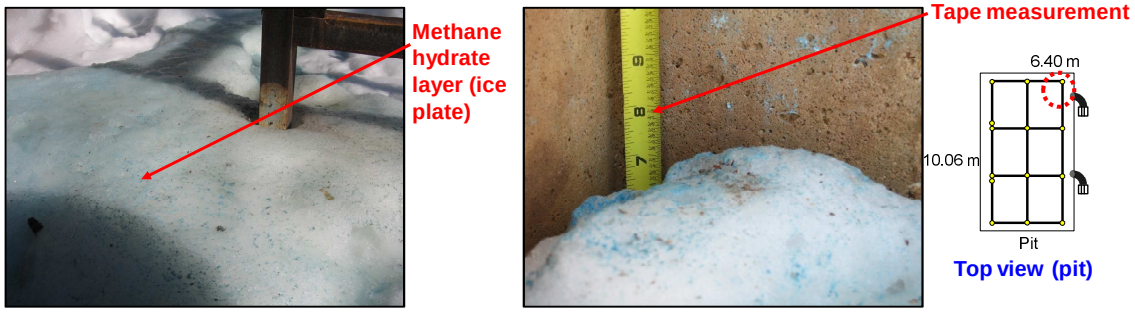

Fig. 38. Observation of ice plate in December 2009 test

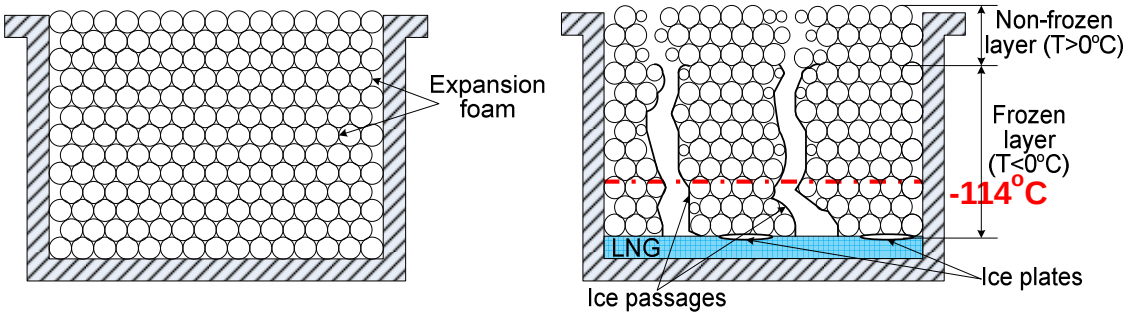

Fig. 39. Schematic model of expansion foam and LNG system

2.4 Conclusion

This chapter summarizes the outdoor LNG spill experiments for evaluating the effectiveness of expansion foam on LNG vapor dispersion. Extensive data analysis was performed to identify key parameters such as: (1) foam collapse rate and mass evaporation rate; (2) effective foam depth; (3) temperature profiles of expansion foam and LNG vapor inside the pit; and (4) the extent reduction of methane concentration.

Key findings from this study are summarized as follows:

- Small-scale test showed that when expansion foam was applied on the LNG pool surface, ice tube passages were formed along the vapor pathways, and foam collapse rate was influenced by contact with LNG and other factors (wind velocity and direction, the direction of foam application, etc.).
- In the medium-scale test, it was confirmed through our temperature readings that the expansion foam can help to warm LNG vapor and causing it to be buoyant. It should be recognized, however, that foam application initially may result in negative effect

on LNG vapor control due to the aggregate vaporization in the initial stage of foam application. This resulted in an initial rapid decrease in vapor temperature followed by excessive vaporization. Therefore, caution should be taken when initiating foam application not to allow fresh water into LNG before foaming. Generating the temperature profiles also allow the identification of minimum effective foam depth, 0.64 m. It is important to note that the effective foam depth should be decided by considering not only the vapor dispersion control but also the pool fire suppression to cover all possible hazard scenarios. In addition, when determining effective foam depth, consideration should be given to foam collapse rate and safety margins to capture underlying nonlinear physical phenomena.

- It is widely assumed that the temperatures of foam and vapor are the same at the same elevation, but here we found them to be different from the temperature contours inside a pit. In addition, it was found that foam temperatures in different locations are significantly affected not only by the characteristics of foam spreading but also by the characteristics of LNG spreading. Thus, consideration should be given when determining the location of foam generator and how many generators should be provided.
- Expansion foam is effective in reducing the methane downwind concentrations, resulting in decreasing LFL and ½ LFL distances. Additionally, results from the gas concentration inside the pit showed that foam application initially increases concentration resulting from larger vaporization and after 9 minutes decreases concentration.

- During foam application, all thermocouples gave much stable temperature readings. This may be attributed to stable heat transfer with the environment, or insulation characteristics of the foam.

We recommend that these findings should be tied to further research initiatives related to pool fire scenarios because the release of LNG into confinement may result in vapor hazard as well as potential pool fire. Therefore, Chapter III focuses on the characteristics of pool fire suppression by foam and heat transfer modeling of foam system on LNG fire. Consequently, the combination of vapor dispersion findings and the pool fire studies will allow for a comprehensive evaluation of foam effectiveness and the key parameters of foam usage for the control of LNG release hazards in confinements.

CHAPTER III

CONTROL OF POOL FIRE

3.1 Introduction

3.1.1 LNG and safety concerns

Liquefied Natural Gas (LNG), which contains mainly methane gas converted into liquid state by super cooling to -162.2 ^{o}C (-260 ^{o}F) at atmospheric pressure, has been widely used as a fuel for industrial and residential purposes [1, 4, 6, 24, 28]. LNG is flammable when the predominantly methane vapor is mixed with air in volumetric concentrations between 5% and 15% [1, 4, 19]. If LNG releases onto ground, a liquid pool will be formed and the existence of immediate ignition sources can result in and sustain a pool fire. If delayed ignition takes place in the vapor cloud during the release of LNG and the formation of liquid pool, then a flash fire may occur and it may result in a pool fire caused by the flash back from the vapor cloud to the LNG pool. The primary hazard of pool fires arise from radiant heat flux emitted by the fire to the people and objects outside the pool fire. Therefore, NFPA 59 A [8] requires a thorough risk assessment of potential release consequences when designing LNG facilities (including terminals). Most notably, the standard requires that LNG storage tanks should have dikes or secondary impounding walls for holding accidental spill from tanks. This standard also requires LNG facilities to design a “thermal exclusion zone” so that thermal radiant flux from an LNG fire will not create damage beyond the property line based on 5

kW/m^2 criterion at ground level for ignition of a design spill [8, 10, 20]. Application of expansion foam can be one of those safety measures for pool fire suppression in terms of NFPA 59 A [8].

According to the definition of NFPA 11 [5], expansion foam can be defined as conglomerates of the air bubbles made by blowing foam solutions (water solution containing foam concentrates), by means of suitable equipment, e.g., foam generators. The foam concentrate, which is mainly composed of surface active agents, plays a role in forming bubbles. NFPA 11 categorizes foam into three ranges of expansion as follows: (1) Low-expansion foam – expansion up to 20; (2) Medium-expansion foam – expansion from 20 to 200; (3) High-expansion foam – expansion from 200 to approximately 1000 [5].

3.1.2 Previous research by other authors

Up to now, very little research and experiments have been done on the application of expansion foam on LNG pool fires, but still present useful knowledge to LNG industries for foam application on LNG.

University Engineers, Inc. [15] investigated the effectiveness of expansion foam on LNG spills onto land in pool fire control by measuring the LNG burning rate and the radiant heat flux emitted by a fire. This research identified that a 0.91 m (3 feet) depth in expansion foam can reduce the radiant heat flux, but it did not define the safe separation distance of the heat flux (5 kW/m^2) for the determination of the thermal exclusion zone. In addition, it was concluded that small bubble foams tend to reduce the mass burning rate while large bubble foams may increase the burning rate during fire control

conditions. This research presented a good understanding of foam effectiveness dependent on bubble size and expansion ratio, but for the fire suppression it did not provide how foams effect the temperature changes, what thickness of foam can be effective, and how radiant heat fluxes vary in different directions. In addition, it did not show the underlying mechanisms of foam changes when contacting with LNG during fire control.

Results of modeling of foam spread and extinguishment in large-scale foam application was reported by Persson et al. in the report of project called FOAMSPEX [22]. The researchers conducted foam spread experiments over water, fuel oil, and lubrication oil with or without fire in a channel and a pool configuration. In the initial stage of foam spreading, the main driving force of the foam spread can be momentum from foam generators or suitable means for foam generation. In the second stage, governing driving force can be differences in gravity forces due to the hydrostatic pressure differences within the foam. On the contrary, the controlling resisting forces can be a viscous friction from the foam blanket against the fuel beneath it in a pool fire. It became apparent in this report that large diameter tanks require higher foam application rates than presently stated in NFPA 11. This research also identified that negligence of foam consumption due to the fire can create an underestimation of the time required to control the fire. However, this research studied only the foam coverage time to create estimations of foam application rates for fuel oils, not LNG. Furthermore, the report does not include the results of foam effectiveness like the degree of reduction of radiant heat flux by foam.

Recently, Suardin et al. [16, 21] at Mary Kay O'Connor Process Safety Center (MKOPSC) conducted a few field tests concerning expansion foam application on LNG pool in College Station, Texas. These tests identified that foam application rates of 10 $L/min \cdot m^2$ are effective for LNG pool fire control on concrete LNG containment pits and the pool fire control time (which is defined as the time required for achieving 90 % radiant heat [5]) is also reduced by increasing the foam application rate. Through these tests it was also observed that the geometric configuration of the containment pit can result in different behaviors in LNG pool fires. However, there are still several knowledge gaps that need to be addressed to obtain a strategy for foam application on LNG pool fire. For instance, the results did not show the changes in the mass burning rate of LNG by foam, temperature profiles of the foam and the fire as a function of elevation, radiant heat flux contours and 5 kW/m^2 distances from the pool fire, or the underlying mechanisms (or phenomena) involved in foam changes when it contacts with LNG during fire control.

Many researchers have been trying to develop LNG pool fire hazard models. With current technology, the most well-known and widely-used pool fire model is the solid flame model. This model assumes that fire is a simple geometrical shape, usually cylinder [1]. The model represents a fire as a surface emitter of radiant heat flux. The mathematical representation of this model [14] is presented by:

$$\dot{q}'' = EF\tau \qquad (6)$$

$\dot{q}''$: Radiant heat flux received by an object

E: Surface emissive power

F: Geometrical view factor between the radiation receiving object and the radiation emitting parts of the fire

τ: Transmissivity of the atmosphere to themal radiation from fire

Based on the solid flame model, the radiant heat flux emitted by a fire is proportional to the surface emissive power (explained as an average thermal radiant flux emitted by the fire over a defined surface of a certain fire shape), the geometrical view factor (used to determine how much radiant heat flux an object receives), and the atmospheric transmissivity (used to consider the fact that the air between the fire and an object can absorb some part of the emitted heat flux). This equation is one of the simplified versions created by assuming that the surface emissive power is constant over the entire surface of the fire and the base diameter of the fire is equal to the burning liquid pool diameter [4, 14].

Using the solid flame model, Parker [29] calculated radiant heat flux from natural gas flame for hazard assessment. In the paper, energy reception rates as a function of distance from the flame center were reported as seen in Fig. 40. It shows that heat emissive power is inversely proportional to the distance of receptors from fires, but it does not show linear relationship. This result can be used to compare with experimental measurements for the validation purpose.

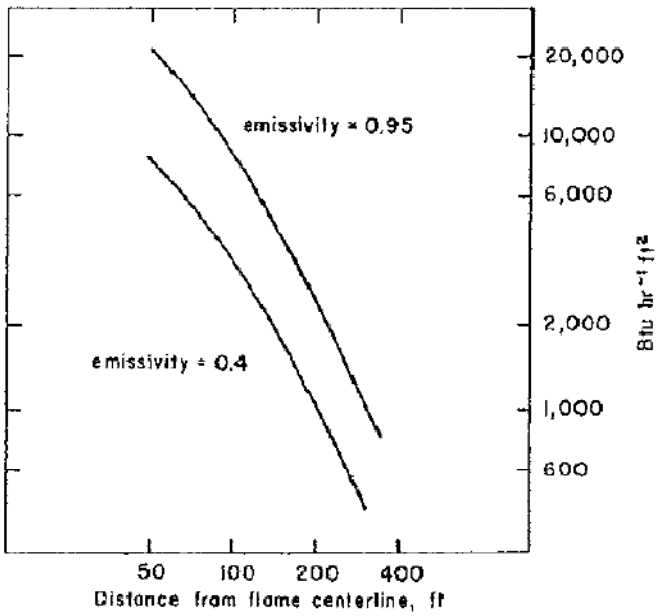

(Adapted from [29])

Fig. 40. Radiant energy reception rates

The surface emissive power (E) and the geometric view factor (F) are functions of flame height, thus it is imperative to identify the fire plume length for modeling the radiant heat flux. Several correlations have been used to compute fire plume length for a fire of a certain diameter and the Thomas correlation [4] has been widely used in the form of the following equation:

$$\frac{L}{D} = AF_c^p (U^*)^q = A\left(\frac{\dot{m}''}{\rho_a\sqrt{gD}}\right)^p \left(\frac{U_{wind}}{\left(\frac{\dot{m}''}{\rho_a}gD\right)^{1/3}}\right)^q \quad (7)$$

L: Height of fire

D: Fire diameter

A, p, q: Correlation constants

ρ_a: Density of air

g: Acceleration due to gravity

$$F_c = \frac{\dot{m}''}{\rho_a \sqrt{gD}}$$

F_c: Combustion Frode number = Dimensionless burning rate

$$U^* = \frac{U_{wind}}{\left(\frac{\dot{m}''}{\rho_a} gD\right)^{1/3}}$$

U^*: Dimensionless wind speed

This equation can also take into account the wind's effect on the length using the dimensionless wind speed term and a correlation constant (q). A common purpose for using expansion foam on LNG pool fires is to control and reduce the radiant heat of fire to allow firefighters to approach and extinguish the fire if needed. It may be useful to develop models so that firefighters and researchers working with flames can estimate the height of fire controlled by the expansion foam against fire diameter for proper fire hazard assessment. However, the current solid flame model may not be used for that purpose without any modification because it does not account for the effects of the foam on LNG fire.

3.1.3 Objectives

Previous researchers discovered that expansion foam has an effect on LNG pool fire control [15, 16, 21, 22]. However, further research is required to fill in research gaps and provide more accurate data on the effects of foam and the properties generated through continued experiments and modeling.

Therefore, the objectives of this chapter in this research were:

- To investigate the effectiveness of expansion foam on LNG pool fire control by identifying the extent of reduction in the radiant heat flux caused by expansion foam in four directions (upwind, downwind, up and down crosswinds) and obtaining heat flux contours emitted by the fire. These findings were used to identify thermal hazard distances on the basis of 5 kW/m^2 heat flux level. In addition, the LNG mass burning rate after foam application and temperature profiles of foam and fire were measured to support the findings on the impacts of foam.
- To observe changes in fire sizes (length) caused by foam and correlate the data to model the equation of fire plume length applied with expansion foam. The equation can be used to estimate foam-controlled fire length as a function of LNG mass burning rates, wind speeds, and pool fire diameters for the radiant heat modeling. Ultimately, the equation can be applied for developing firefighting strategies and emergency response plans to LNG industries which have already installed expansion foam system in their facilities or will incorporate the system into their designs.
- To build theoretical models to understand the underlying mechanisms of foam on LNG pool fire. By using the developed models and obtained experimental data, the effective foam depth for both pool fire suppression and vapor dispersion control is suggested.

3.2 Overview of research

3.2.1 Methodology

In order to achieve the objectives of this research, two methods were executed: (1) medium-scale field tests for gathering experimental measurement data concerned with radiant heat fluxes, fire sizes and temperature profiles; and (2) theoretical study for making foam-controlled fire length models and making expansion foam models with LNG pool fire based on several variables, e.g., temperature and heat. Ultimately, obtained experimental data were used to correlate with the developed models.

3.2.2 Apparatus

Chromega/Alomega thermocouples (type K, Omega Engineering Inc.) with a wire diameter of 6.4 mm and a length ranging from 6.10 m to 10.67 m were used to measure liquid LNG and vapor temperatures. This thermocouple was selected because it is suitable to measure from cryogenic temperature to high temperature of flame (ranging from -270 ^{o}C to 1372 ^{o}C). Each thermocouple was connected to the data acquisition system, which was linked to a computer with an Ethernet cable. The configured software program in the computer was able to simultaneously record the input data every second from the thermocouples, with a standard limit of 2 % (± 2.2 ^{o}C). To ensure all thermocouples for LNG level measurement are working properly in the cryogenic temperature of LNG, they were custom-designed with some protection features. The thermocouple bead was made of Inconel collar, filled with ceramic and the junction of lead wires was insulated with ceramic fiber to prevent moisture accumulation. For the

use of high-temperature conditions, the thermocouples were also protected with abrasion-resistant Inconel overbraid with high-temperature ceramic fiber insulation.

To measure flame emissive power, wide-angle radiometers with 150 degree view (Medtherm Corp.) were used (see Fig. 41). Each radiometer was linked to a data acquisition system and computer. The software program configured in the computer provided a self-generated 10-millivolts output at the design heat emissive power level. This radiometer adopted thermopile type sensor, which can generate mV output. In this sensor, absorbed heat flux at the sensor surface is transferred to an integral heat sink. The difference in temperature between sensor surface and heat sink is used to generate electro-magnetic field (emf) through thermopiles inside the radiometer. A sapphire window attachment to each radiometer was added to eliminate convective heat transfer from fire. In other words, the window attachment was used to measure only radiant heat flux from fire.

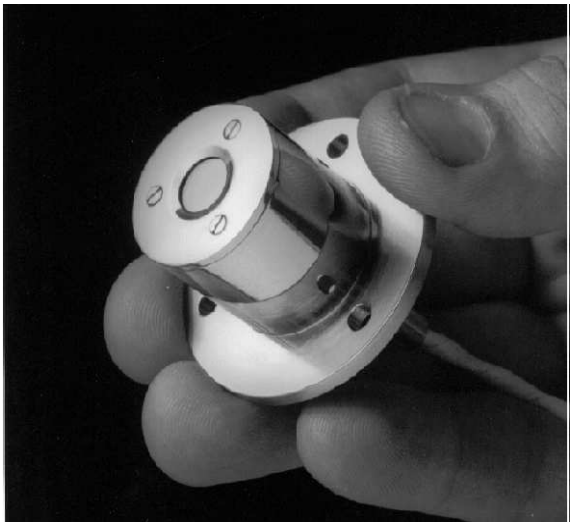

Fig. 41. Example of radiometer (adapted from Medtherm Corp.)

3.2.3 Experimental setup

Outdoor medium-scale experiments were designed to spill LNG into a confined concrete pit to simulate LNG release scenarios in LNG facilities on land. Experiments were carried out at the Brayton Fire Training Field (BFTF), which is one of the affiliates of Texas A&M University. The facility is composed of three concrete pits and its flat ground is also made of concrete.

Two medium-scale field tests were conducted to observe foam effectiveness on LNG fire control and identify key parameters in the large LNG training pit (6.40 m $\times$ 10.06 m $\times$ 1.22 m). As shown in Fig. 42, in the December test 166 thermocouples were installed vertically on steel angle frames inside the pit in sixteen locations to measure the temperatures of expansion foam (or LNG vapors) and the fires. Several thermocouples were installed in 0.64 cm (0.25 inch) distance interval from the pit bottom to measure LNG levels in one location. In addition, four thermocouples (two of them contacted the concrete wall surface and the others were placed near the wall) were installed on each side of the concrete wall to measure the wall surface and foam temperature. Referring to Fig. 42, one wide-angle radiometer was positioned in the center of the pit at 2.9 m height from the pit bottom. The schematic diagram of the concrete pit in the March test is given in Fig. 14. Both tests have similar equipment setup in the pit, but in the December test several modifications were made, for instance additional installation of one radiometer in the pit and changes in locations and numbers of thermocouples.

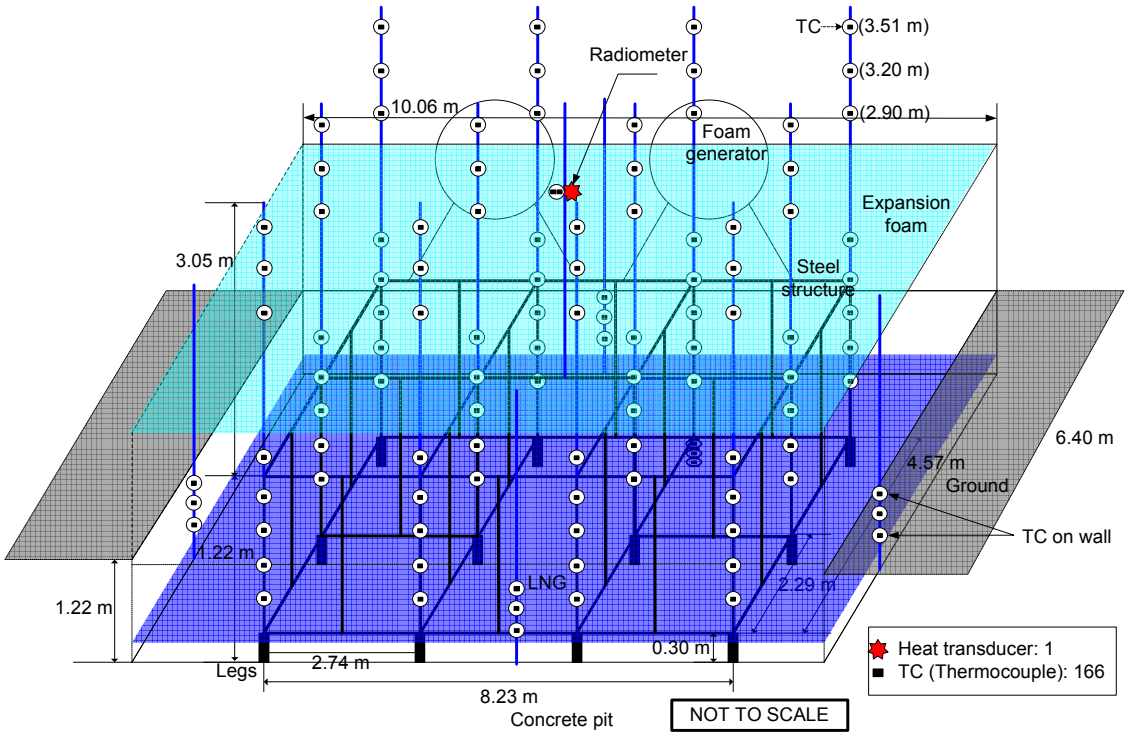

Fig. 42. Setup for medium-scale field test in December 2009

Fig. 43 illustrates detail setup for the radiometer in the pit. As shown in Fig. 43(a) and (b), the radiometer was mounted on the flange of the end of 6.35 cm diameter steel pipe. Two thermocouples were also installed on a steel frame at the same height with the radiometer to calculate heat flux of fire from temperature measurements. As shown in Fig. 43(c), the radiometer was cooled down by flowing cooling water through a 0.48 cm diameter copper tube from one end to the other end. The radiometer was also purged with nitrogen gas through a 0.48 cm diameter copper tube to keep the sapphire window clean from soot or smoke of LNG fire for more precise reading of radiant heat flux. For the protection of radiometer elements such as lead-wire, two water cooling tubes, and nitrogen purging tube from fire, two protective layers were employed: (1) a

5.08 cm (2 inch) diameter fire sleeve hose, which is able to protect continuously to 260 ^{o}C and withstand a molten splash at 1200 ^{o}C, and (2) a 6.35 cm (2½ inch) diameter steel pipe, which is used to protect fire sleeve hose from direct flame impingement.

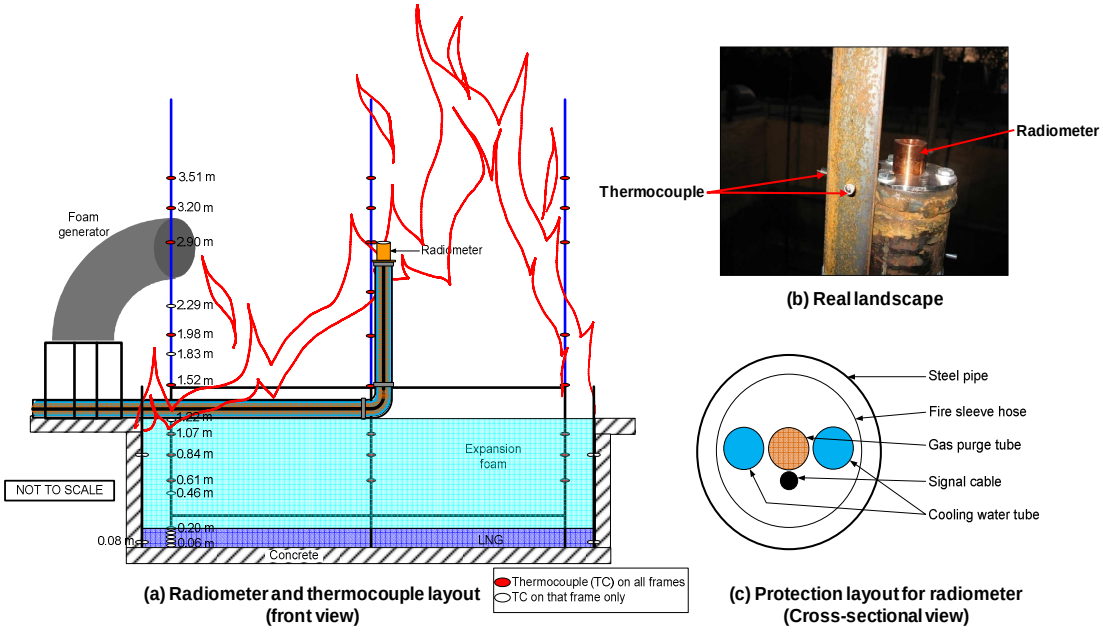

Fig. 43. Radiometer and thermocouple layout in the pit

Fig. 44 presents the actual view of wide-angle radiometer setup outside the pit in the March and December tests in 2009. Each radiometer was mounted on a steel plate at a 0.91 m height, which is recommended by NFPA 11 [5]. The radiometers were stood and positioned by a steel tripod. Fig. 45 depicts the schematic placement of radiometers around the pit. During the March and December tests, prevailing wind directions were opposite, thus accordingly foam generators and the data acquisition system were located in the crosswind. In the March test, more radiometers were placed in crosswind

direction, while in the December test more radiometers were positioned in the downwind. During the March test, one heat flux indicator, which is able to provide a direct readout of radiant heat flux when used with a radiometer, was carried by author so that the author could change the location of R5 and R7 in Fig. 45(a) to identify the distance of the 5 kW/m^2 heat flux. However, during the December test, the author was not able to carry the flux indicator to move the location of R6 and R7 in Fig. 45(b) due to the higher risk of injury downwind of the fire.

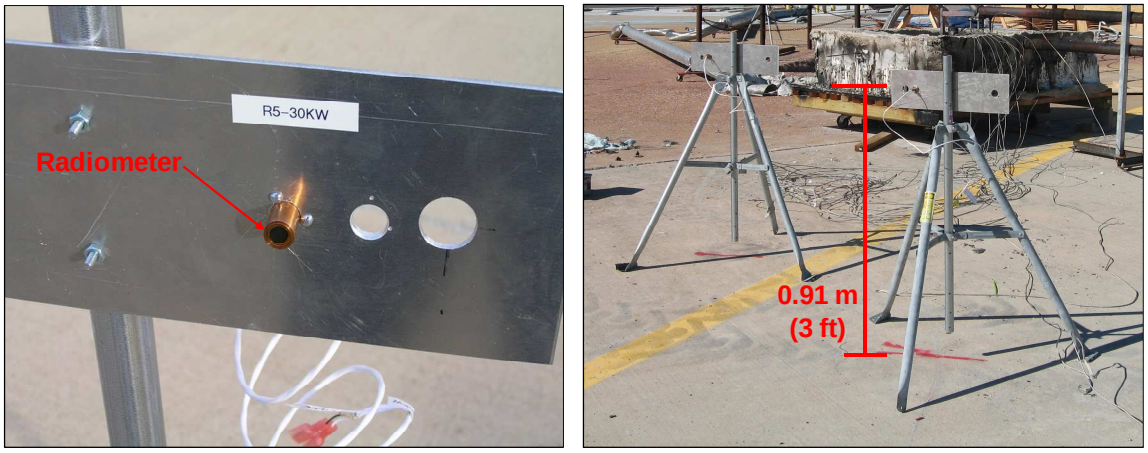

(a) Front view **(b) Rear view**

Fig. 44. Radiometer setup pictures

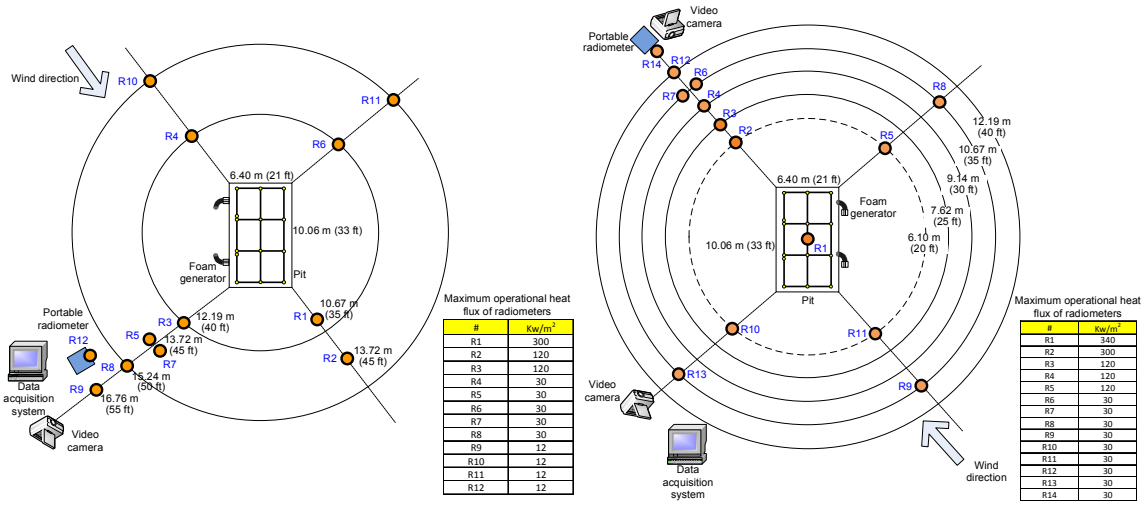

Fig. 45. Setup for radiometers

Fig. 46 illustrates the schematic drawings of the experimental procedure. Initially, LNG was spilled into the pit through a 0.10 meter stainless steel pipeline up to a 0.20 meter (8 inch) depth. For the LNG vapor dispersion control test by expansion foam, as shown in test 1 in Fig. 46, high expansion foam was applied simultaneously by two foam generators and filled the pit up to 2.44 m (8 ft) depth. After finishing test 1 and removing the gas detectors and the wooden walls around the pit, test 2 was initiated from the ignition of the LNG. However, the foam application was suspended until previously applied foam for test 1 disappeared completely because of the LNG pool fire. When a natural LNG pool fire developed during certain time, foam was reapplied onto the fire up to 1.22 m thickness to suppress the fire. The temperature and the radiant heat flux were measured and recorded in every second during the whole test period. Since the results of test 1 in Fig. 46 were mentioned in Chapter II, they will not be considered further in this chapter.

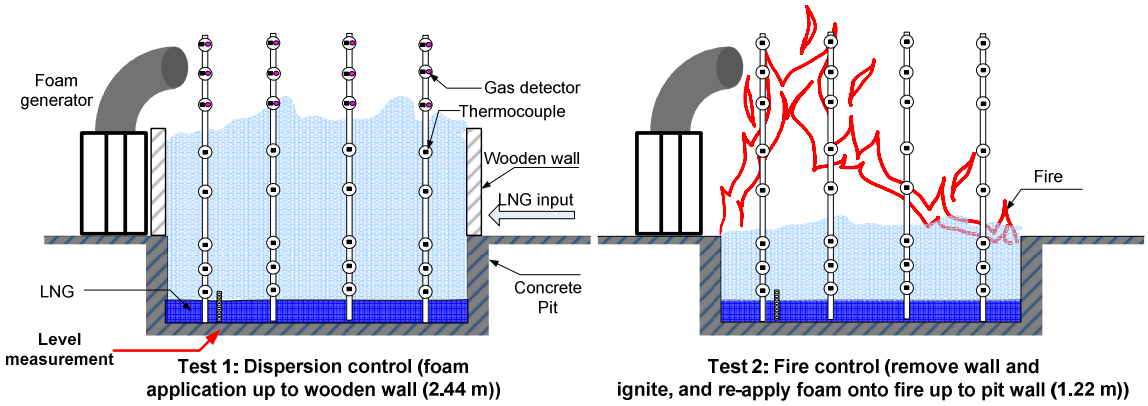

Fig. 46. Experimental procedure

3.2.4 The summary of experiment facts

The summary of experiment facts for the atmospheric and foam conditions during the pool fire field tests are summarized in Table 3.

Table 3 Summary of experiment facts for 2009 pool fire tests

Conditions	Variables	March 2009	December 2009	Note
Atmospheric conditions	Temperature	22.42 ± 0.03 °C	14.31 ± 0.16 °C	
	Wind speed	3.26 ± 0.42 m/s	1.25 ± 0.39 m/s	Maximum wind speed (March test: 6.70 m/s, December test: 1.8 m/s)
	Wind direction	S and SSE&W	N and ENE	
	Relative humidity	51.90 ± 1.73 %	44.17 ± 0.51 %	
	Solar radiation	0	64.00 ± 8.15 W/m^2	During March test, it was night from 7:50 to 7:59 pm.
LNG conditions	Methane composition (%)	99.85	99.87	Other components: nitrogen and ethane
Foam conditions	Expansion ratio	500:1	500:1	Classfied as "high expansion foam"
	Foam application rate	6.5 l/m^2·min	6.5 l/m^2·min	
	Foam concentrate	Jet-X	Jet-X	Components: HMIS surface active agents, ethyl alcohol, lauryl alcohol, glycol, inorganic salts

3.3 Test results

3.3.1 Measurement of fire height

To identity the foam effectiveness on LNG fire control, we attempted to measure the fire plume length as an initial step. Fig. 47 shows actual landscape of LNG pool fire before and after foam application. The still photos were taken by a video camera which was placed at a fixed location in a crosswind direction. It is apparent in Fig. 47 that the freely-burning LNG fire grew (Fig. 47(a)), right after the foam application the fire grew larger (Fig. 47(b)) and then decreased significantly after a certain period of time, post application (Fig. 47(c)). However, this analysis was not able to provide continuous flame length profiles and quantified values for the reduction of the fire length due to foam application.

Therefore, here we attempted to obtain the fire plume length over time from the video file using ImageJ software, which is a free downloadable, Java-based image processing program developed by National Institutes of Health [30]. This method is briefly described as follows: (1) a video file is loaded into ImageJ program, which converts the file into multiple frames, (2) a measurement scale is set by drawing a vertical line over the image of the foam generator supports at 1.22 m height, and (3) the program analyzes the fire length in each frame individually and saves the estimated results. By using this method, Fig. 48 was produced to represent the profile of fire plume length over time. As seen in Fig. 48, the fire height increased steadily up to 13.13 m during free burn (36 seconds), and then foam was applied subsequently at 37 seconds. Right after foam application the flame grew up to 17.17 m. It can be explained that prior

to full foam development a certain amount of initial fresh water ingress from the foam generators onto the LNG pool and also rapidly draining foam increased the evaporation rate of LNG, thus resulting in exaggeration of the fire's intensity [5]. During the test, foam was applied into a concrete pit of 64.83 m^2 area at 6.5 $L/m^2 \cdot min$ foam application rate. At 5 seconds after foam application, the fire height had begun to decrease since the accumulated foam was effective at reducing fire heat feedback to the LNG pool. Approximately 55 seconds after foam application, it was ultimately observed that the fire plume length reached a stable limit at 5.13±0.38 m (i.e., 61% reduction in the free-burn fire height, 13.13 m, prior to foam application). It is implied that the expansion foam was finally able to reach a steady state between the fire and the LNG. Consideration, however, should be given to the fact that the fire, during free burn, could not fully develop since during the test the foam had to be applied earlier than the moment of full development to protect the concrete props and other equipment. Thus, it is possible that the percentage in fire height reduction could be larger than 61 %. As shown by Fig. 48, even after the stable control moment a peak in fire length was observed at the range of 200 sec to 210 sec. We believe that it was caused by intermittent reapplications of foam to keep 1.22 m thickness and during the periods of peak fire height the foam was lower than 1.22 m. This continuous fire length measurement is compared with radiant heat flux profiles measured by radiometers in section 3.3.5.1 to identify the relationship.

Fig. 47. Pictures of fire before and after foam application

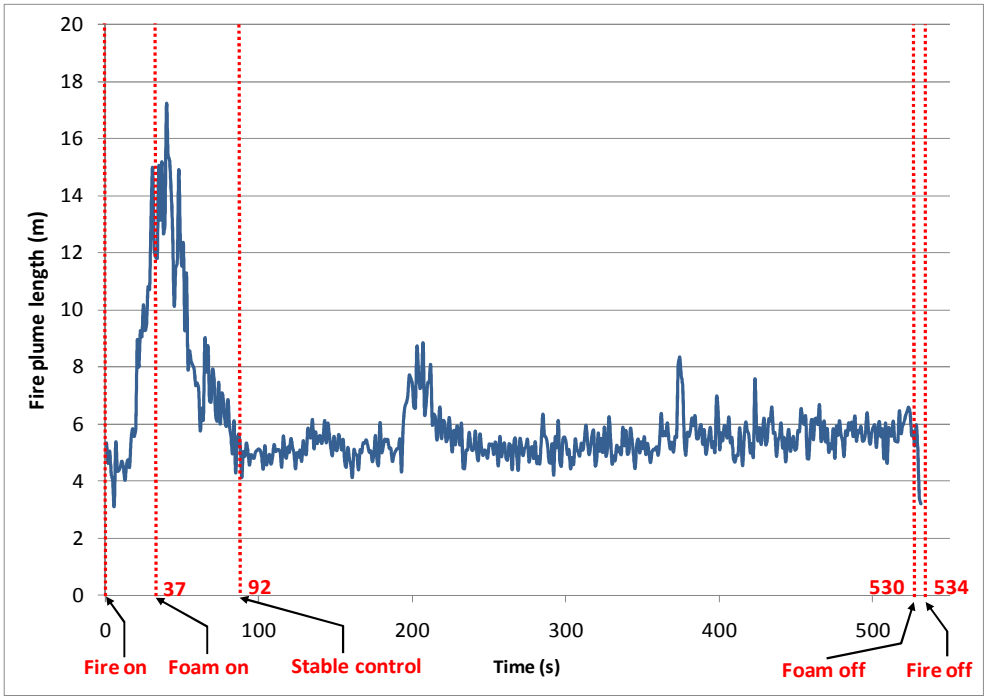

Fig. 48. Fire plume length over time

3.3.2 Mass burning rate

The mass burning rate of LNG is one of the key parameters in predicting how fast the fire burns and to model the fire plume length and the radiant heat flux. The

experimentally measured mass burning rates (or liquid regression rates) of LNG on concrete or land were reported in literature [1, 4]. Babrauskas [26] reported the mathematical analysis of the pool burning rate of flammable liquid on the basis of heat transfer principles and an experimentally correlated model in his paper. An attempt, however; has not been made to obtain the LNG burning rate applied with the use of expansion foam. We believe that it will be useful to model fire characteristics post foam application for identifying foam effects.

In this experiment, an attempt was made to obtain the mass burning rate of LNG post foam application from the temperature measurements of thermocouples, which measure a temperature ranging from -270 ^{o}C to 1372 ^{o}C. The thermocouples were mounted on a steel frame within the LNG levels. The levels of LNG were observed by checking the position of thermocouples and the time in which each thermocouple read out the LNG boiling temperature, -162 ^{o}C. Subsequently, the level changes were converted into mass burning rate using the LNG density (450 kg/m^3 [19, 26]) and the dimensions of the pit. As seen in Fig. 49, the mass burning rate after foam discharge was initially high due to larger fire size, but after reaching steady state control (approximately 55 seconds after foam discharge, see Fig. 48) by expansion foam on pool fire, it became stabilized at smaller values.

Fig. 50 depicts graphically the mass burning (or evaporation) rates of LNG gathered from literature. Fig. 50 also presents the burning rates from this work conducted by MKOPSC. During the March test in 2009, the average burning rate with 1.22 m thick foam was 0.082±0.002 kg/m^2·sec and in the December test a lower value of

0.062±0.005 kg/m^2·sec was measured. We believe that atmospheric conditions affected the results, since wind speed and ambient temperature at the March test were higher than at the December test. It is physically clear that higher atmospheric temperature increases the mass burning rate because it provides more convective heat to the LNG pool. Regarding wind effects, several articles reported that the burning rate of a hydrocarbon pool (e.g., hexane, gasoline, and diesel) increased in wind to a certain level [26, 31]. Therefore, the outcomes of the burning rates are valid. Additionally, those burning rates are smaller than the rates from the pool fire on land and on water, without applied foam. This is a sensible result because 1.22 m foam is capable of reducing the burning rate by reducing the heat feedback of a fire to the LNG pool. It is also clear that the evaporation rate of the LNG on concrete without fire (0.012±0.001 kg/m^2·sec) should be smaller than the rates from the pool fires despite foam uses. As mentioned at section 2.3.2, the mass evaporation rate of LNG during foam control without fire was reported as 0.009±0.002 kg/m^{2}s. The value is slightly smaller than the vaporization rate in case of LNG spill on concrete without foam application. It is believed that the expansion foam subdued the LNG vaporization due to the less heat transfers of solar radiation and atmospheric convection by blanketing effect of the foam. It should be recognized, however; that the value (0.009±0.002 kg/m^{2}s) only reflected the mean value after reaching a steady state of foam and LNG system, without considering the initial rise of vaporization due to the water input to LNG when the foam discharges.

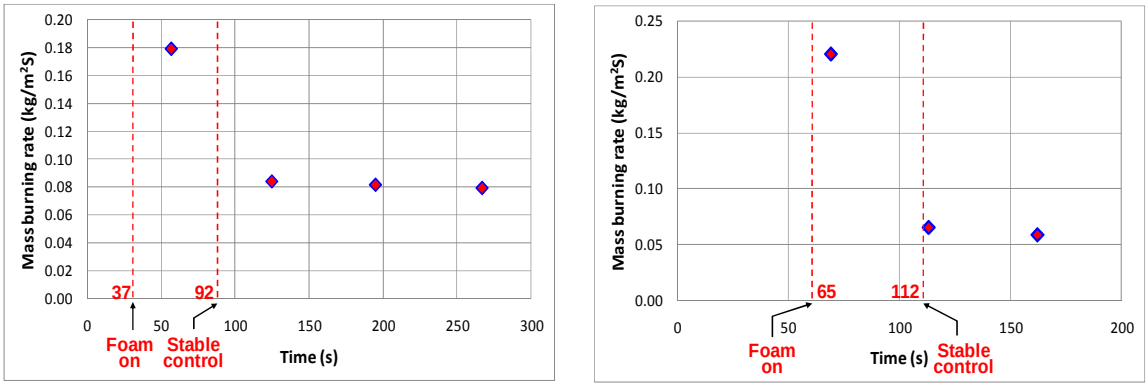

Fig. 49. Mass burning rate of LNG after foam application

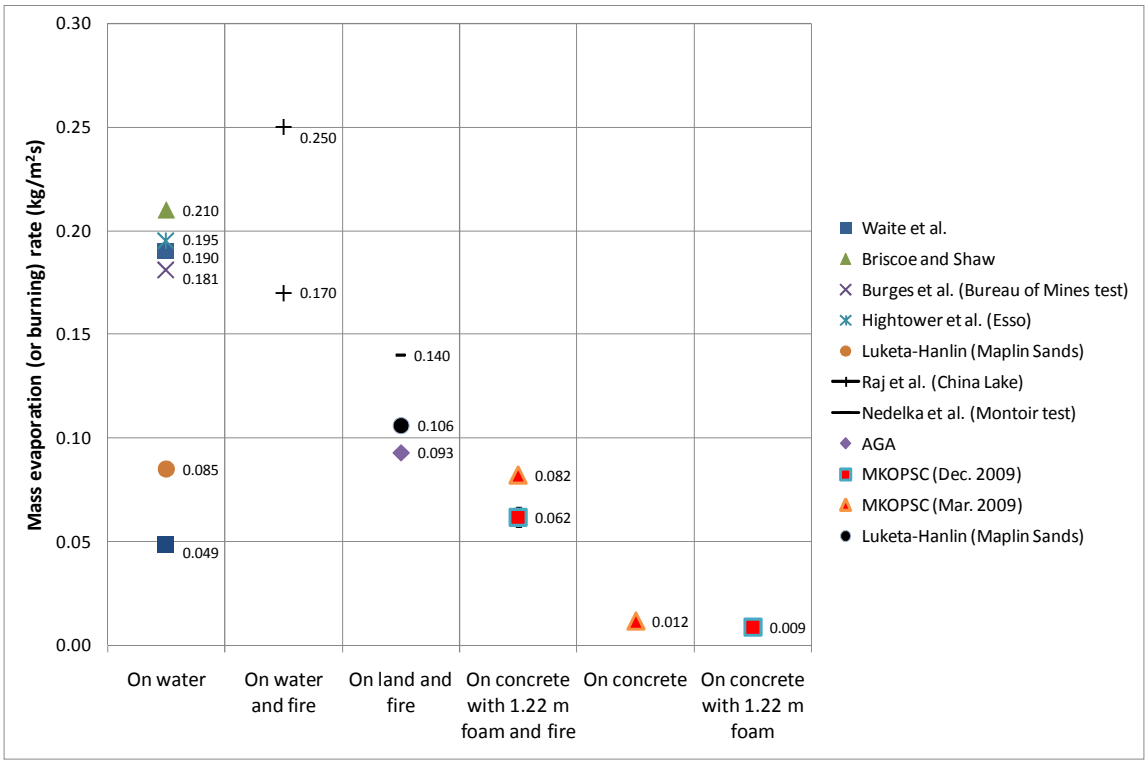

Fig. 50. Summary of mass burning (or evaporation) rate [1, 4, 14]

3.3.3 Temperature in the flame

It is uncertain whether expansion foam has an effect on flame temperature. To answer this question, approximately 35 thermocouples were installed to measure flame temperature at different heights in the pit. For the purpose of high-temperature application, the thermocouples contained double protection features: (1) abrasion-resistant Inconel overbraid and (2) high-temperature ceramic fiber insulation. Fig. 51 and Fig. 52 provide the temperature profiles of the LNG flame over time at three different heights. At the start of the burn, the temperatures were increasing quickly due to the fast development of the fire. When the foam was applied, both figures show that flame temperatures increased for some period of time and then fluctuated continuously. In the March test, the LNG fire was able to reach up to a temperature of 951 ^{o}C at the B0 location after the utilization of foam (referring to Fig. 51). We believe that the fluctuation and indefinite pattern in the flame temperature is caused by the moving and/or pulsating nature of fire. It is not, therefore; feasible to conclude that the amount of expansion foam can affect the flame temperature. However, it is certain in Fig. 51 and Fig. 52 that the flame temperature of an LNG pool fire decreases in height as found in an article with hexane pool fire [32]. Those figures also confirmed that the flame temperature differences among those three thermocouples are different; dependent on the location in the flame (i.e., the temperature difference at B1 location is greater than the one at B0 location). This is perhaps attributable to different fire intensities in the pit caused by different compositions of methane-air mixture due to wind effects, foam spreading characteristics, physical geometric differences, etc. There is no doubt that the

flame temperature distribution in the pit is affected by the action of induced wind. As seen in Fig. 53, the flame temperature distribution was tilted by prevailing wind direction, not symmetrical. It was attempted to identify the difference in flame temperature contours before and after foam application as shown in Fig. 53(a) and (b). However, the difference with current findings was not able to be determined because a major contributing parameter can be wind direction rather than foam application and spreading direction. It should be also recognized that placing of foam generators in an upwind position will provide higher efficiency on controlling fire due to easier application of foam by prevailing wind speed force. Caution must be taken, however; in determining the location of foam generators and the foam application rate because flame temperature in the downwind is higher than other areas, thus resulting in more hazardous conditions.

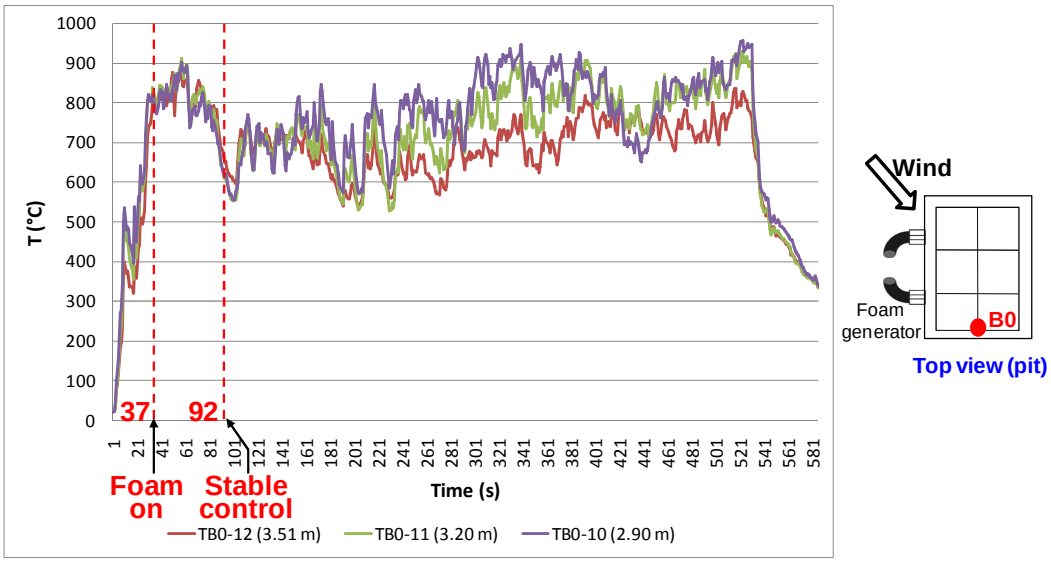

Fig. 51. Temperature profile of fire at B0 location in the pit

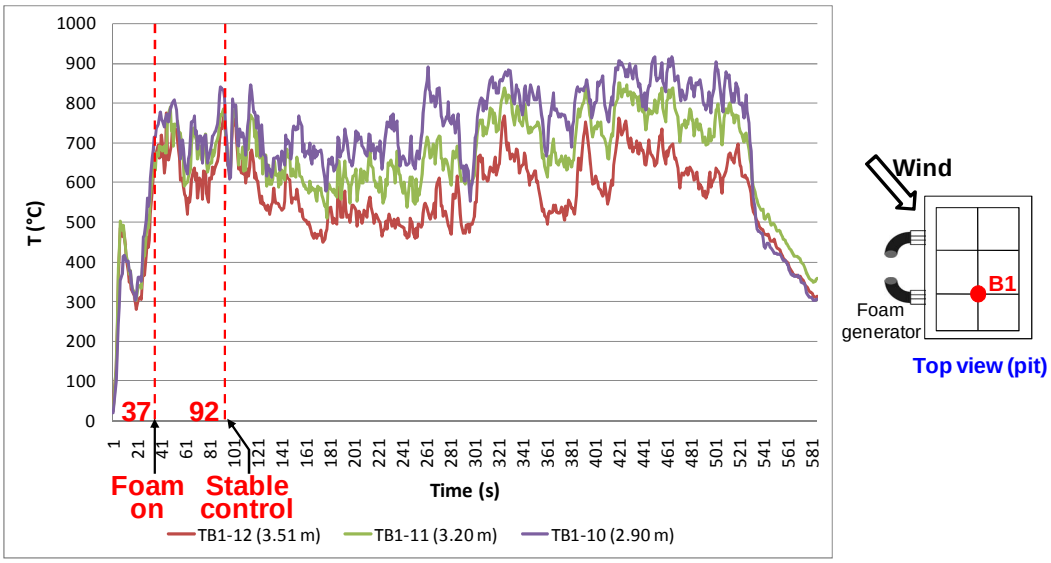

Fig. 52. Temperature profile of fire at B1 location in the pit

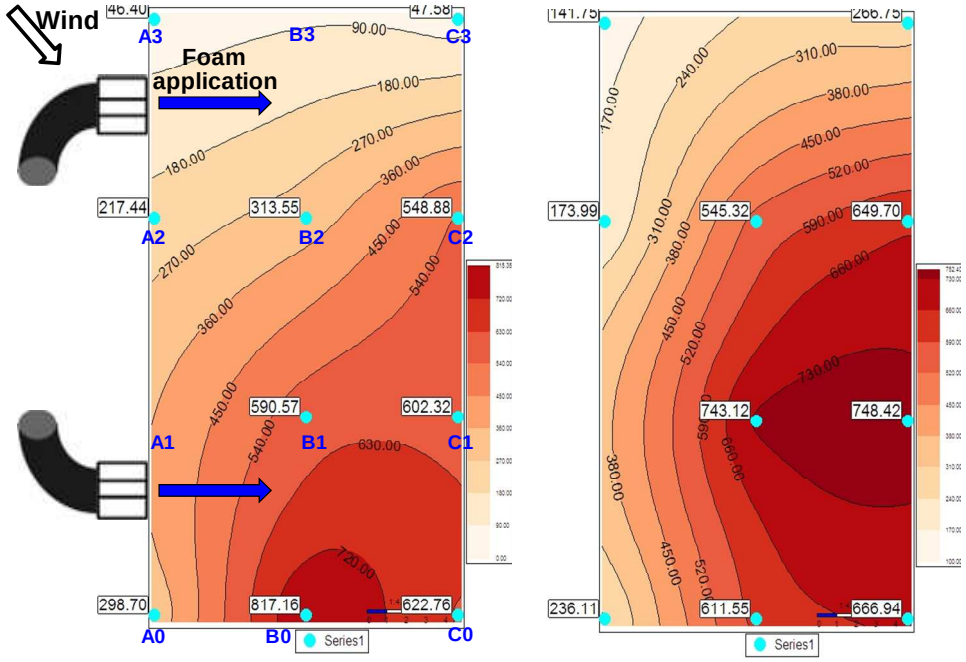

(a) 1 to 5 s before foam on

(b) Stable fire control by foam (48 to 52 s after foam on)

Fig. 53. Temperature contours of fire at 3.20 m height inside a pit

3.3.4 Temperature profile of foam

It is useful to measure the foam temperature when investigating minimum effective foam depth and making schematic models of foam in the fire cases. The minimum effective foam depth is one of the crucial parameters for foam system design since it will permit the determination of foam application rate and the number of foam generators needed. In section 2.3.3, a minimum effective foam depth for LNG vapor dispersion control was determined as 0.64 m. However, the effective foam depth should be determined considering both incident scenarios of LNG vapor dispersion and pool fire to cover major potential incidents. Hence we attempted to decide effective foam depth in the pool fire case. Foam effectiveness on fire suppression is mainly dependent on whether foam bubbles are intact in fire or not. It may be explained in terms of two aspects: (1) the water component of the bubble surface will be evaporated when it is heated up to its boiling point (100 ^{o}C) and this phenomenon will consume some portion of heat from fire as a type of latent heat of water, and (2) the aggregate of intact foam bubbles is capable of making a deficiency in oxygen concentration in the foam layer, thus resulting in suffocation of the fire within this foam layer. It is therefore imperative to identify the depth of foam from the top surface in which the temperature is less than 100 ^{o}C. Fig. 54 illustrates temperature profiles of six thermocouples inside the pit. Fig. 54(a) shows that some of the thermocouples installed at 0.84 m height measured temperatures greater than 100 ^{o}C even during a period of stable fire control post foam application. Most thermocouples at 0.61 m height, however; measured below 100 ^{o}C temperature as seen in Fig. 54(b). This implies that a 0.61 m (1.22 m foam level minus

0.61 m of thermocouple height) foam depth can provide heat block from the fire to the LNG pool to reduce fire length and flame emissive power. It can be therefore concluded that by considering both the pool fire and the vapor dispersion scenarios, the foam depth should be greater than or equal to 0.64 m, which is the limit for the mitigation of vapor cloud hazard from section 2.3.3. For the real application in the LNG industries, however; the foam depth should be determined by associating with additional factors, such as unexpected loss, collapse/shrinkage of the foam and safety margin.

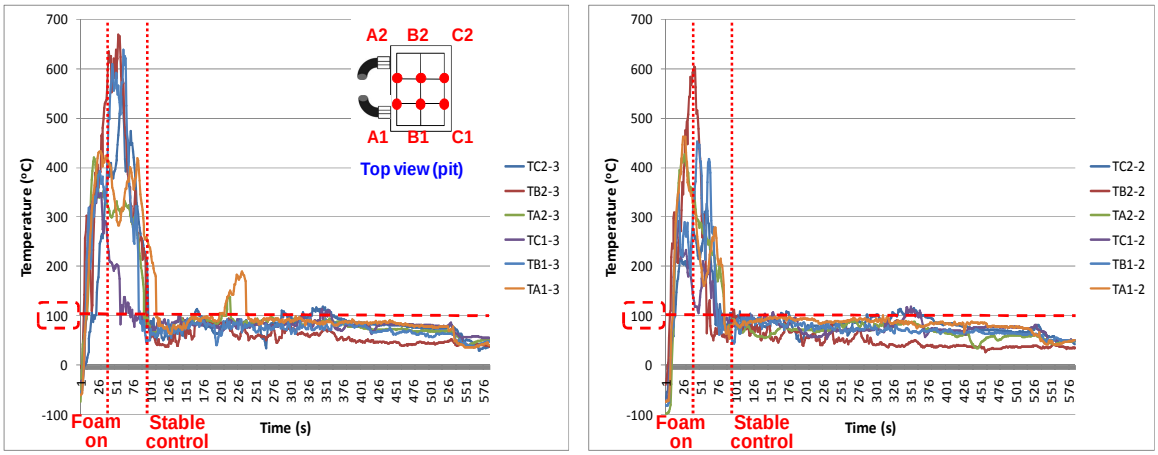

(a) Temperature at 0.84 m height

(b) Temperature at 0.61 m height

Fig. 54. Temperature profile of foam at 0.84 m and 0.61 m height during fire test

It had been unknown in theoretical LNG-foam system modeling that during fire tests expansion foam could have a frozen layer (and/or ice plates). Here we attempted to answer this question with the temperature profiles of the foam. Fig. 55 depicts temperature profiles of three thermocouples installed at 13.97 cm or less height for level measurement of LNG during the March fire test. These thermocouples initially were in

LNG, thus reading the temperature at the LNG boiling point (-162 ^{o}C). When the LNG was vaporized due to the influence of the fire and the atmosphere, the thermocouples were covered by layers of foam. As shown in Fig. 55, after foam application all thermocouples were giving temperature regions below 0 ^{o}C for some time periods despite the flame still burning, thus these regions are referred to as the "frozen layer" of foam in this research. These periods when a frozen layer was present were different depending on the height of each thermocouple. It was observed that lower thermocouples have longer frozen periods as was expected. It implies that as the position of the foam gets lower, then the foam has more influence in the heat balance from the LNG pool than from the fire. In the December test ice layers were observed when the test was completed, as seen in Fig. 56, even if ambient temperature was 14.31±0.16 ^{o}C. We believe that the ice layer was methane hydrate, which contained some volume concentration of methane because vaporized methane might be captured within the ice structure when it was passing through the frozen layer of foam. It is also believed that the formation of ice plates is affected by several factors, e.g., the duration of fire tests using the foam and ambient temperature. During the December test, the duration of the foam controlled fire test was 17 minutes, while it was only 9 minutes in the March test. Because of this, we were able to observe ice plates only during the December test. It was also determined that the thickness of the ice plates is also different based on location within the pit. It was observed that the thickness part of the ice at Northwestern corner of the pit was around 5.08 cm (2 inch). On the other hand, the Eastern edge of the pit had thicker ice layers, greater than 17.78 cm (7 inch). It can be explained that the expansion

foam at the Eastern edge had relatively longer contact time with LNG than any of the other locations since two foam generators were placed near the Eastern edge of the pit, thus resulting in the formation of thicker ice plates. An article by Vesovic [18] states that the formation of ice layer reduces the evaporation rate due to decreasing the temperature difference between LNG and the heating source (e.g., foam and fire). Therefore, it has become clear that this ice layer formed by foam can help to reduce the mass burning rate, thus creating a reduction in fire length and fire emissive power. For the foam-LNG system modeling, these ice plates should be included to cover the effect on the vaporization rate.

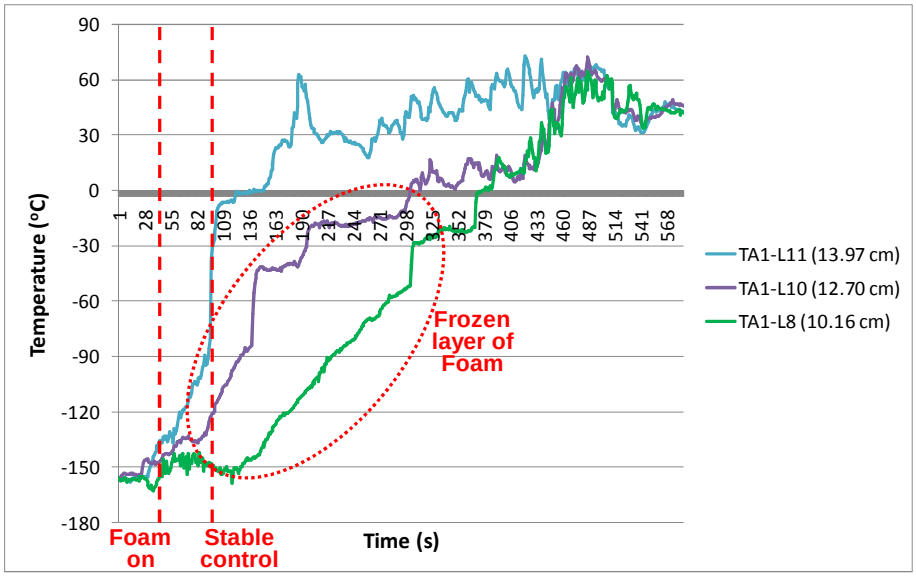

Fig. 55. Temperature profiles of foam at 13.97 cm or less height during fire at the March test

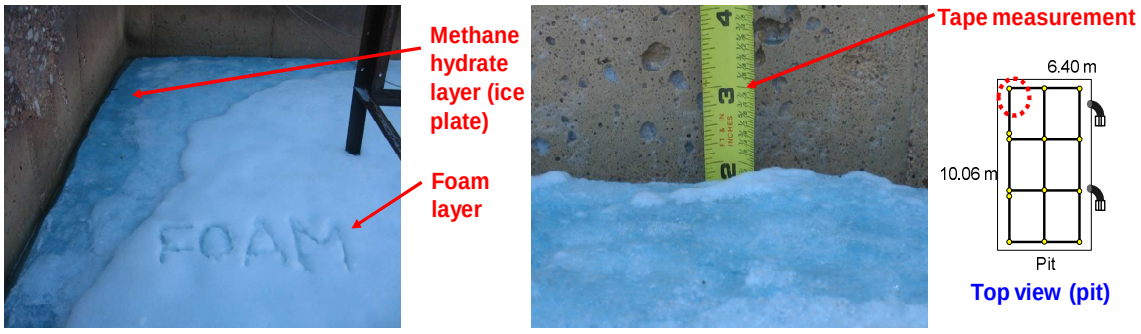

Fig. 56. Observation of ice plate after fire test

3.3.5 Radiative heat flux

3.3.5.1 Heat flux profiles of fire

LNG pool fire emits a radiative heat flux to its surroundings and it can have an adverse impact on humans and objects. Therefore, it is recommended by U.S. Regulations and NFPA 59A standard [8, 14] that exclusion zones around LNG fires on the basis of a 5 kW/m^2 heat flux should be evaluated for LNG facility design. Herein, in this study, we attempted to identify how much expansion foam can reduce the thermal hazard zone by measuring flame emissive power from wide-angle radiometers. Fig. 57 presents radiative heat flux profiles of the LNG pool fire measured by two radiometers (R8 and R9) positioned in the crosswind boundary at 15.24 m and 16.76 m distance respectively from the LNG fire base during the March test. It is clearly shown that after foam application heat fluxes decreased up to 90% in 55 seconds. In addition, two heat flux curves show exactly the same profiles and the radiometer (R8) closer to the fire reads higher values than the radiometer (R9) set farther. This indicates that the

radiometer data is valid. These patterns in heat flux caused by the foam were also observed similarly in the December 2009 test. Fig. 57 also includes flame length curve in blue color which is identical to the curve in Fig. 48. It is clearly shown that heat flux profiles have a close similarity to the curve in plume length over time. This implies that the radiant heat flux of fire is a strong function of the flame height. This relationship also can be explained through the study of the solid flame model as shown in equation (6) in section 3.1.2. According to the model, radiant heat flux is a function of mean surface emissive power (E), geometric view factor (F), and atmospheric absorption (τ). It has been reported by several papers that surface emissive power can be calculated experimentally with visible flame height and its value is dependent on the geometry of the fire, especially plume height [1, 14, 17, 33]. Geometric view factor is the fraction of energy emitted by the fire to the object on the basis of the view of geometric shapes from emitter (fire) and receiver. Previous researchers made mathematical models for view factor calculations and it was discovered that the view factor is proportional to the fire length [34, 35]. Therefore, it became apparent that the heat emissive power is strongly dependent on the height of flame as shown in Fig. 57.

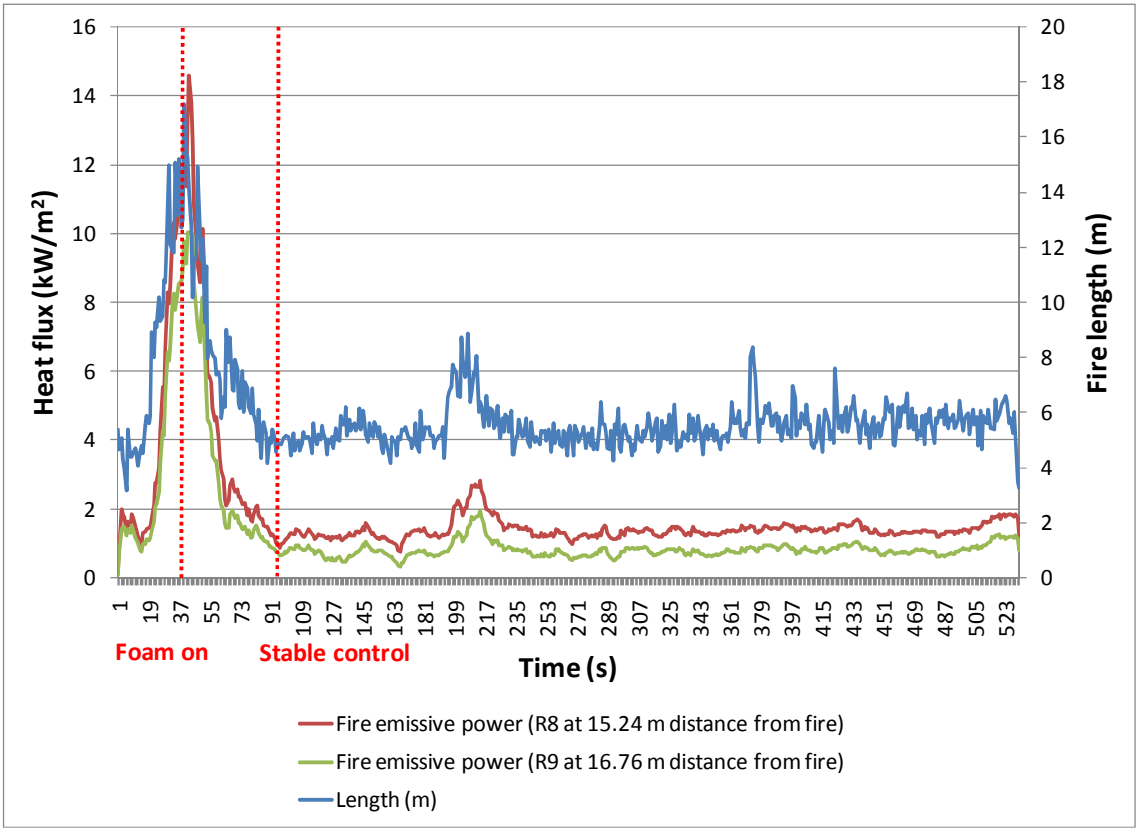

Fig. 57. Heat flux and fire length

In this research, an attempt has been made to identify the extent of the reduction of the radiant heat flux by the foam application. In order to quantify the heat flux reduction, a comparison was made between the mean value of heat flux before foam discharge (from 32 s to 36 s) and the mean heat flux after reaching a stable control by the foam application (from 92 s to 96 s; 55 seconds after foam discharge at 37 s). Fig. 58 includes several shapes of data. Each shaped datum represents the measurement in different wind direction (e.g., diamond: downwind, triangle: down crosswind, square: up crosswind, cross: upwind). In these data, the color-filled data represent measurements

after foam application and the vacant shapes indicate the data before foam discharge. It is shown in Fig. 58 that the radiant heat fluxes of the pool fire in four wind directions decreased ranging from 62 % to 91%. One interesting fact was found that the fire heat emissive powers in the downwind and the down crosswind were more reduced than the fire heat fluxes in the upwind directions. This is attributed to the higher thermal emissions of the pool fire to the radiometers or receptors in the downwind direction due to the fire tilt and the shift by the wind influence.

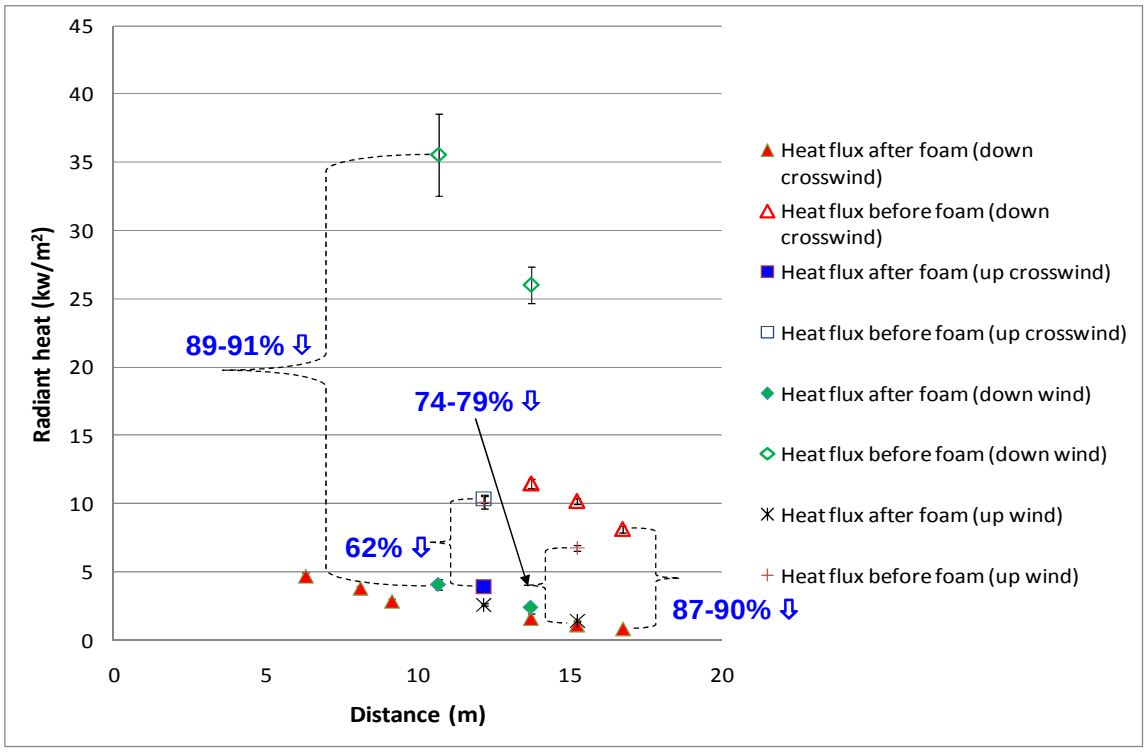

Fig. 58. Heat flux reductions of pool fire by foam application

3.3.5.2 Estimation of thermal exclusion zone (5 kW/m^2)

Here we attempted to identify the thermal exclusion zone, which is a safe separation distance from the source of the fire. In the March test, more radiometers were placed in the down crosswind direction to comply with the requirements of NFPA 11 [5]. Thus, the mean values of radiometer measurements before foam discharge (from 32 s to 36 s) and after reaching a stable control by foam application (from 92 s to 96 s) were plotted as shown in Fig. 59. In order to identify the distance of 5 kW/m^2 flux, the linear regression approaches were made. The trendlines show high R^2 values (0.9831 for the heat flux before foam application and 0.9658 for heat flux post foam utilization), which imply the equations are valid to represent the trend of data. Based on the obtained equations, the thermal threshold distances before and after foam application were estimated to be 19.69 m and 4.51 m, respectively. It became apparent that the expansion foam reduced the safe separation distance of the LNG pool fire with 64.83 m^2 basis up to 77 %. However, the magnitude of this reduction could be larger if free-burn of LNG were fully developed, but in this test foam had to be applied earlier than the moment of fully development due to safety concerns. It should be also noted that the reduction of thermal threshold distance can be varied in different wind directions. Uncertainty may arise by using the linear regression estimation for the 5 kW/m^2 distances from the small number of data. Further validations are recommended to conduct with more measurement data in various different distances. Additionally, the needs to build the thermal exclusion zone with heat flux contours still should be fulfilled to obtain the realistic pictures of exclusion zone.

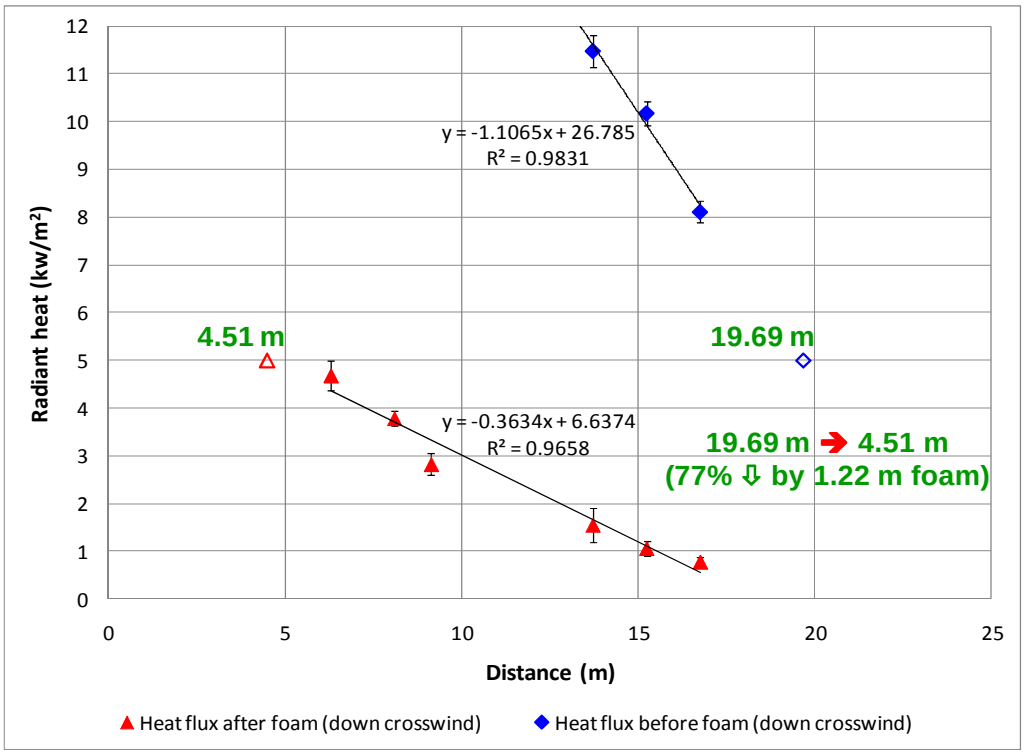

Fig. 59. Safe separation distances of LNG pool fire in down crosswind

To accomplish the needs of exclusion zone, in the December test, ten radiometers positioned around the pit (64 m^2 area) and one radiometer placed at the center of the pit to measure the heat fluxes of fire. During the test, foam was applied at 65 seconds after the fire initiation and radiant heat flux reached a stable control status at approximately 48 seconds after foam discharge (at 113 seconds after fire start). In order to consider fluctuation of heat flux due to flame variation with time, we employed mean values in 5 seconds before and after foam application, and after reaching steady fire by foam (time intervals of mean values are referred in the sub titles of Fig. 60). Fig. 60 presents three contours of flame emissive power in the same scale used by 3DFieldPro, which is one of the commercially available graphic tools. The program produced the contours in each

picture by considering the distribution and interrelation of measured data. Each figure includes a red color contour, which represents the thermal threshold distance of 5 kW/m^2 heat flux. Fig. 60(a) depicts heat flux contours measured right before the foam application to represent the largest heat flux values. As seen in Fig. 60(b), when foam was applied to an LNG pool fire, initially the thermal hazard distance increased slightly. However, when fire was controlled by the foam at steady state burning, the threshold distance decreased significantly as shown in Fig. 60(c). This trend agreed with the profiles of fire height and radiative heat flux in Fig. 48 and Fig. 57. During the 2009 December test, wind speed was 1.25±0.39 m/s, which was relatively low. Thus, the shapes of the contours became a rough circle without any significant alterations.

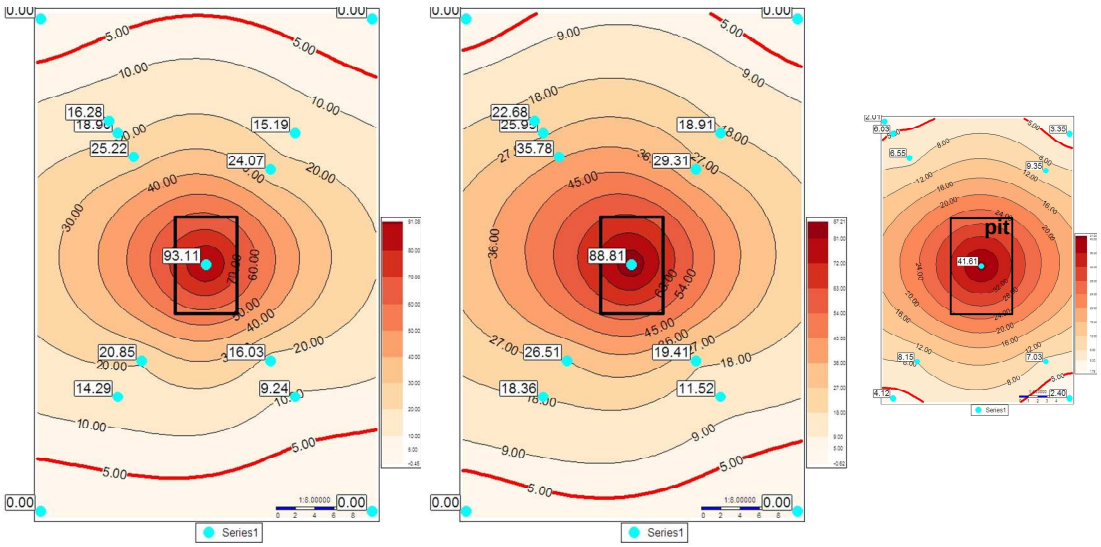

(a) 1 to 5 s before foam on

(b) 1 to 5 s after foam on

(c) Stable fire control by foam (48 to 52 s after foam on)

Fig. 60. Changes of heat flux contours by foam

During the December test, more radiometers were positioned in the downwind direction to identify the most conservative separation distance. Fig. 61 illustrates the changes of measured fire emissive power by foam application as a function of distance from the fire base in the downwind direction. As explained in Fig. 58, the color-filled data depict measurements from the radiometers and the void data represents calculated distances on the basis of coordinates of 5 kW/m^2 contours in Fig. 60 given by 3DFieldPro program. It is clearly shown in Fig. 61 that the application of expansion foam initially increased flame emissive powers and after reaching a stable control status decreased the heat flux from 68 % to 88 % dependent on the distances of radiometer from the fire base. This does clearly present a good agreement with the profile of flame height as shown in Fig. 57.

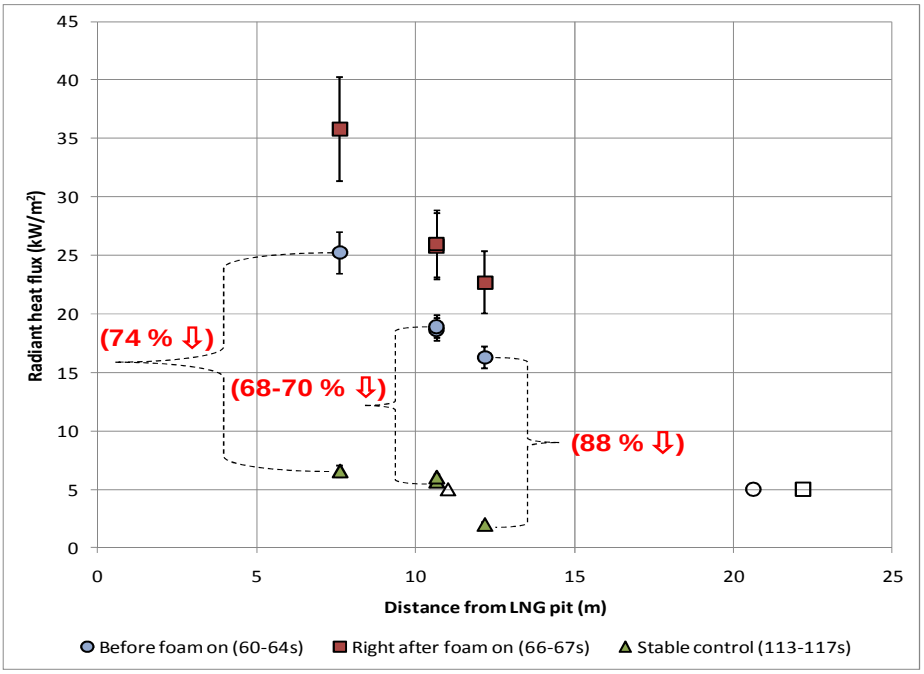

Fig. 61. Radiant heat flux changes by foam application in downwind

Furthermore, to identify the differences of foam influences on the safe separation distance in different wind directions, the distances of the 5 kW/m^2 heat flux were estimated on the basis of obtained contours corresponding to the wind direction as seen in Fig. 62. It became apparent in Fig. 62 that thermal threshold distance was reduced ranging from 47 % to 52 %, due to the application of 1.22 m thick foam. In this test, as shown by Fig. 62, the radiative heat fluxes in four wind directions were reduced similarly by the foam. It is believed that this is attributed to the relatively lower wind speed, 1.25±0.39 m/s, thus resulting in less wind effect on the fire shape (tilt and shift). However, one question that may arise is why the distance was reduced only 52 % even though radiative heat flux decreased up to 88 % in the same time span. It may be explained that flame emissive power is not inversely proportional to the distance from the fire source to the receptor with a magnitude of -1 due to the effect of the geometric view factor and atmospheric transmissivity. Another important issue is that further studies on scale-up of these findings as a function of several factors (e.g., LNG spill size) are required to apply for real industry facilities.

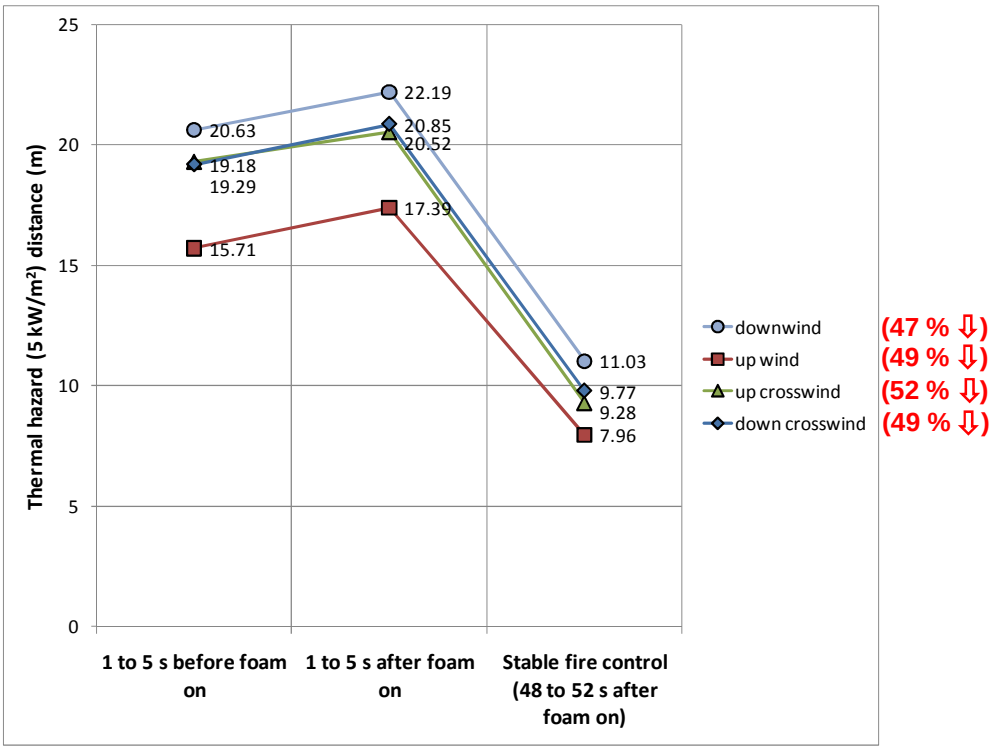

Fig. 62. Reduction of thermal hazard distance by foam

In the December test, a wide-angle radiometer with 150^{o} view was installed in the center of pit and was exposed to the LNG flame. Fig. 63 shows two curves: red curve is heat flux profile measured by the radiometer and blue one represents computed flux using the Stefan-Boltzman equation. The heat flux measurements by the radiometer were calibrated with 360^{o} view to be comparable to the thermocouple measurements because the thermocouples were exposed to fire in 360 degree angles. When the fire was initiated, the heat flux measurements showed initial dramatic increase and subsequent decrease in 45 seconds. We believe that this phenomenon was caused by the presence of ice layers which were formed during the vapor dispersion test. Before the ignition of LNG, methane vapors were accumulating inside the pit. When the LNG was ignited, the

ignition made an initial big fire which was also observed by a recorded video. The fire size subsequently decreased due to the consumption of the accumulated LNG vapor and the existence of the ice plates. When the fire was able to melt ice layers, the fire grew quickly again and then decreased because of subsequent foam application. The profile of the measured heat flux reflects this fire dynamics. However, this profile was not sensitive to the fire changes by foam as much as the heat flux curves measured by radiometers placed outside the pit. It can be explained that the radiometer inside the pit was continuously, directly exposed to the methane flame, thus resulting in relatively smaller influence in the heat flux by foam application.

We attempted to compute the heat fluxes using the temperature measurements by two thermocouples, which were placed at the same position with the radiometer. Babrauskas [26] suggested that the radiative heat flux of pool fire might be calculated with following equation:

$$q_r = \sigma T_f^4 (1 - e^{-k\beta D}) \quad (8)$$

Here σ is the Stefan-Boltzmann constant (5.67×10^{-11}kW/m^{2}K^4) and T_f is an effective equivalent grey-gas flame temperature. The emissivity of flame is related to its pool diameter (D), absorption-extinction coefficient of the flame (k) and mean-beam-length corrector (β). These empirical constants of LNG are also given in the literature [26]. Equation (8) was used to calculate the heat flux profile of the LNG pool fire shown as the blue curve in Fig. 63. It became apparent that measured and simulated heat flux profiles showed big discrepancies. It may be explained that the fire itself is not a blackbody and the assumption of grey-gas radiation is rather simplified [26]. Even if

average blackbody temperature is generally used ranging from 872 °C to 927 °C according to Atallah et al. [36], relatively lower temperatures (e.g., 600 °C to 800 °C) were used in the computation process of the heat flux in Fig. 63. In addition, an article reported that Stefan-Boltzmann equation may not be used for predicting the flame emissive power because of the uncertainty in the predicted emissivities and flame temperature [35]. It is therefore evident that the computation of fire emissive power using the Stefan-Boltzmann equation may create unacceptable uncertainty.

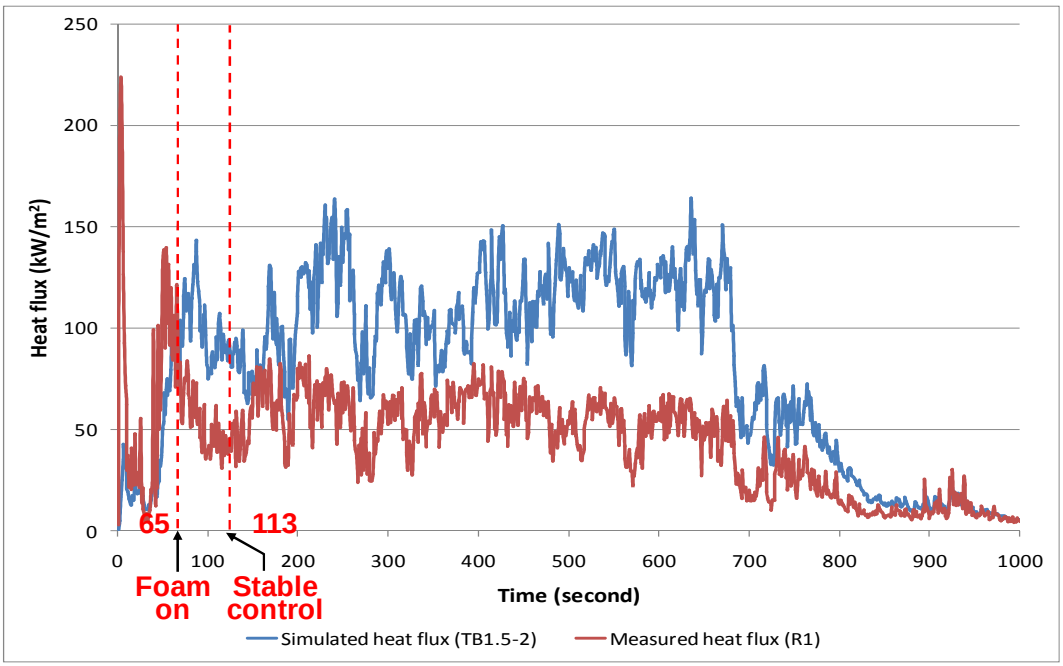

Fig. 63. Profile of heat flux measured inside LNG flame

3.3.6 Simplified model of LNG-foam system with fire

For the control of LNG vapor dispersion by foam, a simplified model of LNG and expansion foam was proposed in section 2.3.7. Similarly, in this section, we developed a model for a foam and LNG system in fire for potential theoretical modeling on the basis of previously stated experimental observations as seen in Fig. 64. Based on Fig. 54, Fig. 55, and Fig. 56, it is assumed that expansion foam produce three layers: a foam breaking layer, a non-frozen layer, and a frozen layer. It was assumed that expansion foam will be applied continuously or intermittently to keep a certain level of foam thickness. The foam breaking layer represents the layer in which foam bubbles are collapsed by the evaporation of water content due to boiling in fire. The temperature of this layer is greater than or equal to 100 ^{o}C. This layer may be able to reduce fire temperature to some extent due to the absorption of latent heat of the water boiling from fire heat, but it may not contribute to reduce the fire size significantly because it cannot impact on LNG vaporization reduction. The non-frozen layer, where the temperature ranges from 0 ^{o}C to 100 ^{o}C, is mainly composed of intact foam bubbles. This layer is effective at reducing fire height and vaporization rate due to suffocation of oxygen in the fire mechanism and insulation of the fire's heat feedback to the LNG pool. Thus, the depth from the top surface of foam to the interface between the foam breaking layer and the non-frozen layer can be a threshold value for the minimum effective foam depth on pool fire control. The bottom layer of foam can be a frozen layer (including ice plates), with its temperature below 0 ^{o}C. This layer may include ice tubes for passing vaporized LNG vapor, ice plates, and a bulk of frozen foam. The mechanics of the formation of

this layer can be explained as follows: (1) foam bubbles collapse due to the influences of fire and air and water contents of foam bubbles drain through the foam layers by gravity force to the LNG pool and (2) the drained water loses heat caused by contacting with LNG and cold vapor and becomes ice plates (or frozen layers). This frozen layer may be beneficial to reduce the fire height and the mass burning rate by reducing temperature differences between foam and LNG and also by blocking the fire's heat feedback to the LNG pool. In the interface of the non-frozen layer and the frozen layer, the latent heat of water in the foam due to freezing should be also taken into account the heat balance modeling.

In order to build the heat balance model of the LNG-foam system in the fire, several heat sources should be considered as seen in Fig. 64. If it is assumed that LNG is the system of interest, LNG may have several positive heat sources as follows: radiative ($q_{f,r}$) and convective heat input ($q_{f,c}$) from fire, heat input from the bottom side of the expansion foam ($q_{foam,c}$), conductive heat from the concrete ground and walls (q_g), solar radiation (q_r), convective heat transfer from the atmosphere (q_a), and the latent heat of water in the foam due to freezing ($q_{L,f}$). However, the solar radiation (q_r) and the convective heat transfer from atmosphere (q_a) may be negligible since they are relatively a lot smaller than other heat sources and they are mostly absorbed in the foam layers, thus not reaching to the LNG pool. In addition, it may be assumed that conductive heat input from the concrete walls may be neglected to make the model simpler, because the conductive heat input from the concrete ground is much larger than the wall conductive heat transfer, especially in the case of the large areas of confinement (e.g., the dike area

of an LNG storage tank). Therefore, we are able to model a one-dimensional conduction equation as shown at the bottom of Fig. 64. There could be some negative heat sources for the LNG system regarding the heat balance, such as latent heat of LNG for evaporation ($q_{L,LNG}$) and latent heat of water in the foam due to boiling ($q_{L,b}$). However, the latent heat of water in the foam due to boiling ($q_{L,b}$) may be neglected because it is not significantly influential on the LNG pool due to the existence of the non-frozen and frozen layers. Therefore, a total heat balance equation of LNG can be expressed as follows:

$$q_{f,c} + q_{f,r} + q_{foam,c} + q_g + q_r + q_a + q_{L,f} = q_{L,LNG} + q_{L,b} \quad (9)$$

If we consider several negligible factors stated above, then equation (9) can be simplified into the next expression:

$$q_{f,c} + q_{f,r} + q_{foam,c} + q_g + q_{L,f} = q_{L,LNG} \quad (10)$$

This heat balance equation can be used to solve the heat balance problems that arose from the incident scenarios of LNG pool fire control by foam and to calculate the mass burning rate post foam application. Caution must be used, however; in employing these equations whenever the system of interest is different than this (for instance, if the system of interest is the expansion foam, not LNG). In that case, the heat balance should be modified correspondingly.

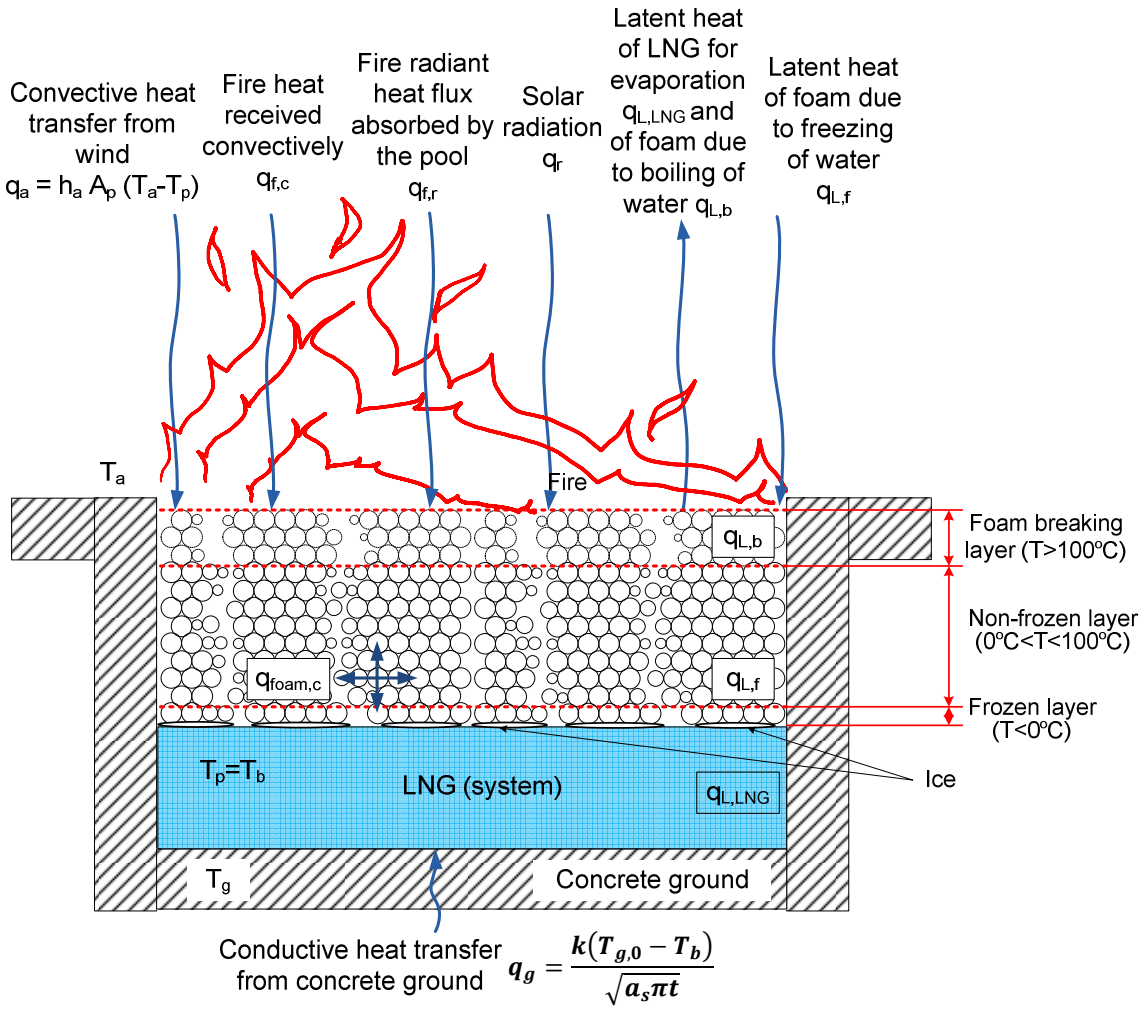

Fig. 64. Schematic model of LNG and expansion foam system with fire

3.4 Discussions

It is imperative to know the relationship between fire diameter and height to compute experimental values of surface emissive power of LNG pool fires [4]. To accomplish this purpose, the Thomas correlation of fire plume length for the diameter of fuel pools as seen in equation (3) (see section 1.2.1) has been widely used in fire

modeling. In addition, it was found by Thomas that the correlation made a good agreement with the data for industrial fuels burning when the diameter of the pools is less than or equal to 22.9 meters (D ≤ 22.9 m) [4, 14, 36]. However, at this moment, any correlation of fire plume length-diameter with foam application has not been developed yet. This correlation may be useful to compute the reduction of thermal heat flux by foam discharge and to consider providing credits in determining safe separation distances and plant layout to industries for using the foam system as an independent layer of protection. Herein, we proposed the correlation with an application of 1.22 m thick foam in the following expression using measured data of the mass burning rate ($\dot{m}''$), plume length (L), and equivalent pit diameter (D: 9.06 m) in this chapter as given by equation (11) and as seen in Fig. 65.

$$\frac{L}{D} = 17.40F^{2/3} \tag{11}$$

It was stated in Fig. 65 that the ratio of L to D has a mean value of 0.62, and its standard deviation is 0.07. This equation has an assumption that the Thomas correlation may also be valid in the case of fires with foam suppression (if D ≤ 22.9 m). It is therefore assumed as seen in Fig. 65 that the fire length-diameter correlation post foam application has the same slope in the Thomas correlation as well as this work. This assumption may have a rationale because expansion foam can only affect fire dynamics physically, not affect chemical combustion reactions (or combustion dynamics). Consequently, this correlation may provide a good initiative for further studies to researchers of interest, even if further tests and efforts for the correlation with experimental data are still required to validate the correlation.

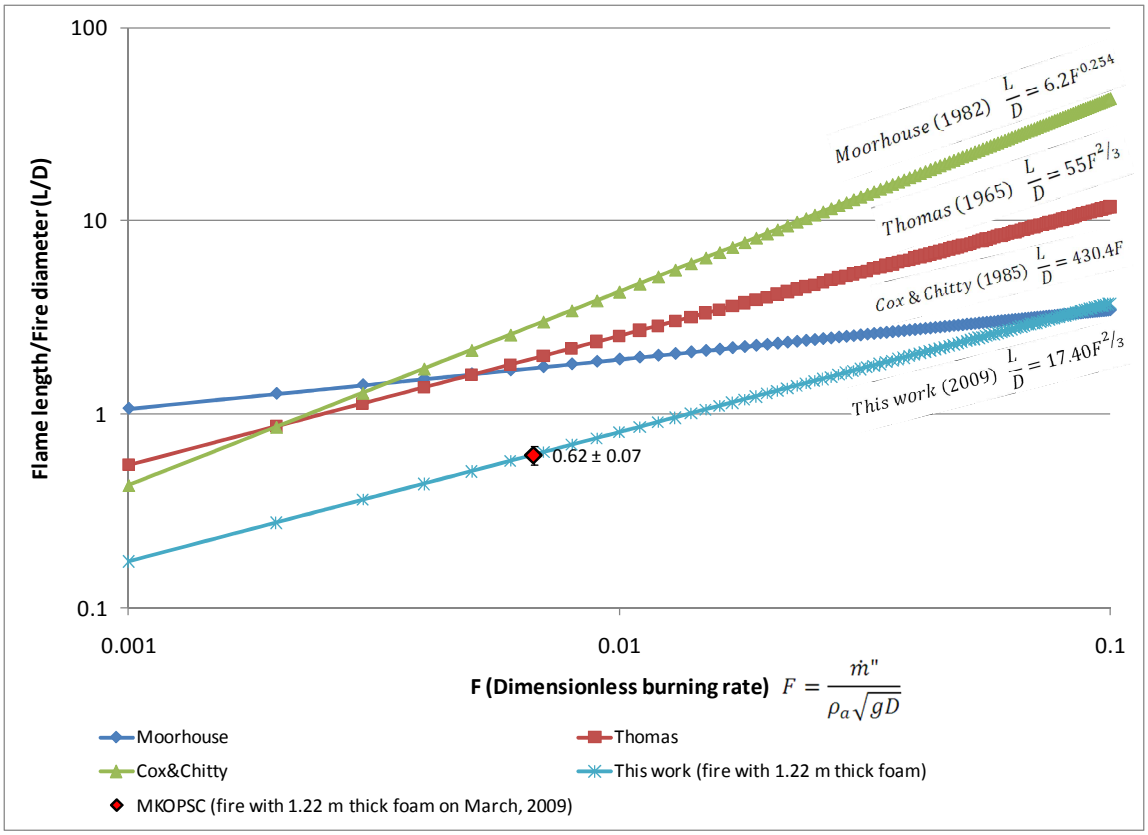

Fig. 65. Experimental correlation of fire height and diameter with 1.22 m thick expansion foam (adapted and modified from [4, 14])

Another interesting observation was that paper labels attached to thermocouples for LNG level measurement have survived even after the pool fire test in the March test as shown in Fig. 66. This can be explained with following sequential mechanisms. When LNG was ignited, the paper labels were dipped into the LNG pool. Thus the labels could not be burned due to non-existence of oxygen within the LNG layers. While LNG was vaporizing continuously and when expansion foam was subsequently applied, the labels were covered by multiple foam layers. Therefore, the LNG fire could not burn the paper

labels due to the deficiency of oxygen in the foam layers. To support this statement, the temperature profiles of the thermocouples for LNG level measurement at A1 location in the pit were provided as seen in Fig. 67. It depicts that all thermocouples presented temperatures below 100 ^{o}C even if fire was present throughout the whole period of test. It can be therefore concluded that the expansion foam can suppress LNG fires by decreasing oxygen concentration, which is required for the fuel combustion mechanism within the foam layers.

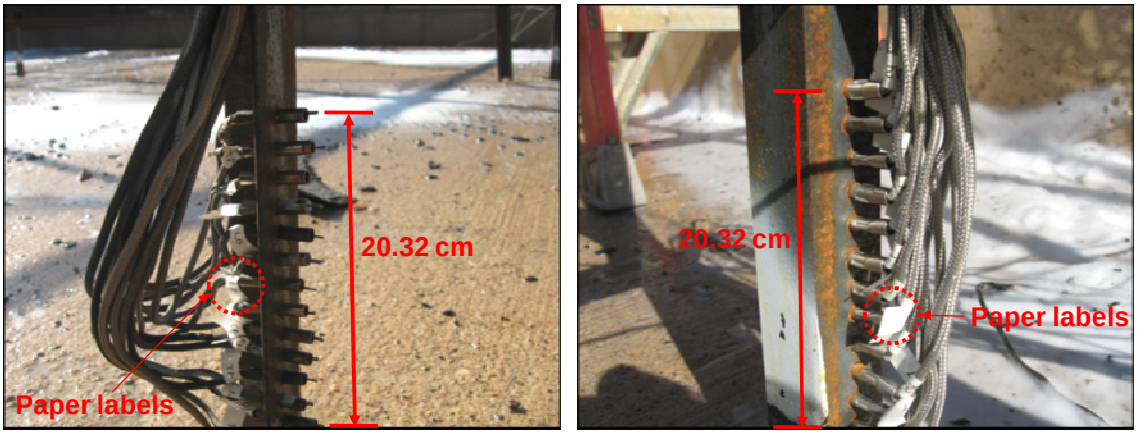

(a) A1 location in the pit (b) A2 location in the pit

Fig. 66. Paper labels of thermocouples for LNG level measurement

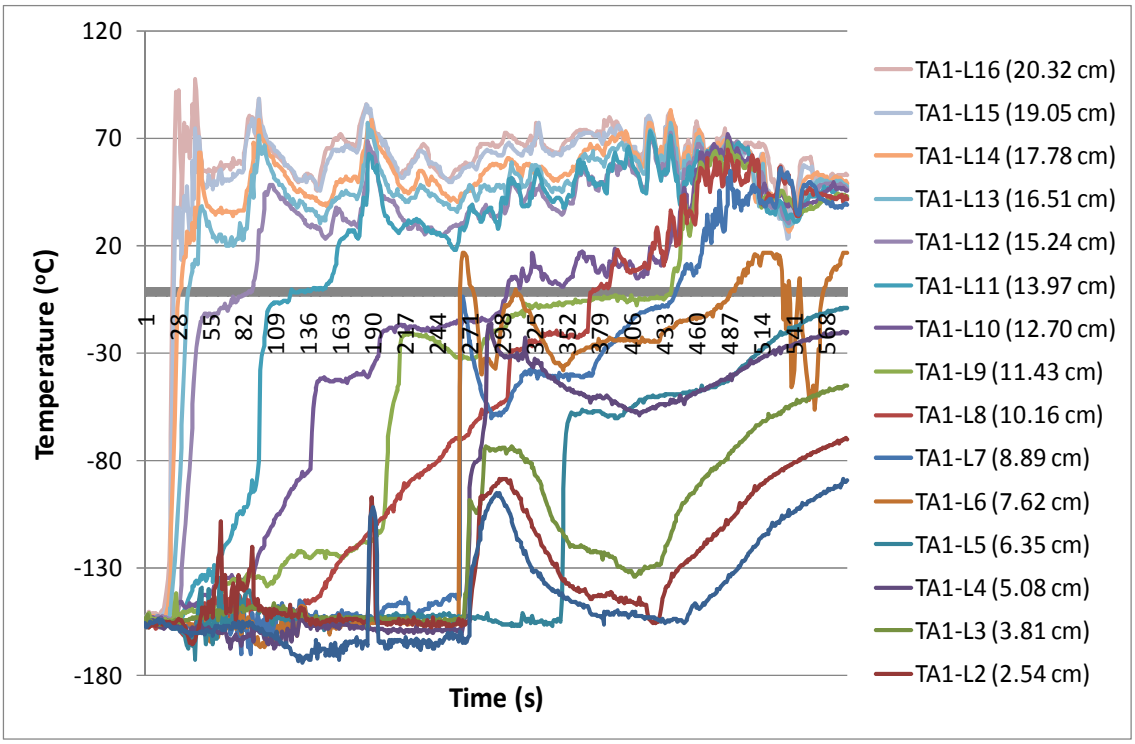

Fig. 67. Temperature profiles of thermocouples for LNG level measurement

3.5 Conclusions

This chapter provided the summary of the LNG field tests for evaluating the foam effectiveness on LNG pool fire control. Additionally, a wide range of data analysis was reported to identify important parameters such as: (1) mass burning rate; (2) effective foam depth; (3) relationship between the fire height and the radiative heat flux; (4) thermal exclusion zone; and (5) the correlation of LNG plume length for the diameter with foam application. A model of the LNG-foam system in the fires was also suggested for future theoretical calculation. Several critical findings are summarized as follows:

- It was confirmed through photographic analysis of the fire that expansion foam can reduce the fire height at least 61 % due to a reduction in fire heat feedback to the LNG pool by the foam insulation effect.
- The measurement of the mass burning rate of LNG with 1.22 m thick foam was achieved in this research. It was compared with other measurements to show its validity. It was found that the mass burning rate with foam is smaller than the burning rate in case of a pool fire on water and on concrete without foam application. It was also concluded that the burning rate with foam in fire is larger than the vaporization rate in case of a spill on concrete without fire and foam application.
- A minimum effective foam depth for pool fire control was determined as 0.61 m through the analysis of temperature data of the foam during the fire tests. However, the effective foam depth was selected as 0.64 m, which is a minimum effective foam depth for vapor dispersion control, because the depth should be chosen as the larger value between pool fire and vapor dispersion control to cover both incident scenarios.
- In this chapter, we identified that the expansion foam is capable of reducing the thermal hazard distance up to 52 % by the analysis of radiometer measurements. In addition, it was shown that flame emissive power is a strong function of flame height due to the effects of the geometric view factor and the surface emissive power.

- From the temperature analysis and observations after the pool fire test, a schematic model of the LNG and expansion foam with the fire was proposed. It was observed that expansion foam applied onto LNG pool fire have three layers: a foam breaking layer, a non-frozen layer, and a frozen layer. One of the interesting findings is that in spite of the pool fire, frozen layers (and/or ice plates) of foam can be formed. We believe that these frozen layers may reduce the mass burning rate of LNG further due to blocking fire heat feedback to the LNG pool and reducing temperature differences between foam and LNG.

CHAPTER IV

CONCLUSIONS

4.1 Summary and conclusions

This dissertation presents experimental evidence of the effectiveness of expansion foam on the control of LNG vapor dispersion and pool fire. To associate with the experimental findings, theoretical studies and calculations were conducted in parallel.

The literature review was performed on the phenomena of foam control on the LNG vapor dispersion and pool fire. Several previous studies were conducted to study foam effectiveness on LNG control, but many research gaps were identified through these literature studies. For example, minimum effective foam depth and the extent of reduction of vapor exclusion zone and thermal exclusion zone were not investigated. Additionally, behaviors and internal changes of foam when it is applied on the LNG pool were not reported in detail. To obtain the best safety and cost benefits of applying expansion foam system to LNG facilities, it is therefore imperative to perform further investigations through outdoor experiments and theoretical modeling described in this research.

Through the small-scale test, it was identified that when expansion foam was applied on the LNG pool surface, ice tube passages were formed along the vapor

pathways. Foam collapse rate was also measured allowing the determination of minimum effective foam depth and foam application rate.

In the medium-scale tests, it was confirmed through temperature measurements that the expansion foam can assist to warm LNG vapor and promote its buoyancy. It should be recognized, however; that foam application initially may result in negative effects on LNG vapor control due to excess vaporization in the initial stage of foam application. Generating temperature profiles of foam layers also assists in the determination of the minimum effective foam depth, 0.64 m, for mitigating vapor dispersion hazards. In order to reduce thermal hazards of LNG pool fire, the effective foam depth was determined to be greater than or equal to 0.61 m through the analysis of foam temperature data during the pool fire test. For mitigating both vapor cloud and fire risks, a larger value of two minimum effective foam depths should be chosen. Therefore, it was concluded that the thickness of expansion foam should be at least 0.64 m. For the actual application in LNG industries, however; the effective foam depth should be decided by associating this recommended thickness and additional factors, such as unexpected loss, foam collapse/shrinkage and safety margin.

In the medium-scale tests, it was also identified that expansion foam is effective in reducing the methane downwind concentrations, resulting in decreasing LFL and ½ LFL distances up to 80 % and 89 % respectively. Additionally, it was discovered that the expansion foam is capable of reducing the thermal hazard distance (5 kW/m^2 heat flux) up to 52 % through the analysis of radiometer measurements.

Based on the findings from small and medium scale tests, two schematic models of LNG and expansion foam system with/without fire were proposed. In case of fire mitigation tests, it was observed that expansion foam may form three layers when it is applied to an LNG pool fire: a foam breaking layer, a non-frozen layer, and a frozen layer (including ice plates). During the vapor cloud mitigation tests, it was found that foam may have two layers when it is applied to an LNG pool without fire: a non-frozen layer and a frozen layer. These simplified models were also used to develop energy and heat balance models.

Consequently, it can be concluded on the basis of these findings that expansion foam has beneficial effects on reducing both LNG vapor cloud exclusion zone and thermal exclusion zone when reaching to a stable control status. However, it should be noted that the foam application could result in initial negative influences due to increasing the vapor production rate. The more specific summaries of findings are provided in sections 2.4 and 3.5.

4.2 Recommendations for further research

This study provided extensive experimental data analysis obtained from the outdoor field tests to simulate potential incident scenarios in real LNG facilities. This work also proposed simplified models of the LNG and foam system for controlling vapor cloud and pool fire. Herein, we recommend that these findings should be tied to further research initiatives for the theoretical heat transfer modeling of the foam system on an LNG pool with/without fire. This will permit computational calculation of

effective foam depth, foam application rate, and mass evaporation (or burning) rate in terms of LNG pool sizes.

During the December test, prevailing wind direction was shifted from the weather-forecasted direction. This resulted in relatively lower values of methane concentration and fire emissive power measurements because all sensors were placed corresponding to the weather-predicted wind direction. It is believed that this affected the shape of the contours of methane concentration and radiant heat flux around the LNG pool to some extent. Thus, further tests with the same methodology adopted in this research are needed to make up this weakness.

This research was based on the LNG release case into a concrete pit with 64.83 m^2 area. However, actual LNG facilities may have different or significantly larger areas of released LNG pools. For instance, it is certain that the area between LNG storage tank and surrounding dike in LNG import terminals is significantly larger than this concrete pit area. Therefore, additional tests using different size pits are required to cover more possible release scenarios. Another important issue is that further studies on the scale-up of these findings as a function of several factors (e.g., LNG spill size) are required for application to actual industry facilities.

In measurement of the mass evaporation (or burning) rate using thermocouples, there may exist some degree of uncertainty due to the fluctuation of temperature readings. Even though the vaporization measurements can still provide good approximated experimental results, there is some room for improving LNG level measurement techniques. For example, multiple techniques such as use of

thermocouples and differential pressure-meters can be employed at a test site. Additionally, use of multiple locations of level measurement is also recommended, if there is uncertainty in horizontal plane of the floor bottom of simulated LNG containments or test props.

Foam collapse rate should be identified to determine minimum effective foam depth and foam application rate for real industry application. Thus, foam collapse rate during the LNG vapor cloud mitigation tests was measured in this study. However, in order to cover potential fire scenarios as well, foam regression rate during fire suppression should be also identified. This may be obtained by following steps: (1) measure radiant heat flux with a certain thickness of foam, (2) turn off the foam application and wait until the foam is consumed completely in the fire, (3) investigate the time in which heat flux comes back to the level of free-burn pool fire, and (4) obtain time difference between the investigated time in step 3 and the foam-off time, and then divide the foam thickness (or volume) with this time difference to obtain the foam regression rate.

In this research, a correlation of fire plume length-diameter with an application of 1.22 m thick foam was proposed. This correlation may be useful to compute the reduction of thermal heat flux by utilizing foam and to consider providing credits to industries for using the foam system as an independent protection layer when determining safe separation distances and plant layout. However, this correlation requires further tests with foam in different size LNG pools to cement the relationship.

Nowadays, the interest for control on LNG release onto water has been increasing due to higher demands of LNG marine transportation. However, the control measures of spilled LNG and fire on water have not studied or developed comprehensively. Therefore, further research should be performed to secure LNG safety in marine transportations, for instance:

- Study the characteristics of expansion foam on water (foam spreading, collapse rate): The impacts of expansion foam on ground release control of LNG have been identified in this research. However, the tests for determining the foam effectiveness on LNG spill onto water were not performed in depth. Thus, the characteristics of expansion foam on water (e.g., foam spreading, collapse rate) should be identified using various sizes of confinements or pits.
- Study the effectiveness of expansion foam and its alternatives (e.g., AFFF (Aqueous Film-Forming Foam)) on pool fire suppression.

REFERENCES

[1] A. Luketa-Hanlin, A review of large-scale LNG spills: Experiments and modeling, J. Hazard. Mater. 132 (2006) 119-140.

[2] P. Cleaver, M. Johnson, B. Ho, A summary of some experimental data on LNG safety, J. Hazard. Mater. 140 (2007) 429-438.

[3] K. Takeno, T. Ichinose, K. Tokuda, R. Ohba, Effects of high expansion foam dispersed onto leaked LNG on the atmospheric diffusion of vaporized gas, J. Loss. Prev. Process Ind. 9 (1996) 125-133.

[4] P.K. Raj, LNG fires: A review of experimental results, models and hazard prediction challenges, J. Hazard. Mater. 140 (2007) 444-464.

[5] NFPA 11A, Standard for low, medium, and high-expansion foam, 2002 edition, National Fire Protection Association, Quincy, MA, February 2002.

[6] R.P. Koopman, D.L. Ermak, Lessons learned from LNG safety research, J. Hazard. Mater. 140 (2007) 412-428.

[7] E.S. Yoon, M.S. Mannan, K.S. Park, K.H. Kim, Safety analysis for LNG terminal focused on the consequence calculation of accidental and intentional Spills, in: 8th Annual Symposium of Mary Kay O'Connor Process Safety Center. (2005) 200-218.

[8] NFPA 59A, Standard for the production, storage, and handling of liquefied natural gas (LNG), 2001 Edition, National Fire Protection Association, Quincy, MA, February 2001.

[9] L. Myron, D.C.N. Casada, The current status of LNG facility standards and regulations, Process Saf. Prog. 24 (2005) 152-157.

[10] P.K. Raj, Field tests on human tolerance to (LNG) fire radiant heat exposure, and attenuation effects of clothing and other objects, J. Hazard. Mater. 157 (2008) 247-259.

[11] D.A. Crowl, J.F. Louvar, Chemical process safety - Fundamentals with applications, second ed., Prentice Hall PTR, Upper Saddle River, NJ, 2002.

[12] B.R. Cormier, Computational fluid dynamics for LNG vapor dispersion modeling: A key parameters study, PhD dissertation at TAMU, College Station, TX, 2008.

[13] J.A. Fay, Model of spills and fires from LNG and oil tankers, J. Hazard. Mater. 96 (2003) 171-188.

[14] P.K. Raj, Large LNG fire thermal radiation: Modeling issues and hazard criteria revisited, Process Saf. Prog. 24 (2005) 192-202.

[15] University Engineers, Inc., An experimental study on the mitigation of flammable vapor dispersion and fire hazards immediately following LNG spills on land, Washington, DC, 1974.

[16] J.A. Suardin, The application of expansion foam on liquefied natural gas (LNG) to suppress LNG vapor and LNG pool fire thermal radiation, PhD dissertation at TAMU, College Station, TX, 2008.

[17] M. Hugues, P.K. Raj, Thermal emission and other characteristics of large liquefied natural gas fires, Process Saf. Prog. 26 (2007) 237-247.

[18] V. Vesovic, The influence of ice formation on vaporization of LNG on water surfaces, J. Hazard. Mater. 140 (2007) 518-526.

[19] M.A. Rana, Y. Guo, M.S. Mannan, Use of water spray curtain to disperse LNG vapor clouds, J. Loss. Prev. Process Ind. 22 (2009) 1-12.

[20] H. Jerry, S. Tom, LNG vapor cloud exclusion zones for spills into impoundments, Process Saf. Prog. 24 (2005) 181-186.

[21] J.A. Suardin, Y. Wang, M. Wilson, M.S. Mannan, Field experiments on high expansion (HEX) foam application for controlling LNG pool fire, J. Hazard. Mater. 165 (2009) 612-622.

[22] B. Persson, A. Lonnermark, H. Persson, FOAMSPEX: Large scale foam application—modeling of foam spread and extinguishment, Fire Technol. 39 (2003) 347–362.

[23] The Netherlands Organization of Applied Scientific Research (TNO), Methods for the calculation of physical effects, third ed., The Hague, The Netherlands, 1997.

[24] F. Briscoe, P. Shaw, Spread and evaporation of liquid, Prog. Energy Comb. Sci. 6 (1980) 127-140.

[25] R.B. Bird, W.E. Stewart, E.N. Lightfoot, Transport phenomena, second ed., John Wiley & Sons, Inc, New York, 2001.

[26] V. Babrauskas, Estimating large pool fire burning rates, Fire Technol. 19 (1983) 251-261.

[27] M.A. Rana, B.R. Cormier, J.A. Suardin, Y.C. Zhang, M.S. Mannan, Experimental study of effective water spray curtain application in dispersing liquefied natural gas vapor clouds, Process Saf. Prog. 27 (2008) 345-353.

[28] R. Ohba, A. Kouchi, T. Hara, V. Vieillard, D. Nedelka, Validation of heavy and light gas dispersion models for the safety analysis of LNG tank, J. Loss. Prev. Process Ind. 17 (2004) 325-337.

[29] R.O. Parker, Calculating thermal radiation hazards in large fires, in: Conference Proceedings of NFPA Annual Meeting (1973), St. Louis, MO.

[30] T.J. Collins, ImageJ for microscopy, Biotechniques, 43 (2007) 25-30.

[31] J.M. Chatris, J. Quintela, J. Folch, E. Planas, J. Arnaldos, J. Casal, Experimental study of burning rate in hydrocarbon pool fires, Combustion and Flame. 126 (2001) 1373-1383.

[32] E.I. Planas-Cuchi, J. Casal, Flame temperature distribution in a pool-fire, J. Hazard. Mater. 62 (1998) 231-241.

[33] Raj, P.K., A review of the criteria for people exposure to radiant heat flux from fires. J. Hazard. Mater. 159 (2008) 61-71.

[34] R.O. Weber, Analytical models for fire spread due to radiation, Combustion and Flame. 78 (1989) 398-408.

[35] B.C. Davis, D.F. Bagster, The computation of view factors of fire models: 1. Differential targets. J. Loss. Prev. Process Ind. 2 (1989) 224-234.

[36] S. Atallah, D.S. Allan, Safe separation distances from liquid fuel fires, in: The Central States Section of the Combustion Institute Meeting (1970), Houston, TX.

APPENDIX A

Methane concentration profiles outside the pit during 2009 December test.

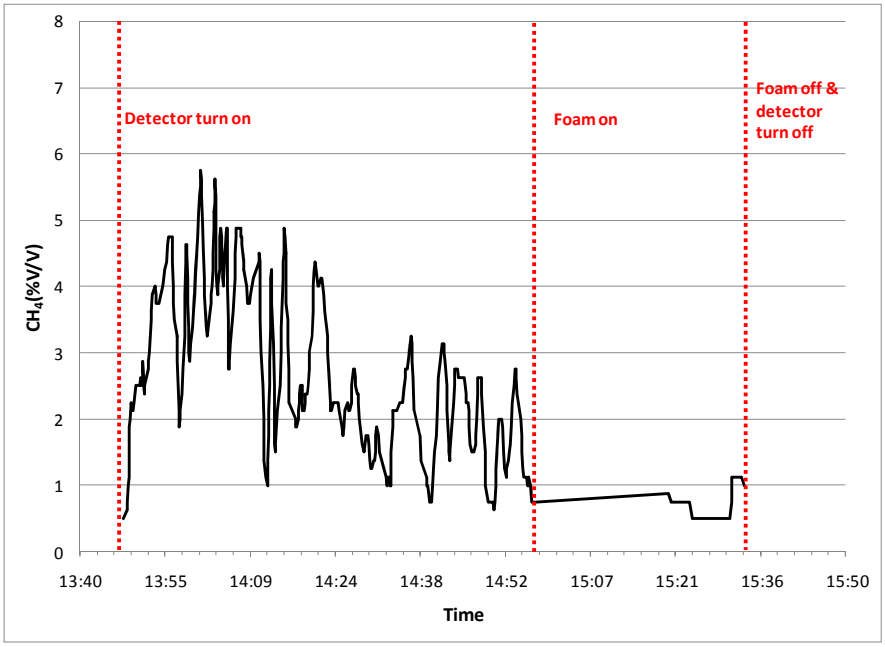

(a) GD 41 Full

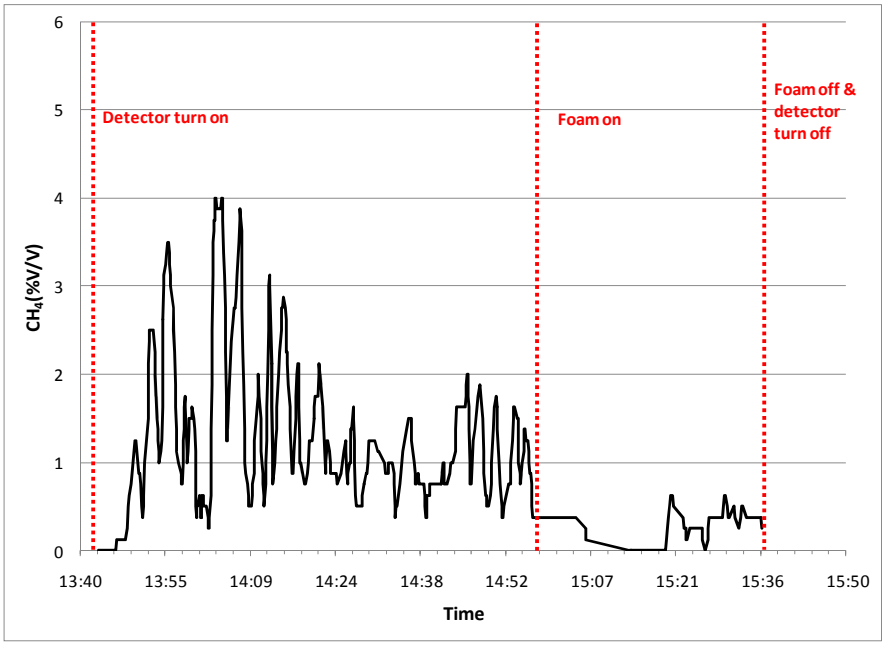

(b) GD 42 Full

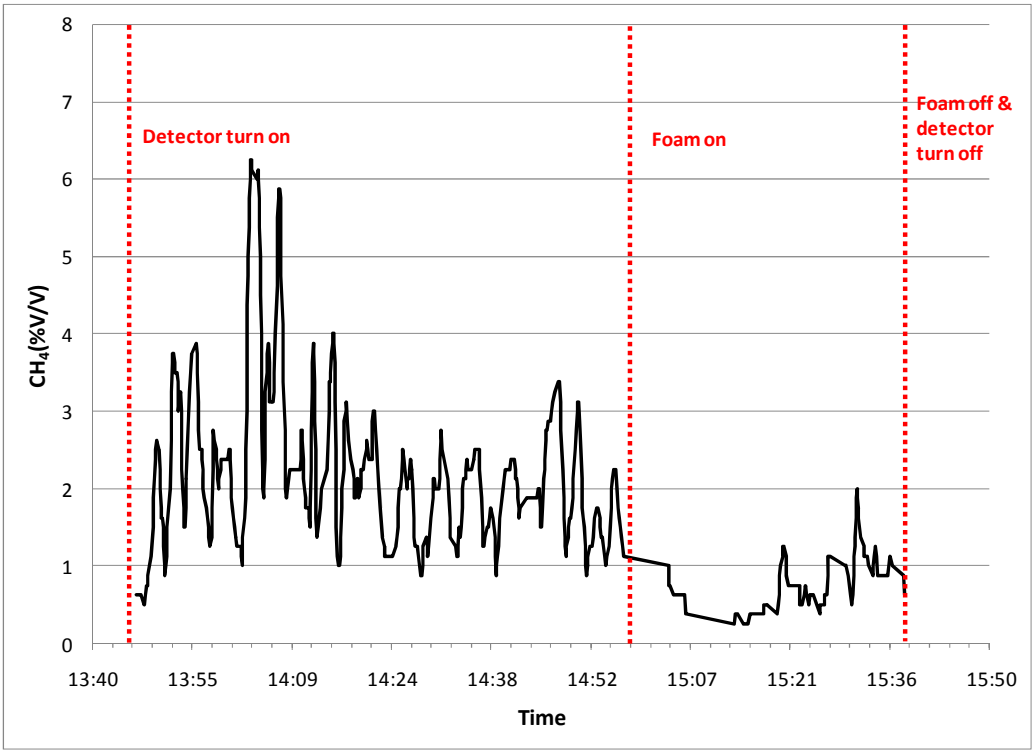

(c) GD 43 Full

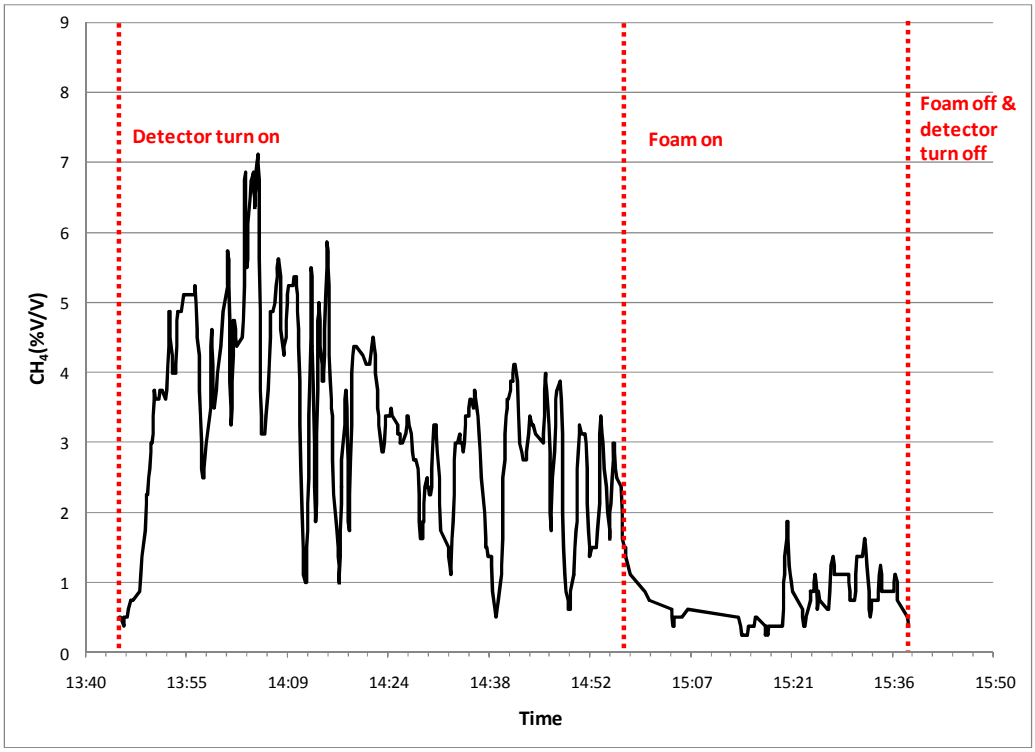

(d) GD 44 Full

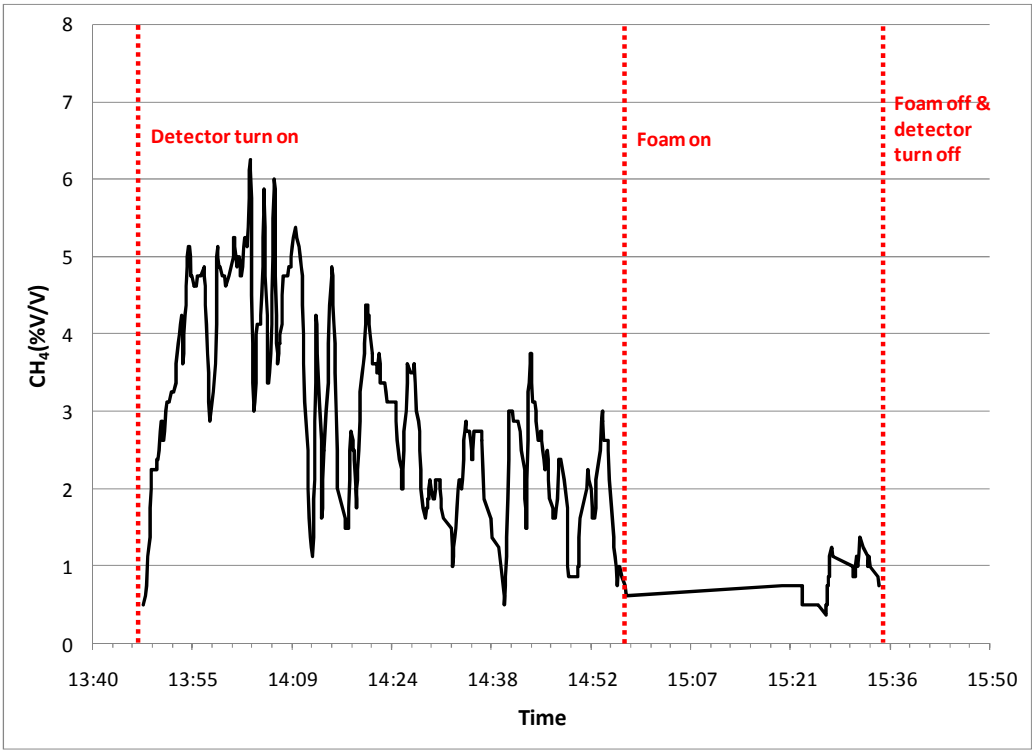

(e) GD 45 Full

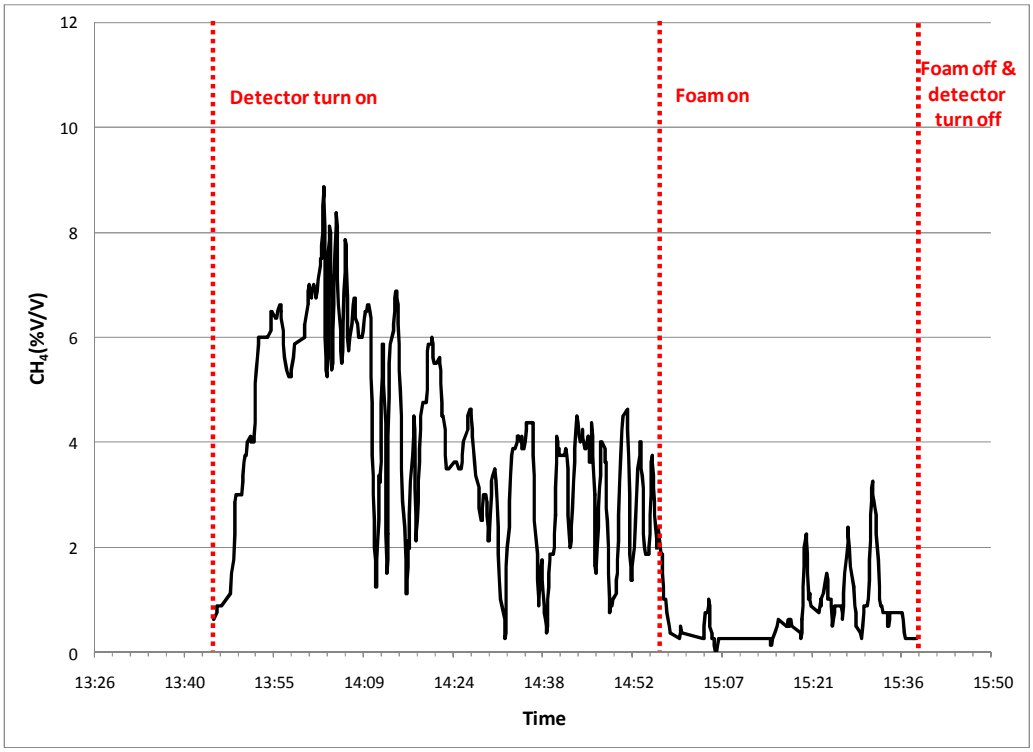

(f) GD 46 Full

VITA

Name Geun Woong Yun

Address Mary Kay O'Connor Process Safety Center, Room 200, Jack E. Brown Building, Texas A&M University, 3122 TAMU, College Station, TX 77843-3122

Email address geunwoong@gmail.com

Education

- B.S., Chemical Engineering, SungKyunKwan University, 1997
- M.S., Mechanical System Engineering, YonSei University, 1995
- M.S., Chemical Engineering, Texas A&M University, 2007
- Ph.D., Chemical Engineering, Texas A&M University, 2010

Employment Safety Engineer and Research Scientist, Korea Gas Safety Corporation, 1996 -2005

Qualifications

- LOPA Training Certification, MKOPSC, 2007
- Certification of OSHA PSM NEP Training, MKOPSC, 2010
- Certification of PHA Leadership Training, MKOPSC, 2010
- Certification of Best Practices – Pressure Relief Systems, MKOPSC, 2009
- Certification of 2008 Engineering Ethics, MKOPSC, 2008
- Certification of LOPA (Layer of Protection Analysis) Training, MKOPSC, 2007
- Certification of SIL (Safety Integrity Level) Verification Training, MKOPSC, 2006
- Design Corrosion Control Certification, NACE (The Corrosion Society), 2004
- Certified Welding Inspector Certificate, AWS (American Welding Society), 2003
- Gas Safety Expert Certificate, Human Resources Development Service of Korea, 1996
- Occupational Safety Expert Certificate, Human Resources Development Service of Korea, 1995